We cannot solve our problems

with the same thinking we used

when we created them.

Albert Einstein (1879 – 1955)

Members of the jury

Prof. dr. Sven Hendrix, Universiteit Hasselt, Diepenbeek, Belgium, president
Prof. dr. Virginie Bito, Universiteit Hasselt, Diepenbeek, Belgium, promoter
Prof. dr. Wilfried Mullens, Universiteit Hasselt, Diepenbeek, Belgium, co-promoter
Prof. dr. Bert Brône, Universiteit Hasselt, Diepenbeek, Belgium
Prof. dr. Jean-Michel Rigo, Universiteit Hasselt, Diepenbeek, Belgium
Prof. dr. Jolanda van der Velden, VU University Medical center, Amsterdam, The Netherlands
Prof. dr. Casper Schalkwijk, Maastricht University Medical Centre, Maastricht, The Netherlands

Table of Contents

List of figures

List of tables

List of Abbreviations

Aβ	Amyloid-béta
ADAM10	A Disintegrin and metalloproteinase domain-containing protein 10
AGE-R1	Advanced glycation end product receptor 1
AGE-R2	Advanced glycation end product receptor 2
AGE-R3	Advanced glycation end product receptor 3
AGEs	Advanced glycation end products
ALT-711	4,5-dimethyl-3-phenacylthiazolium
Ang II	Angiotensin II
AP	Action potential
AWT	Anterior wall thickness
BSA	Bovine serum albumin
BW	Body weight
CaMKII	Ca^{2+}-calmodulin-dependent protein kinase II
cAMP	Cyclic adenosine monophosphate
CD36	Cluster of differentiation 36
Cdc42	Cell division control protein 42
CEL	Carboxyethyllysine
CICR	Ca^{2+}-induced Ca^{2+}-release
CML	N-carboxymethyllysine
CO	Cardiac output
cRAGE	Cleaved RAGE
CS	Citrate synthase
CTGF	Cytokine connective tissue growth factor
CVD	Cardiovascular disease
DCM	Diabetic cardiomyopathy
DN-RAGE	Dominant-negative RAGE
ECC	Excitation-contraction coupling
ECL	Enhanced chemiluminscence
EDP	End-diastolic pressure
EDV	End-diastolic volume
EF	Ejection fraction

ELISA	Enzyme-linked immunosorbent assay
eNOS	endothelial nitric oxide synthase
esRAGE	Endogenous secreted RAGE
ESV	End-systolic volume
ET-1	Endothelin 1 (ET-1)
F_{act}	Active force
F_{pass}	Passive force
FS	Fractional shortening
GOLD	Glyoxal lysine dimer
GTP	Guanosine triphosphate
HF	Heart failure
HPLC	High-performance liquid chromatography
HR	Heart rate
HMGB-1	High-mobility group box-1
HMW-AGEs	High molecular weight advanced glycation end products
HW	Heart weight
I_{Ca}	Ca^{2+} current
IFN-γ	Interferon gamma
IGF1	Insulin-like growth factor 1
IL-6	Interleukin 6
ISO	Isoproterenol
Jak	Janus kinase
L/L_0	Systolic cell length/diastolic cell length
LAD	Left anterior descending
LCCs	L-type Ca^{2+} channels
LMW-AGEs	Low molecular weight advanced glycation end products
LOX	Lysyl oxidase
LTBP	Latent binding protein
LV	Left ventricle
LVEDD	Left ventriclar end-diastolic diameter
LVESD	Left ventriclar end-systolic diameter
LVP	Left ventricular pressure
LVW	Left ventricular weight
MAPK	Mitogen-activated protein kinase

X

Max dP/dt	Maximum peak time derivative
MG-H1	Methylglyoxal-derived hydroimidazoline
MI	Myocardial infarction
Min dP/dt	Minimum peak time derivative
MOLD	Methylglyoxal lysine dimer
NAC	N-acetyl-L-cysteïne
NADPH	Nicotinamide adenine dinucleotide phosphate
NCX	Na^+/Ca^{2+} exchanger
NF-κB	Nuclear factor kappa B
NO	Nitric oxide
NT	Normal tyrode
PI3-K	Phosphatidylinositol-3 kinase
PFA	Paraformaldehyde
PKA	Protein kinase A
PLB	Phospholamban
PLB16	Phospholamban on serine 16
PLB17	Phospholamban on threonine 17
PLP	Pyridoxal 5-phosphate
PM	Pyridoxamine
PVDF	Polyvinylidene fluoride
PWT	Posterior wall thickness
RAGE	Receptor for advanced glycation end products
RCS	Reactive carbonyl species
ROS	Reactive oxygen species
RNA	Ribonucleic acid
si-RNA	Small interfering ribonucleic acid
RT	Room temperature
RT_{50}	Half-time relaxation
RyR	Ryanodine receptor
S_{circ}	Circumferential strain
SDS-PAGE	Sodium dodecyl sulfate polyacrylamide gel electrophoresis
SEM	Standard error of the mean
SERCA	Sarcoplasmic reticulum Ca^{2+} ATPase
SI	Sphericity index

SR	Sarcoplasmic reticulum
SR-A	Scavenger receptor class A
SR_{circ}	Circumferential strain rate
sRAGE	Soluble RAGE
STAT	Signal transducers and activators of transcription
STE	Speckle tracking echocardiography
STI	Speckle tracking imaging
SV	Stroke volume
τ fast	Fast time constant
τ slow	Slow time constant
TBS-T	Tris-buffered solution Tween-20
TBP	TATA box binding protein
TGF-β1	Transforming growth factor β1
TL	Tibia length
TNF-α	Tumor necrosis factor α
TTC	Triphenyl tetrazolium chloride
TTP	Time to peak of contraction
UR	Untwist rate
UP-LC/MS/MS	Ultra-performance liquid chromatography tandem mass spectrometry
VCAM-1	Vascular cell adhesion molecule-1
VEGF	Vascular endothelial growth factor
V_m	Resting membrane potential
YWAHZ	Tyrosine 3-monooxygenase/tryptophan 5-monooxygenase activation protein zeta

1

GENERAL INTRODUCTION AND AIMS

1.1 General introduction

Demographic data of the United Nations demonstrate that the percentage of the world population aged 65 and older is increasing every year [1]. Among others, cardiovascular diseases (CVDs) are commonly experienced by the elderly population. CVDs comprise coronary ischemic heart disease, congenital cardiovascular diseases, arrhythmias, myocardial infarction, atherosclerosis and heart failure (HF). Of these, HF is the most often diagnosis for hospitalized patients aged over 65 [2].

HF is the final stage of many heart diseases characterized by the inability of the heart to pump blood to meet the energy demand of the body. Two main types of heart failure have to be distinguished: systolic dysfunction and diastolic dysfunction. Systolic dysfunction indicates that the heart is unable to maintain cardiac output, better known as forward failure (reduced ejection fraction). At the basis of this process lies increased afterload or impaired contractility due to loss of myocytes (apoptosis) or myocyte function. Diastolic dysfunction indicates that diastolic filling is impaired, also known as backward failure (preserved ejection fraction). Impaired diastolic filling, for instance due to increased stiffness or impaired diastolic relaxation of cardiomyocytes, results in diastolic dysfunction [3, 4].

A variety of cardiac pathologies can lead to HF: atherosclerosis, hypertension, cardiomyopathy, coronary artery disease and myocardial infarction. Myocardial infarction reflects cell death of the cardiac myocytes caused by prolonged ischemia, which is the result of a perfusion imbalance between oxygen supply and demand [5].

As a result of modern medicine, most of the symptoms experienced by HF patients can be managed, reducing the amount of discomfort and slowing down progression of the adverse condition. The underlying problem, however, is barely treated. Besides recommending a healthy lifestyle, clinicians often treat HF patients with diuretics, aldosterone antagonists, ACE inhibitors or β-blockers. Although a lot of ground-breaking discoveries have already been made and knowledge about the molecular processes inducing HF expanded, a lot of key processes still have to be understood in order to reduce the mortality of CVDs.

One of the steps in that process is the discovery of new players in the pathogenesis of HF.

Over the past few years, advanced glycation end products (AGEs) have been indicated as such a potential target [6-8]. AGEs are proteins and/or lipids that become glycated and oxidized after persistent contact of reducing sugars (*e.g.* glucose) or short-chain aldehydes (*e.g.* glycolaldehyde) with amino groups and/or a high degree of oxidative stress [9, 10]. AGEs can also be categorized based on their molecular weight: low-molecular weight AGEs (LMW-AGEs) and high molecular weight AGEs (HMW-AGEs). In this thesis we investigate the role of HMW-AGEs in cardiac dysfunction.

1.2 Objectives of the study

In this thesis, we further investigated the role of HMW-AGEs in cardiac dysfunction. In particular, we hypothesized that HMW-AGEs play a deleterious role in the development and progression of cardiac dysfunction and that blocking AGEs formation could attenuate the cardiac phenotype in cardiac dysfunction. To test this hypothesis, we focussed on several objectives:

1. Investigate the role of HMW-AGEs on cardiac function *in vivo* in a rat model with increased circulating HMW-AGEs levels (**Chapter 3**). We tested whether HMW-AGEs *per se* are a cause for cardiac dysfunction.

2. Investigate the role of HMW-AGEs on cardiomyocyte function in a rat model with increased circulating HMW-AGEs levels (**Chapter 4**). We hypothesized that the altered morphology and function *in vivo* is not only the result of extracellular remodeling but also the result of structural and functional remodeling at the cardiomyocyte level.

3. Determine the acute effects of HMW-AGEs on rat cardiomyocytes (**Chapter 5**). In this chapter, we determined whether HMW-AGEs could alter cardiomyocyte function not only chronically, but also acutely.

4. Determine the role of AGEs formation inhibitor pyridoxamine (PM) in myocardial infarction (MI) (**Chapter 6**). We hypothesize that pre-treatment with PM can limit LV remodeling in rats with MI and therefore improving cardiac outcome.

2

Advanced glycation end products (AGEs) and cardiovascular dysfunction: focus on high molecular weight AGEs

2.1 Advanced glycation end products

Glycation is a major cause of spontaneous damage to cellular and extracellular proteins of living organisms [11]. AGEs are proteins and/or lipids that become glycated and oxidized after persistent contact of reducing sugars (*e.g.* glucose) or short-chain aldehydes (*e.g*. glycolaldehyde) with amino groups and/or a high degree of oxidative stress [9, 10]. AGEs can be found exogenously in both cigarettes and in our western diet, in particular during the processing of foods leading to an irreversible chemical modification of amino acids and a loss of essential amino acids in the diet and a decreased protein digestibility [12-16]. To date, two large databases are available with the content of carboxymethyllysine (CML), a commonly measured AGEs, in more than 500 food items in order to estimate daily dietary AGEs intake. Foods rich in both protein and fat, mostly of animal origin, and cooked at high and dry heat (e.g. broiling, grilling or frying) are the richest dietary sources of AGEs [17, 18]. In addition to external sources of AGEs, this reaction can also occur endogenously, yielding to the formation of AGEs *in vivo*. The accumulation of AGEs in the body is a natural process that occurs with senescence. AGEs are produced in the body, are found in the plasma and can also accumulate in various tissues, including cardiac tissue. However, increased circulating AGEs has been described to arise at early lifetime, in particular in settings of cardiovascular diseases. Elevated levels of AGEs were first associated with diabetes, where it was thought that AGEs formation was exclusively the result of increased blood sugar concentrations [19]. However, recent literature have extended this view and have shown that AGEs accumulation occurs also in pathological situations independent of diabetes such as cardiac dysfunction, renal failure and Alzheimer disease [20-23].

2.2 Formation of AGEs *in vivo*

As summarized in Figure 2.1, the formation of AGEs *in vivo* occurs by three independent pathways: the Maillard reaction, the polyol Pathway and during increased oxidative stress. During all three reactions, the synthesis of AGEs leads to the formation of reactive carbonyl species (RCS), such as glyoxal, glycolaldehyde, methylglyoxal and 3-deoxyglucosone [10, 24-26]. These reactive intermediates can further react with circulating proteins leading to additional

AGEs formation. As shown previously, the larger source of AGEs formation is the enzymatic Maillard reaction [12]. Briefly, an unstable Schiff base is formed by the reaction of a reducing sugar with amino groups of proteins, nucleic acids or lipids. The reversible Schiff base can evolve into Amadori products by molecular rearrangements. These Amadori products can be transformed into RCS to form AGEs like glucosepane, known to be involved in the pathogenesis of diabetic complications [27-29]. Alternatively, these products can be fragmented by oxidation, which results in the generation of AGEs such as CML or pentosidine [13, 25, 29-31]. These two major AGEs molecules were shown to be associated with a higher risk for mortality and inversely correlate with ejection fraction, independent to confounding factors, such as renal function [32, 33]. The two-step enzymatic polyol pathway is also an important pathway responsible for AGEs formation [13, 34]. During this reaction, glucose is reduced to sorbitol by aldose reductase, which is in turn, converted to fructose by sorbitol dehydrogenase. The generation of different fructose metabolites (fructose-1-P and fructose-3-P) leads to RCS, which in turn generates AGEs by the reaction with monoacids. Finally, elevated levels of oxidative stress promote the oxidation of monosaccharides such as glucose, ribose or fructose by catalytic metals and O_2, as a process known as autoxidation, resulting in the formation of α-dicarbonyl compounds, such as methylglyoxal [25, 29]. Methylglyoxal can react with a free lysine group leading to the formation of carboxyethyllysine (CEL) or methylglyoxal lysine dimer (MOLD). Additionally, lipid peroxidation is also a substantial source of reactive intermediates such as glyoxal or methylglyoxal. The reaction of glyoxal with a free lysine group results in CML or glyoxal lysine dimer (GOLD) while the reaction with an arginine group forms hydroimidazolines [25, 29].
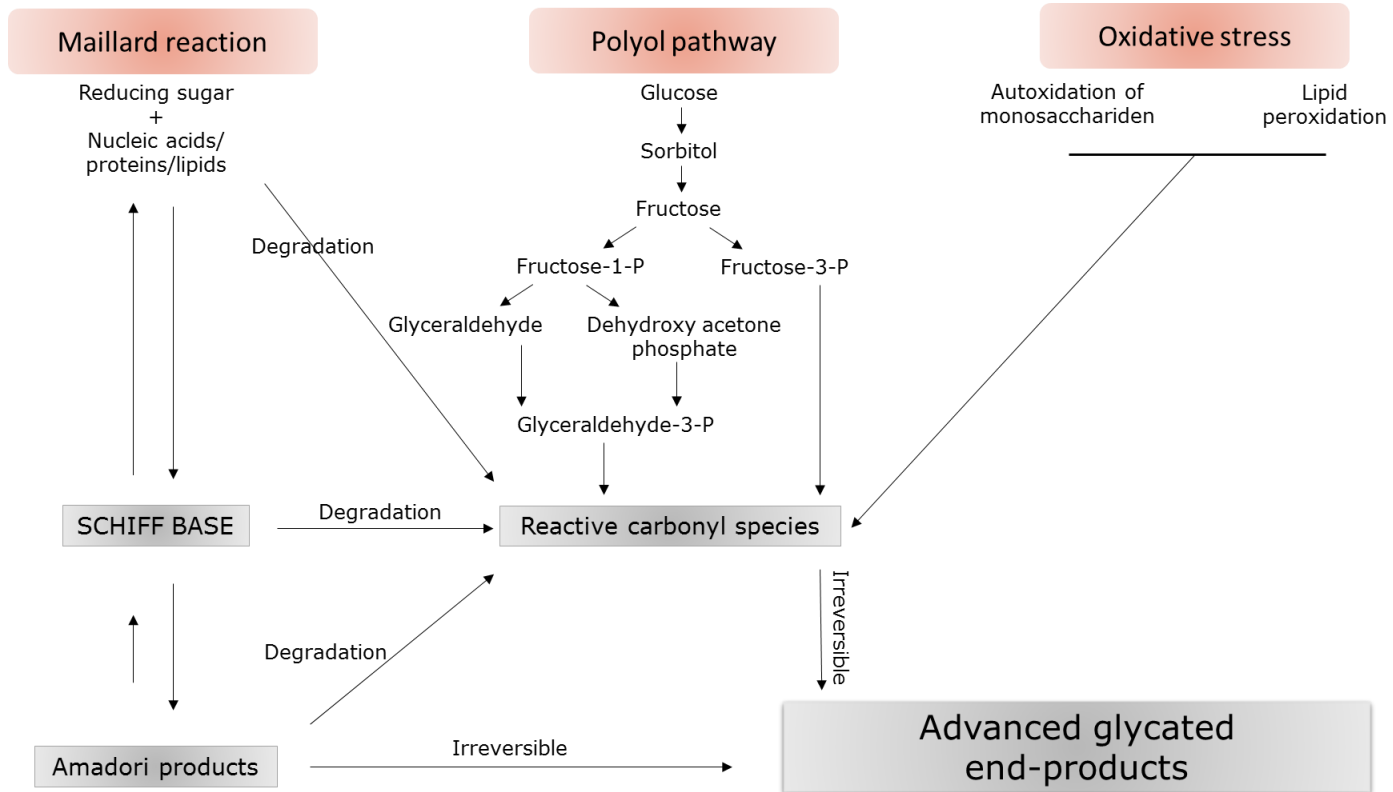
Figure 2.1 Formation of AGEs via Maillard, polyol and oxidative stress pathways. The *in vivo* formation of AGEs occurs via three different pathways: the non-enzymatic Maillard reaction, the Polyol pathway and during increased oxidative stress.

Glucose is one of the most reactive sugars in biological systems. It had been thought that elevated levels of glucose play a primary role in the Maillard reaction. However, the degradation of glucose can generate powerful glycation reagents such as glycolaldehyde, glyceraldehydes, glyoxal and methylglyoxal [35-37]. The plasma levels of these RCS are much lower than those of glucose. However, they have been shown to induce protein glycation about 20,000-fold faster than glucose [38]. It is known that the formation of AGEs can result from the action of RCS independent of high glucose levels [35, 39, 40]. In healthy subjects, the levels of glycated products on plasma proteins is less than 3%. However, in pathological situations such as in diabetes, this level can increase up to three fold resulting in the development of a pathological phenotype [41-43]. Conversely, plasma levels of glyoxal, methylglyoxal and glycolaldehyde are increased in patients with diabetes [37, 42].

Glycolaldehyde, a short chain aldehyde, is *in vivo* present in our body [44-47]. It is practically impossible to determine the physiological concentration of free glycolaldehyde. Indeed, due to its reactive properties, glycolaldehyde interacts very fast with amino residues of proteins [24, 34]. Several studies estimated its concentration to be between 0.1 and 1 mM [48-50]. Glycolaldehyde can be formed *in vivo* as a by-product of protein glycation or from L-serine by myeloperoxidase-hydrogen peroxidase-chloride system of phagocytic leukocytes [39, 44, 51]. Glycolaldehyde can also be generated by metal- or peroxynitrite-catalyzed oxidation of ascorbic acid, oxidative degradation of polyunsaturated fatty acids or metal-catalyzed oxidation of serine [52, 53]. However, there is evidence showing that glycolaldehyde also plays a role in pathological situations [54, 55]. In addition, the reaction between glycolaldehyde and amino acids can lead to the formation of AGEs such as CML and glycolaldehyde-pyridine [37, 56]. The deleterious effects of glycolaldehyde-derived AGEs have also been proved in *in vitro* studies. Koike *et al.* demonstrated that glycolaldehyde-derived AGEs induces apoptosis of vascular smooth muscle cells [57]. Morita *et el.* reported that these AGEs play a pivotal role in endothelial dysfunction in diabetes [58]. Additionally, several reports showed increased levels of this AGEs subtype in diabetic patients, therefore indicating a role for modification of proteins with aldehydes in this setting [56, 59, 60].

2.3 (Patho)physiological effects of AGEs on the heart

As already mentioned, the accumulation of AGEs in the body is a natural process that occurs with ageing, when the turnover rate of proteins is reduced [61]. It is known that AGEs contribute to the development and progression of cardiovascular dysfunction by 2 major mechanisms: cross-linking tissue proteins (*e.g.* extracellular matrix proteins and/or intracellular proteins) and binding to their cell surface receptor for advanced glycation end products (RAGE) (Figure 2.2) [7, 30].
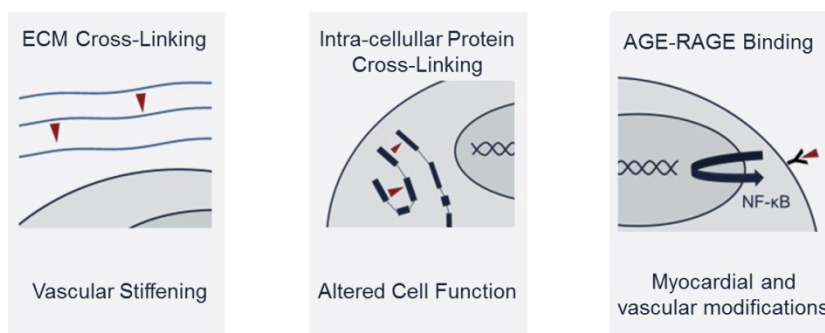
Figure 2.2 The deleterious effects of AGEs. AGEs have deleterious effects via 2 major mechanisms: cross-linking of extracellular and intracellular proteins and/or binding to their cell surface receptor for advanced glycation end products (RAGE).

2.3.1 Cross-linking proteins

Cross-linking of extracellular matrix proteins (*e.g.* collagen, vibronectin and laminin) with AGEs is an important physiological process for tissue integrity and stability, without compromising flexibility [7]. However, through AGEs-AGEs intermolecular covalent bonds or cross-linking that are highly resistant to hydrolytic turnover, AGEs alter the physiological properties of proteins in the extracellular matrix [27]. Cross-linking of myocardial and/or vascular collagen affects tissue mechanical properties and leads to decreased vascular elasticity, myocardial flexibility and promote vascular and myocardial stiffness [30, 62-64], resulting in diastolic dysfunction. Studies report that inhibitors of AGEs formation (*e.g.* with pyridoxamine) or breakers of AGEs cross-links (*e.g.* 4,5-dimethyl-3-phenacylthiazolium chloride, ALT-711) can limit AGEs-induced myocardial structural changes [65, 66].

Glycation and cross-linking of intracellular proteins lead to impaired cell function by linking intracellular proteins involved in the excitation-contraction coupling (ECC) [67]. The ECC is the process from electrical excitation to contraction of the cardiomyocyte (Figure 2.3) [68]. In brief, the electrical stimulation of the cardiomyocyte gives rise to an action potential, a transient depolarization of the membrane potential, able to trigger a transient increase in cytosolic Ca^{2+} (*i.e.* the Ca^{2+} transient) via L-type Ca^{2+} channels (LCCs). In addition, Ca^{2+} influx through the Na^+/Ca^{2+} exchanger (NCX) merely occurs at low local intracellular $[Ca^{2+}]$, high local intracellular $[Na^+]$ and when E_m is more positive than $E_{Na/Ca\ exchanger}$ (± -32 mV). The LCCs are the main pathways for Ca^{2+} entry in ventricular myocytes that will, ultimately, switch on the contractile machinery and initiate cell contraction. The structure of the cardiac dyad is important for ECC to occur. In this organization, LCCs are located within the sarcolemma of the transverse tubules (T-tubules) in close proximity to the sarcoplasmic reticulum (SR) Ca^{2+} release channels, *i.e.* ryanodine receptor (RyR). In ventricular myocytes, Ca^{2+} release from the SR via the RyR is the major source of the intracellular Ca^{2+} concentration rise during the ECC. This release is triggered by a local increase in intracellular Ca^{2+} concentration near the Ca^{2+} release channels in the SR, the RyR [69], through a process called Ca^{2+}-induced Ca^{2+} release (CICR). CICR is considered the main mechanism involved in the ECC in ventricular myocytes. Elevation in free $[Ca^{2+}]_i$ causes Ca^{2+} binding to the myofilament protein troponin C, resulting in activation of the myofilaments and ultimately to myocyte contraction during systole. During diastole, a decline in free $[Ca^{2+}]_i$ is needed for relaxation to occur. Relaxation occurs mainly through the SR Ca^{2+} ATPase (SERCA), the sarcolemmal NCX, the sarcolemmal Ca^{2+} ATPase, and the mitochondrial Ca^{2+} uniporter, the two latter pathways being less important for Ca^{2+} removal during a single beat. The function of SERCA is inhibited by the regulatory transmembrane protein of the SR, phospholamban (PLB). Dephosphorylated PLB bind to SERCA, which inhibits SERCA activity by reducing its affinity for Ca^{2+}.
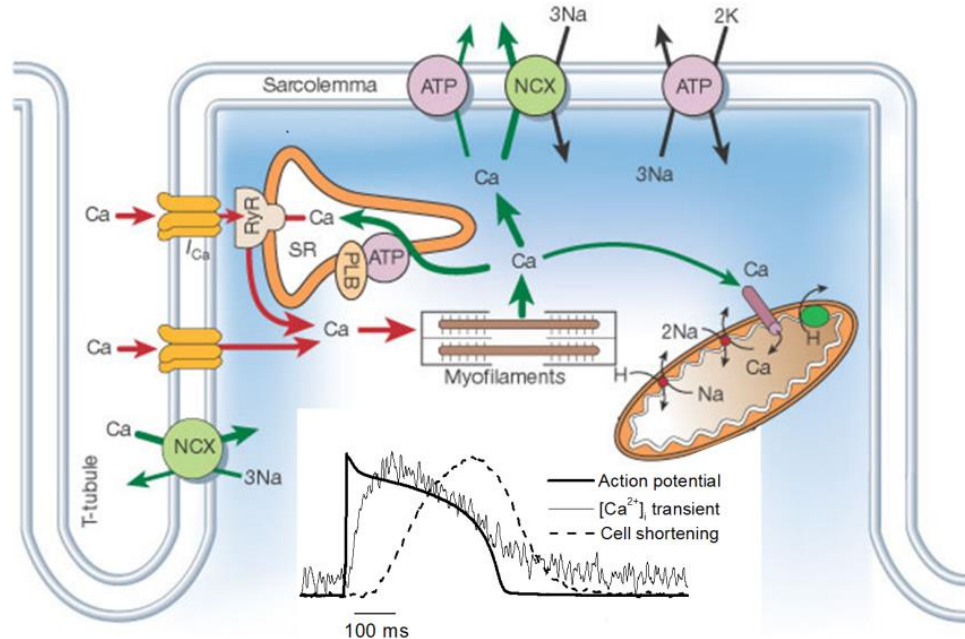
Figure 2.3 Excitation-contraction coupling in cardiomyocytes. The upstroke of the action potential (AP) stimulates an inward Ca^{2+} current (I_{Ca}) in the ventricular myocytes. Calcium enters the myocytes mainly via the L-type Ca^{2+} channels (LCCs), although some Ca^{2+} influx may be provided by the Na^+/Ca^{2+} exchanger (NCX) in reverse mode. This Ca^{2+} activates the ryanodine receptors (RyRs), leading to Ca^{2+} release from the sarcoplasmic reticulum (SR) and activation of the myofilaments. During relaxation, the free intracellular Ca^{2+} is removed by the SR Ca^{2+} ATPase (SERCA), NCX in forward mode, the sarcolemmal Ca^{2+} ATPase and the mitochondrial Ca^{2+} uniporter. SERCA function is modulated by phospholamban (PLB). Modified from Bers DM 2002.

PLB can reversibly become phosphorylated by cyclic adenosine monophosphate (cAMP)-dependent protein kinase A (PKA) or Ca^{2+}-calmodulin-dependent protein kinase II (CaMKII), resulting in the relief of the SERCA inhibition at high $[Ca^{2+}]_i$ [70-72]. Overall, potential alterations of Ca^{2+} homeostasis in cardiac myocytes result in significant alterations in contraction and relaxation of the whole heart [73].

AGEs are able to cross-link the domains of the RyR and SERCA pump leading to alterations in Ca^{2+} homeostasis [74, 75]. It has been reported in diabetic cardiomyopathy that AGEs cause RyR dysfunction, seen as a decrease in its ability to bind the specific ligand ryanodine and alterations in its sensitivity to Ca^{2+}, resulting in a decreased cardiac contractility [74]. Impairment of SERCA by AGEs alters Ca^{2+} removal and therefore directly alters relaxation leading to diastolic dysfunction [76, 77]. In addition, because SERCA alterations will impair SR Ca^{2+} content, subsequent cardiomyocyte contraction will also be altered in time. Kranstuber *et al.* have shown that Ca^{2+} handling in cardiomyocytes isolated from diabetic rats treated with ALT-711, a cross-link breaker, can be partially restored. These data suggest that AGEs are a cause for ECC alterations at the cellular level leading to an impaired relaxation at the organ level [78].

2.3.2 Binding to receptors and differential effects

AGEs are able to bind to a diversity of receptors, the most studied AGEs receptor being RAGE. RAGE belongs to the immunoglobulin superfamily of cell surface molecules characterized as low-affinity, pattern-recognition receptors [16]. RAGE has the ability to bind a wide range of ligands including the S100/calgranulins family of pro-inflammatory molecules, high-mobility group box-1 protein (HMGB-1), β-sheet fibrils, amyloid-β peptide (Aβ) and the $β_2$-integrin Mac-1 [79]. RAGE is present on many cell types including macrophages, lymphocytes, fibroblasts, endothelial cells and cardiomyocytes [64, 80, 81]. Generally, in physiological conditions, expression of RAGE is rather low in cardiac tissue and is thought to have a protective role by generating non-specific inflammatory responses. However, in myocardial infarction or ischemia-reperfusion, RAGE

expression is up-regulated, indicating a potential deleterious role of AGEs, RAGE and AGEs/RAGE interaction under these pathological situations [22, 82, 83].

There are different isoforms for RAGE. The full length RAGE receptor has an extracellular region containing one V-type immunoglobulin ligand binding domain (variable) and two C-type immunoglobulin domains [84] [85]. RAGE has a single hydrophobic transmembrane α-helix domain and a highly charged short cytosolic tail (43 amino acids), which is essential in transducing the signal from the cell surface to downstream pathways [32, 79]. Besides the full length RAGE, four other RAGE isoforms, including dominant-negative RAGE (DN-RAGE), N-terminally truncated RAGE, cleaved RAGE (cRAGE) and endogenously secreted RAGE (esRAGE) could exist on the membrane of different celltypes or in the circulation (Figure 2.4). DN-RAGE lacks the intracellular signaling domain and binds AGEs without inducing signal transduction. As a consequence this isoform can help in the scavenging of AGEs. N-terminally truncated lacks the V-type domain and is unable of binding ligands.
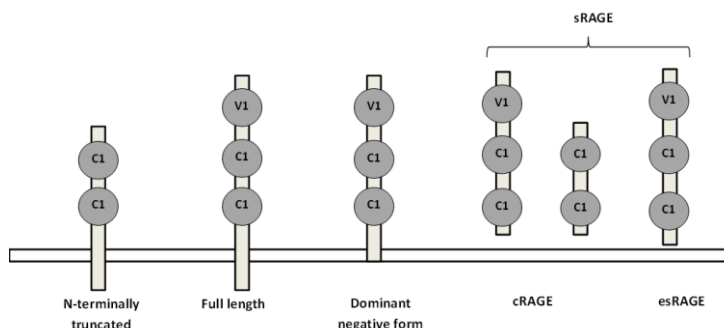
Figure 2.4 The different isoforms of RAGE. Five different isoforms can be distinguished namely N-terminally truncated, full length, dominant negative form, cRAGE and esRAGE.

Other receptors for AGEs, namely soluble RAGE (sRAGE), advanced glycation end product receptor 1 (AGE-R1, oligosaccharyl transferase-48), advanced glycation end product receptor 2 (AGE-R2, 80K-H phosphoprotein) and advanced glycation end product receptor 3 (AGE-R3, galactin-3) will also not elicit an intracellular signal after binding to AGEs. AGE-R1 has been studied the most. Data suggest that they could contribute to the clearance and possible

detoxification of AGEs [86, 87]. AGE-R1 accelerates the uptake and removal of AGEs and blocks cellular AGEs-RAGE mediated generation of ROS and proinflammatory cytokines [88, 89]. AGE-R1 will be also discussed in 'Detoxification of AGEs'.

AGEs/RAGE signaling pathway

Activation of the AGEs/RAGE signaling pathway has been studied in animals and/or human models of heart failure [90, 91]. Nielsen *et al.* reported that RAGE activation plays an important role in the development of cardiac dysfunction in type 2 diabetes [92]. In a rat model of diabetic cardiomyopathy, they showed that RAGE inhibition was able to prevent reduced systolic function and cardiac stiffness. Increased circulating AGEs and upregulation of RAGE at the cellular level were confirmed in cardiomyocytes isolated from diabetic rats. However, involvement of the AGEs/RAGE axis is not limited to the diabetic situation. Non-diabetic mice subjected to ischemia-reperfusion had an increased cardiac RAGE expression [82]. Cardioprotective effects of RAGE were also demonstrated by Bucciarelli *et al.* in isolated perfused hearts subjected to ischemia/reperfusion [93]. In addition, Aleshin *et al.* showed a reduced infarct size and improved cardiac performances was demonstrated in a mouse model of myocardial infarction with genetic deletion of RAGE, further emphasizing the overexpression and deleterious role of RAGE in ischemic injury [94].

At the cellular level, human RAGE overexpression was shown to alter Ca^{2+} homeostasis, characterized by reduced intracellular Ca^{2+} levels and a delayed Ca^{2+} uptake in cardiomyocytes [95]. Further emphazising the role of AGEs/RAGE axis, Ma *et al.* reported a decreased cell shortening of cardiomyocytes exposed to AGEs for 2 h [96]. The AGEs-induced changes in the contractile properties of these cardiomyocytes were ablated by an anti-RAGE antibody. Finally, Yan *et al.* reported that AGEs/RAGE interaction impaired intracellular Ca^{2+} handling by promoting SR Ca^{2+} leak, which is an important mechanism for AGEs/RAGE-induced cardiac dysfunction [97]. Altogether, these data demonstrate a link between AGEs/RAGE interaction and cardiac ECC at the cellular level, further

suggesting a potential direct role of AGEs and AGEs/RAGE interaction in cardiac dysfunction.

Binding of AGEs to the full length RAGE activates a range of signaling pathways (Figure 2.5). AGEs-RAGE interaction activates mitogen-activated protein kinases (MAPKs), members of the Ras family, phosphatidylinositol-3 kinase (PI3-K), guanosine triphosphatases (GTPases) and cell division control protein 42 (Cdc42) [8, 25, 27, 30]. This will upregulate the expression of nuclear factor kappa B (NF-κB), which in turn leads to enhanced transcription of genes such as endothelin-1, vascular cell adhesion molecule-1 (VCAM-1) tissue factor, E-selectin, vascular endothelial growth factor (VEGF) and increases ROS generation [98]. Furthermore, NF-κB is responsible for activation of inflammatory cytokines, tumor necrosis factor α (TNF-α) and interleukin 6 (IL-6) and triggers the transcription of lysyl oxidase (LOX) gene [99, 100]. LOX is an extracellular, matrix-embedded protein that causes cross-linking of collagen fibrils, resulting in the deposition of insoluble collagen. Additionally, NF-κB activation stimulates RAGE expression, thereby creating a positive feedback loop. AGEs/RAGE interaction also activates members of the janus kinase – signal transducers and activators of transcription (JAK-STAT) signaling family. AGEs/RAGE interaction can also activate nicotinamide adenine dinucleotide phosphate (NADPH) oxidase, the main reactive oxygen species (ROS) source in cardiomyocytes. It has been shown that ROS play an important role in the development of cardiac dysfunction by impairing the structure and function of proteins, lipids and nucleic acids, altering ECC at the cellular level [30]. The increase in NADPH oxidase by AGEs/RAGE interaction is also known to stimulate NF-κB. In conclusion, emerging data suggest AGEs to be an important mechanism contributing to ROS production and increased oxidative stress in the heart [98, 101].
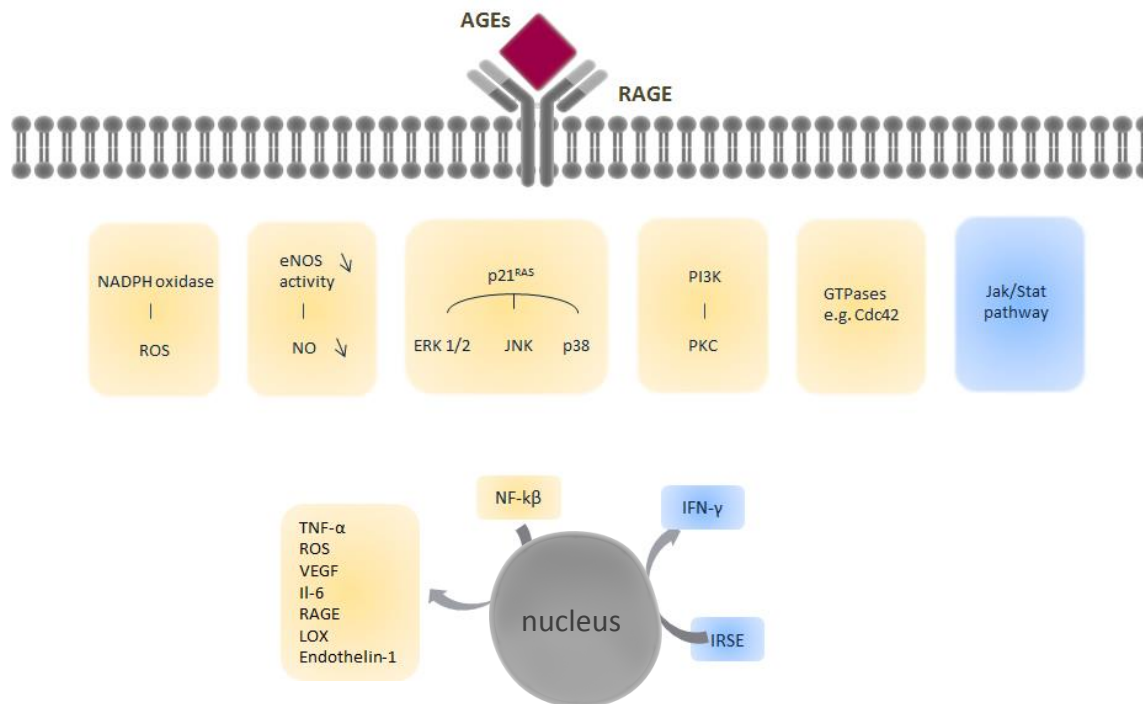
Figure 2.5 The AGEs/RAGE signaling. AGEs/RAGE interaction stimulates multiple signaling pathways, such as Jak/Stat, NADPH oxidase, mitogen activated protein kinase (MAPK) including p38, extracellular regulated (ERK)-1/2 and c-Jun N-ternminal kinase (JNK). AGEs-induced signaling pathway leads to the activation of transcription factors such as nuclear factor (NF-κB) or IFN-stimulated response elements (ISRE), which will stimulate the production of cytokines or growth factors.

At the cellular level, Zhang *et al.* demonstrated a decreased cell shortening in adult rat cardiomyocytes as well as a prolongation of the contraction and relaxation in response to AGEs exposure for 12 h [102]. The observed AGEs-induced changes were contributed to increased oxidative stress.

Furthermore, binding of AGEs to RAGE can inhibit the nitric oxide (NO) activity. In addition, AGEs are also able to decrease the levels of NO by reducing the endothelial NO synthase (eNOS) activity. By reducing the bioavailibity of NO, AGEs promote cardiac stiffness [103]. Finally, AGEs/RAGE interaction increases vascular permeability, causing impaired cardiac wall kinetics and contributing to cardiac dysfunction [104, 105]. At the cellular level, Hegab *et al.* demonstrated alteration of intracellular calcium homeostasis in neonatal cardiomyocytes due to AGEs stimulation [106]. Their data support the activation of AGEs/RAGE axis that may stimulate NADPH oxidase and hence the production of ROS. Increased ROS levels may alter the observed Ca^{2+} handling by S-nitrosylation of important proteins involved in the ECC such as RyR [106].

Detoxification of AGEs

Soluble RAGE (sRAGE) is the secretory circulating isoform of RAGE with cRAGE and esRAGE as members (Figure 2.4). cRAGE is produced by proteolytic cleavage at the cell surface mediated by a disintegrin and metalloproteinase domain-containing protein 10 (ADAM 10). esRAGE, also named as the C-terminally truncated form, is formed of removal of the transmembrane region via alternative splicing. Several studies reported a protective effect for sRAGE and/or esRAGE in various disorders by contributing to AGEs clearance [22, 107-110]. However, its potential protective role remains controversial as sRAGE is also associated with impaired outcome of HF patients [111-113]. In that context, Prasad *et al.* reported that not only AGEs or sRAGE levels but examing the combination or the ratio of both is essential to elucidate the exact potential benefical role of sRAGE [107, 114].

AGEs can bind to a variety of receptors, including AGE-R1, AGE-R2, AGE-R3 and some members of the scavenger receptor family such as scavenger receptor class A (SR-A) and cluster of differentiation 36 (CD36) [25]. AGE-R1 is a single transmembrane integral protein, which is not capable to transduce cellular

signals upon binding of AGEs. AGE-R1 was proven to be protective in diabetic complications as it promotes AGEs removal and inhibits ROS production [16]. Indeed, several studies have reported decreased levels of AGE-R1 in patients with diabetes mellitus and chronic renal failure [86, 115-117]. In addition, it has been shown that AGE-R1 is an efficient scavenger for AGEs in hepatic sinusoidal cells and macrophages. In that context, AGE-R1 could have an important role in detoxification and clearance of AGEs, most likely via endocytosis in pathological situations [118-120].

2.4 Several ways to classify the different AGEs subtypes

Due to the several AGEs-precursors, AGEs are a heterogeneous group of molecules of which not all structures are known yet. To date, there are seven immunochemically different classes of AGEs identified in sera of type 2 diabetic patients [26, 36] which are glucose-derived AGEs, fructose-derived AGEs, glyceraldehyde-derived AGEs, glycolaldehyde-derived AGEs, glyoxal-derived AGEs, methylglyoxal-derived AGEs and 3-deoxyglucosone-derived AGEs [26].

2.4.1 Classification of AGEs based on their fluorescent properties: cross-linking vs non-cross-linking AGEs

Based on their chemical structure, AGEs can be classified in three types: fluorescent cross-linking AGEs characterized by aromatic chemical structures (*e.g.* glyoxal lysine dimer, pentosidine and crossline), non-fluorescent cross-linking AGEs (*e.g.* imidazolium dilysine and glucosepane) and non-cross-linking AGEs (*e.g.* CML and pyrraline) [29]. Due to aromatic chemical structures, some AGEs molecules, such as pentosidine, have autofluorescence properties. Pentosidine and CML are the best characterized AGEs molecules [10]. Furthermore, CML is the most abundant AGEs structure *in vivo* and is therefore often used in studies as a surrogate for the 'representative' AGEs molecule [121, 122]. However, it has been demonstrated that our western diet contains more than only CML [18, 123]. In addition, as shown in several studies, CML is not always associated with the severity of the disease [124, 125]. Therefore, although important, as CML may represent only a part of all AGEs molecules in our body, it should not be used as the only surrogate for total AGEs.

(A) Fluorescent Cross-linking AGEs:

Pentosidine

Crossline

(B) Non-Fluorescent Cross-linking AGEs:

Glucosepane

MOLD (Methylglyoxal lysine dimer)

(C) Non-Cross-linking AGEs:

CML (Carboxymethyl-lysine)

Pyrraline
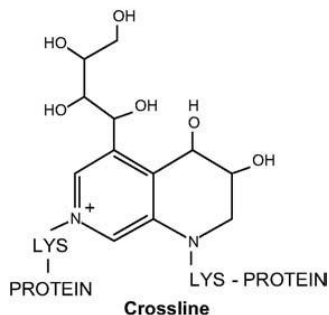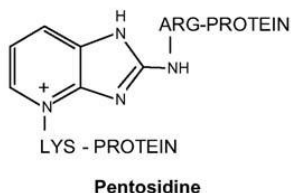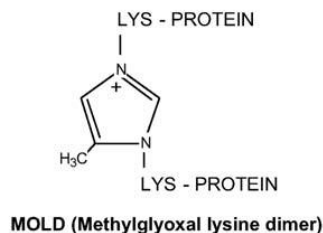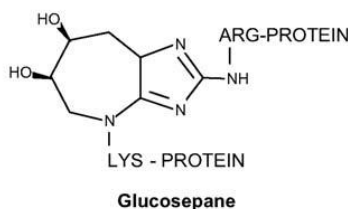
Figure 2.6 Chemical structures of three types of AGEs. (A) Fluorescent cross-linking AGEs such as pentosidine and crossline, (B) non-fluorescent cross-linking AGEs such as a glucospane and MOLD, (C) non-cross-linking AGEs such as CML and pyrraline. [25]

2.4.2 Classification of AGEs based on their molecular weight: LMW-AGEs vs HMW-AGEs

AGEs can also be categorized based on their molecular weight: low-molecular weight AGEs (LMW-AGEs) and high molecular weight AGEs (HMW-AGEs). There is no clear boundary between LMW-AGEs and HMW-AGEs. Gerdemann *et al.* defined LMW-AGEs as proteins with a molecular mass lower than 12 kDa [126], while HMW-AGEs display a molecular mass higher than 12 kDa [126]. To date, HMW-AGEs are considered to be protein-bound molecules while LMW-AGEs are free proteins or peptide-bound proteins [127, 128]. At the moment, very little is

known on the chemical structure and effects of HMW-AGEs. Indeed, most studies focus on the effects of the LMW-AGEs as their chemical structure is known and a broad diversity of enzyme-linked immunosorbent assays (ELISAs) are commercially available to detect and measure LMW-AGEs in plasma. At the moment, the quantification of AGEs in general relies mostly on CML, CEL and pentosidine, members of LMW-AGEs. Because these molecules are more stable, quantification of LMW-AGEs from blood or urine samples is easier compared to other AGEs molecules, including HMW-AGEs [17, 18].

However, in our western diet, AGEs formed during heat treatment can range from LMW-AGEs to protein-bound and aggregated with a HMW, *i.e.* HMW-AGEs [129]. Therefore, distinguishing LMW-AGEs from HMW-AGEs may be essential in understanding the role of AGEs in the pathogenesis of cardiac stiffness and cardiovascular diseases in general as the prevalence is increasing tremendously.

2.5 LMW-AGEs *vs* HMW-AGEs: absorption, distribution and detoxification

In normal circumstances, cellular proteins undergo proteosomal degradation which is highly efficient and mostly complete, leading to the release of bioavailable amino acids [128, 130]. However, because AGEs-modification masks the target for proteosomal digestion, AGEs are characterized by resistance to proteolytic degradation. It has been demonstrated that incomplete degradation of the proteins results in the formation of LMW-AGEs [128]. LMW-AGEs, such as CML, can be absorbed via simple diffusion, while peptide-bound AGEs use peptide transporters to cross the epithelium [131, 132]. The absorption of AGEs is thought to be around 10% in both human and rodent circulation from which about two-thirds are retained in tissues [133, 134]. Once absorbed, it has been thought that LMW-AGEs are readily distributed throughout the body, about 60% of the AGEs being bound to the liver and kidneys after 72 h. In addition, it has been shown that AGEs accumulation can also be observed in lungs, heart and spleen [133]. However, this study focused only on the distribution of CML and CEL specifically and not on total AGEs, comprising HMW-AGEs. In that context, one could expect that, due to their high molecular weight, distribution of HMW-AGEs throughout the body is slower. However, this remains speculative and further investigation is required. Concerning detoxification, Thomas *et al.* reported that renal clearance is the most important mechanism for removal of LMW-AGEs in

the body [135]. It was thought that in contrast to LMW-AGEs, HMW-AGEs may not be very extensively absorbed due to insufficient degradation by gastrointestinal enzymes and their bioavailability [136]. As a consequence, HMW-AGEs have been shown to have a slow and inefficient absorption rate [137]. Furthermore it has been reported that only 2% HMW-AGEs were recovered in urine after consuming food with HMW-pentosidine [138]. However, recently, Poulsen *et al.* showed that the amount of CML recovered in urine was independent of the molecular weight, indicating that both HMW-AGEs and LMW-AGEs (*i.e.* CML) are absorbed and excreted to a comparable extent [129]. Further fate of HMW-AGEs may in addition depend on factors such as their exact structure, host diet, gut environment *etc.* that remain unknown at the moment.

Regarding AGEs metabolism, it is thought that AGEs are not substrates for enzyme systems involved in detoxification by phase 1 and 2 enzymes [25]. It has been shown that endogenous AGEs are metabolized by innate defense and/or intracellular degradation after receptor-dependent uptake such as AGE-R1, AGE-R2 and AGE-R3. Binding of AGEs to these receptors stimulates receptor endocytosis. This mechanism may contribute to the detoxification and clearance of LMW-AGEs [119, 120]. However, it is unknown whether these receptors contribute to the detoxification of HMW-AGEs specifically.

2.6 LMW-AGEs *vs* HMW-AGEs: cardiovascular effects

Deuther-Conrad *et al.* demonstrated a higher toxic potential of LMW-AGEs compared to the HMW-AGEs, characterized as a higher degree of cellular damage, likely related to their capacity to bind to AGEs receptors [128, 139]. As described in several reports, LMW-AGEs are at the moment considered to be the best marker of disease status. Many studies have indeed shown that CML levels correlate to a certain extent with the severity of the phenotype in diabetic as well as in non-diabetic chronic HF patients [140, 141]. It is commonly admitted that CML, and LMW-AGEs in general, contribute to abnormal Ca^{2+} handling, contractile protein alterations and altered energy metabolism in cardiac muscle [142]. However, CML is a non cross-linking AGEs compound. It is therefore unlikely that CML could *per se* induce cardiac stiffness, suggesting the involvement of other members of the AGEs family in the development of cardiac dysfunction [143]. Additionally, Berg *et al.* concluded that serum levels of total AGEs, but not

serum levels of CML specifically, correlated with cardiac relaxation. This study suggests that other members of the AGEs family, causing cross-linking, could correlate with the observed cardiac stiffness [144]. In that context, Miura *et al.* reported that not only serum levels of CML but rather non-CML AGEs correlate with the severity of the diabetic phenotype [145]. In contrast to the CML-AGEs, they have shown that non-CML AGEs contribute to diabetic complications such as systemic vascular complications, microalbuminuria, clinical nephropathy and hemodialysis [145].

Furthermore, others have demonstrated that as opposed to CML-AGEs, only non-CML AGEs levels were significantly associated with clinical parameters of glycemic control such as HbA1c and fasting blood glucose [143]. Sharp *et al*. found no significant correlation between vascular disease in type 1 diabetic patients and LMW-AGEs serum levels [146]. This was confirmed in a study of Thomas *et al.*, where no link between macrovascular disease and LMW-AGEs was observed [135]. Finally, in patients with congestive heart failure, no changes were observed in plasma CML concentrations [124]. These data indicate that despite being an important parameter, CML solely is not a reliable marker in heart failure. In that context, total AGEs content, including HMW-AGEs levels could be of great importance as new markers in heart failure [124]. It even appears that complex AGEs, which have a higher molecular weight, provide the highest pathogenic potential in type 2 diabetes compared to LMW-AGEs [147]. Indeed, plasma levels of HMW-AGEs were shown to be significantly increased in diabetic patients compared to controls [127]. This was also seen in a study from Kilhovd *et al.*, where levels of AGEs with a wide range of molecular weights, but not CML, were increased in serum levels of patients with coronary heart disease and type 2 diabetes [125].

The deleterious effects of HMW-AGEs are mainly attributed to cross-linking, because protein-bound AGEs are considered to have a high affinity for proteins leading to tissue retention [136, 148]. In addition, cross-links of AGEs are resistant to proteolytic degradation, which delays their turnover [149, 150]. Finally, Poulsen *et al.* demonstrated no changes in RAGE gene expression after 2 weeks HMW-AGEs diet, indicating that the mechanism of action of HMW-AGEs unlike LMW-AGEs, is independent of the activation of the RAGE receptor [129].

2.7 Anti-AGEs therapies

As already mentioned, the adverse effects of increased AGEs levels have been reported in cardiovascular diseases. Therefore targeting AGEs is an important strategy as a therapy. The intervention against AGEs can be classified into different strategies: AGEs formation inhibitors, AGEs cross-link breakers, AGEs receptor blockers, AGEs receptor signaling blockers and AGEs scavengers. Besides these specific therapies against AGEs, there are also some therapies which are more general and not-specific targeting AGEs such as adequate glycaemic control, antioxidant activity and changing lifestyle.

2.7.1 AGEs formation inhibitors

Due to deleterious effects associated with increased AGEs levels, identifying agents/molecules able to prevent AGEs formation is mandatory.

The first AGEs formation inhibitor, aminoguanidine, was discovered by Brownlee *et al.* who demonstrated a reduced diabetes-mediated arterial wall protein cross-linking in rats treated by aminoguanidine [151]. Aminoguanidine is a highly reactive scavenger of reactive carbonyl intermediates (early active glycation products) in the Maillard reaction due to its nucleophilic nature [24, 30, 152]. The beneficial effects of aminoguanidine have been widely demonstrated in the 1990s in experimental models of diabetes. In diabetic nephropathy, treatment with aminoguanidine (1 g/l in drinking water) for 32 weeks reduced albuminuria and caused a reduction of kidney basement membrane thickness [153]. In diabetic retinopathy, treatment with aminoguanidine for 26 weeks (25 mg/kg/day) prevented accumulation of AGEs at branching sites of precapillary arterioles and abnormal endothelial cell proliferation [154]. Finally in diabetic neuropathy, aminoguanidine administration for 8 weeks (25 mg/kg/day) normalized reduction in sciatic nerve blood flow and improved conduction [155]. Additionally, it improved motor nerve conduction velocity and inhibited accumulation of fluorescent AGEs in nerves [156, 157]. To evaluate the safety and efficacy of aminoguanidine, two clinical trials were designed, namely ACTION I with type 1 diabetic patients and ACTION II with type 2 diabetic patients [158, 159]. In both studies, patients were randomized to placebo or to either a low (150 mg ACTION I, 50-300 mg ACTION II) or high (300 mg ACTION I, 100-600 mg ACTION II)

dose of aminoguanidine. Treatment of aminoguanidine improved the secondary end-point measures including proteinuria, kidney function and retinopathy. However, due to adverse effects such as increased levels of liver enzymes and the production of auto-antibodies, ACTION II was not further processed. In conclusion, despite the beneficial effects of aminoguanidine in animal models, translation into the clinic remains limited as it did not achieve successful clinical trials.

Alternative to aminoguanidine, vitamin B derivatives such as pyridoxamine (PM), thiamine and benfotioamine have been used as inhibitors for AGEs formation. In particular PM, a vitamin B6 derivative showed promising properties. Unlike aminoguanidine, PM strongly inhibits CML formation [160]. PM interferes with post-amadori oxidative reactions via the chelation of dicationic metal ions rather than via direct interaction with Amadori products [161]. PM is now considered to have multiple mechanisms of action: scavenging ROS, blocking oxidation of the Amadori intermediate, trapping of reactive carbonyl and dicarbonyl compounds derived from the Amadori compounds and chelation of metal ion catalysts [24].

Like aminoguanidine, the beneficial effects of PM have been demonstrated in animal models of diabetes, where studies demonstrated efficacy in the prevention of renal disease [162-164], vascular pathology [162], hyperlipidaemia [162, 163] and AGEs formation [162, 163, 165].

Degenhard *et al.* demonstrated that treatment of streptozotocin (STZ)-diabetic rats with PM for 7 months (1 g/l in drinking water), caused a reduced albuminuria and plasma creatinine and was able to decrease the levels of CML and CEL in the skin. In the study of Alderson *et al.*, treatment of Zucker obese rats with PM (2 g/l in drinking water) decreased hypertension, vascular wall thickness, CML en CEL levels in the skin, triglycerides, cholesterol and finally normalized albuminuria [162]. In 2014, NephroGenex Inc. announced the start of phase III PIONEER program to test the efficacy of pyridoxamine dihydrochloride (PYRIDORIN). However, recently this clinical trial was stopped due to financial issues. The purpose of this study was to randomize type 2 diabetes patients. Patients received a placebo or 300 mg of twice daily PYRIDORIN. The goal was to investigate the efficacy of PYRIDORIN in time to a 50% increase in serum creatinine. Preliminary results show a doubling of serum creatinine.

Besides the synthetic AGEs inhibitors, plant-derived products like flavonoids and vitamins have been used as AGEs inhibitors. Flavonoids have shown anti-glycation effects through their antioxidant properties [166].

Vitamin E treatment (800 mg/day) in diabetic patients reduced AGEs accumulation in arterial walls of diabetic patients [167]. Ceriello *et al.* showed that vitamin E supplementation (600 mg/day) attenuates serum glycated-albumin levels in patients with diabetes [168]. In addition, in STZ-diabetic rats, vitamin E supplementation for 4 weeks (18 mg/day) suppressed the formation of AGEs [169].

2.7.2 AGEs cross-link breakers

Cross-link breaker, ALT-711 contains a thiazolium structure that is able to break α-carbonyl compounds non-enzymatically by cleaving the carbon-carbon bound between carbonyls [30, 109]. In animal models for diabetes, long term treatment of ALT-711 has been shown to be beneficial in a number of chronic disease states such as atherosclerosis [170, 171], cardiovascular disease [78, 172-175], hypertension [175] and renal injury [176-179]. However, the mechanism of ALT-711 as a cross-link breaker is still controversial. Yang *et al.* demonstrated that the beneficial effects of ALT-711 are in fact not the result of breaking AGEs cross-links [180]. This was confirmed by Mentink *et al.* [174]. As ALT-711 is capable of inhibiting copper-catalyzed oxidation of ascorbate, it has been suggested that ALT-711 instead might act *in vivo* by preventing metal-catalyzed glycoxidation [29, 181]. As a result, ALT-711 has been widely investigated in clinical trials from 2002 to 2010 [182]. In the study of Kass *et al.* 93 patients with hypertension were randomized to oral dose of ALT-711 or placebo. In this study, a daily dose of 210 mg ALT-711 for 56 days improved total arterial compliance in aged humans with vascular stiffening [183]. In the Distensibility Improvement and Remodeling in Diastolic Heart Failure (DIAMOND) trial, 23 patients with diastolic heart failure were enrolled in a 16-week, open-label trial of 420 mg ALT-711 per day. Four months treatment of ALT-711 resulted in a decrease in left ventricular mass and improved diastolic filling [66]. However, despite the beneficial effects in earlier trials, the BENEFICAL trial could not confirm this data. In this clinical trial, 102 patients with systolic heart failure were randomized to either ALT-711 (200 mg) or placebo twice daily for 36 weeks. There were no improvements observed in exercise capacity nor in systolic function of those patients [184]. Finally, two

randomized, double-blind, placebo-controlled studies were performed. In these studies, a combination of exercise with 200 mg of ALT-711 daily was used for 1 year in aging populations [185, 186]. However, these studies could also not confirm the beneficial effects observed in previous trials and in diabetic animal models. To date, no further clinical trials have continued with ALT-711. To summarize, targeting AGEs-induced cross-links remains a challenge.

2.7.3 AGEs receptor signaling blockers

Binding of AGEs to their receptor RAGE activates pro-inflammatory signaling pathways. As RAGE is a pattern-recognition receptor, it can be activated by multiple ligands other than AGEs. Therefore, activation of this receptor is of great biological significance. Inhibition of AGEs/RAGE interaction can be performed with anti-RAGE antibodies. In type 1 and type 2 animal models of diabetes, administration of anti-RAGE antibodies ameliorates the kidney function [187, 188]. Ma *et al.* reported that the observed altered cardiomyocyte function was counterbalanced by anti-RAGE antibodies.

Curcumin is a plant-derived product and capable of blocking the AGEs-RAGE signaling pathway by inhibition of AGEs-induced increase in NF-κB and activator protein-1 activity in human endothelial cells [189]. Treatment with curcumin in rats with diabetic cardiomyopathy (DCM) attenuated myocardial dysfunction, cardiac fibrosis, AGEs accumulation, oxidative stress, inflammation and apoptosis [190]. These results suggest that curcumin may have great therapeutic potential in the treatment of DCM and maybe other cardiovascular diseases. Recently, a systematic review described the effects of curcumin on generation of advanced glycation end products. They reported that except one, all included studies indicated that curcumin is able to prevent AGEs formation and AGEs-induced disturbances with different potential mechanisms [191].

2.7.4 Adequate glycaemic control

An adequate glycaemic control can prevent AGEs accumulation in patients with diabetes mellitus. Controlling blood glucose levels are indirectly inhibiting AGEs-formation, as the concentration of glucose is an important factor for the endogenous formation of AGEs.

2.7.5 Antioxidant activity

As the final step of the Maillard reaction is catalyzed by oxidative stress and metal ions, antioxidant activity is an important factor in anti-AGEs therapy. Scavenging of free radicals, such as hydroxyl and superoxide, decreases the formation of reactive carbonyl species and therefore limits AGEs formation. Additionally, chelators, inhibiting metal-catalyzed oxidation reactions, important to promote AGEs formation, are also important players in the antioxidant approach [24].

2.8.6 Changing lifestyle

Changing our lifestyle is an easy non-invasive anti-AGEs therapy. Our western diet as well as smoking contain high levels of AGEs. Additionally, these dietary AGEs can also bind to RAGE to activate the AGEs-RAGE signaling pathway [18]. Lowering AGEs intake by smoking cessation and low-AGEs diets have been demonstrated to reduce AGEs intake and thereby lowering AGEs levels in the blood [192, 193]. The essential concept in low AGEs diet is a manner of cooking. Stewing or steam-cooking meat will generate much less AGEs than broiling or frying. Finally, exercise has been shown to induce beneficial metabolic changes [194]. Several studies have been reported that exercise training is more helpful than drugs in the secondary prevention of cerebral vascular disease and is as efficient as pharmaceutical therapy in preventing the development of diabetes [195, 196] . Goon *et al.* demonstrated that a tai chi program 2 times per week for 12 months in overweight adult patients resulted in decreased serum AGEs levels [197]. However, these results could not be confirmed by Macias-Cervantes *et al.* where exercise alone did not reduce serum levels of AGEs [198]. However, the combination of low AGEs diet with exercise 3-5 days/week for 20-60 minutes showed promising results. The healthier lipid profile (low levels of triglycerides and higher HDL cholesterol levels) was observed in these patients compared to other treatments combined with decreased levels of circulating AGEs.

3

Cross-linking *versus* RAGE: how do high molecular weight advanced glycation products induce cardiac dysfunction?

3.1 Abstract

Background. Several clinical and experimental studies have demonstrated that advanced glycation end products (AGEs) are associated with adverse cardiac outcome. Growing evidence shows that high molecular weight AGEs (HMW-AGEs) might be as important as the characterized low molecular weight AGEs (LMW-AGEs). To date, the role of HMW-AGEs in the pathogenesis of cardiac remodeling remains unknown. In this study, we investigated whether HMW-AGEs are involved in cardiac dysfunction.

Methods. Healthy rats were daily intraperitoneal (*ip*) injected with 20 mg/kg BSA-derived HMW-AGEs or, as a control, unmodified BSA, during 6 weeks. Cardiac function was assessed with echocardiography. Plasma levels of glucose, AGEs and soluble RAGE (sRAGE) were measured. AGEs, RAGE and lysyl oxidase (LOX) expression were determined by Western blot.

Results. After 6 weeks, animals displayed a sustained increase in circulating total AGEs without hyperglycaemia. HMW-AGEs injections induced cardiac dysfunction characterized by wall hypertrophy, increased heart sphericity, reduced strain and strain rate with preserved ejection fraction. Plasma sRAGE levels were significantly higher compared to control and correlated significantly with decreased strain. RAGE expression, TNF-α and IL-6 remained unchanged. Finally, HMW-AGEs induced prominent cardiac fibrosis associated with an increased LOX expression.

Conclusion. Our data demonstrate that rather than via a specific activation of RAGE, the deleterious effects of HMW-AGEs are likely mediated via an increased collagen cross-linking responsible for the observed cardiac dysfunction.

3.2 Introduction

Heart failure (HF) is a leading cause of mortality and morbidity worldwide and is defined as the inability of the heart to meet the energy demand of the body [3]. The development of HF is a complex process related to a series of physiological and molecular factors characterized by structural and functional disorders that still remain incompletely understood [199].

Advanced glycation end products (AGEs) are proteins and lipids that become glycated and oxidized after persistent contact of reducing sugars (*e.g.* glucose) or short-chain aldehydes (*e.g.* glycolaldehyde) with amino groups and/or a high degree of oxidative stress [9, 10]. The accumulation of AGEs in the body is a natural process that occurs with aging, when the turnover rate of protein is reduced due to glycoxidation [61]. There is growing evidence that AGEs contribute to the development and progression of cardiovascular dysfunction by 2 major mechanisms: cross-linking of intra and/or extracellular proteins or binding to their cell surface receptor for AGEs (RAGE) [7, 30]. AGEs can alter the physiological properties of proteins in the extracellular matrix (*e.g.* collagen), resulting in protein cross-link formation leading to decreased vascular elasticity, myocardial flexibility and promoting vascular and myocardial stiffness. Glycation and cross-linking of intracellular proteins potentially lead to impaired cell function. Additionally, binding of AGEs to their cellular receptor leads to activation of a cascade of cell signaling pathways upregulating RAGE expression, resulting in enhanced cellular oxidative stress, hyper-responsiveness to inflammatory cytokines (*e.g.* Tumor necrosis factor α (TNF-α) and Interleukin-6 (Il-6)) in macrophages and endothelial cells [7, 30]. Alternative splicing or cleavage by matrix metalloproteinases of the full length RAGE receptor can lead to soluble RAGE (sRAGE), which is thought to have a protective effect by scavenging circulating AGEs [30].

Several clinical and experimental studies support the view that AGEs have a significant role in many pathological situations, particularly in cardiac disorders [30, 33, 200]. Increased circulating AGEs levels and tissue accumulation have been reported to occur at early age in patients with diabetes and are associated with adverse outcome [201]. Because the process of AGEs formation and accumulation also occurs in euglycaemia, pathogenesis of AGEs has been shown to be not

restricted to diabetes but to be involved in a larger range of cardiovascular diseases such as myocardial infarction and ischemia-reperfusion [22, 82].

Even if the chemical nature of AGEs *in vivo* remains largely unknown, several classes of AGEs have been however identified and characterized. *In vivo* detectable AGEs are categorized in three groups: fluorescent cross-linking AGEs (*e.g.* glyoxal lysine dimer, pentosidine), non-fluorescent cross-linking AGEs (*e.g.* imidazolium dilysine) and non-cross-linking AGEs (*e.g.* carboxymethyllysine (CML) and pyrraline). These low molecular weight AGEs (LMW-AGEs) were found to be elevated in diabetes [29, 30]. Although high levels of CML and pentosidine have been shown to correlate to the severity of the disease phenotype observed in diabetes, there is growing evidence suggesting that high molecular weight AGEs (HMW-AGEs) might be even more important in pathological settings than the known LMW-AGEs [61, 125, 145, 201, 202]. However, in the clinical setting, defining the effect of HMW-AGEs *per se* on cardiac morphology and function in non-pathological conditions is not easy due to many confounding factors (*e.g.* coexisting cardiovascular diseases and medication). Therefore, whether HMW-AGEs are a potential cause for cardiac dysfunction remains to be elucidated. As such, small animal models have been extensively used during the past decades for the better understanding of the pathophysiological mechanisms leading to myocardial dysfunction. In addition, more recent technological advances in non-invasive imaging (*e.g.* ultrasound echocardiography) have greatly facilitated the assessment of cardiac morphology and function in rodents. Several studies have recently applied speckle tracking imaging (STI) on different small animal models of left ventricular (LV) dysfunction demonstrating that STI-derived strain/strain rate measurements accurately reflect pathology and the time course of HF development in these animals [203-205].

The purpose of this study was to investigate whether HMW-AGEs *per se* are a cause for cardiac dysfunction in rats. Therefore, rats were daily injected with HMW-AGEs for 6 weeks and the effect on heart function was assessed. Conventional and STI echocardiography associated with molecular tools were used to identify the nature of this impairment.

3.3 Materials and methods

This investigation conforms to the EU Directive 2010/63/EU for animal experiments and was approved by a local ethical committee (Ethische Commissie Dierproeven, UHasselt, Diepenbeek, Belgium).

3.3.1 Preparation and characterization of AGEs

HMW-AGEs were prepared based on the method described by Valencia *et al* [206]. Briefly, fatty acid-free and low endotoxin bovine serum albumin (BSA; 7 mg/ml) was incubated with 90 mM glycolaldehyde dimers (Sigma-Aldrich, Diegem, Belgium) in phosphate buffered saline (PBS) (pH 7.4) for 5 days at 37°C (BSA-derived AGEs). A control sample was prepared in parallel by incubation of BSA (7 mg/ml) in PBS. Unreacted glycolaldehyde was removed by dialysis against PBS using a cut-off value of 3.5 kDa and filter sterilized (0.2 µm sterile filter, Sarstedt, Essen, Belgium). Finally, the samples were concentrated using Amicon Ultra Centrifugal Filter Units with Ultracel-50 membrane (Millipore, Brussel, Belgium). A commercially available AGEs sample (Millipore, Brussel, Belgium), prepared in a similar way was used as a positive control. To validate the prepared AGEs, protein patterns of control (BSA alone), HMW-AGEs (BSA-derived AGEs) and the commercially available AGEs (positive control) were examined via sodium dodecyl sulfate polyacrylamide gel electrophoresis (SDS-PAGE) followed by a Coomassie blue staining. In addition, fluorescence intensity of the samples (related to fluorescent AGEs), measured at a protein concentration of 1 mg/ml, was detected at excitation/emission wavelengths of respectively 370/460 nm using a fluorescence reader (Bio-Rad Laboratories, Temse, Belgium) [207, 208].

3.3.2 Experimental protocol

Thirteen Sprague-Dawley rats (150-180 g) (Charles River Laboratories, L'Arbresle, France) were subjected to daily intraperitoneal (*ip*) injection of 20 mg/kg BSA-derived AGEs (HMW-AGEs, N=9) or an equal amount of unmodified BSA (Control, N=4) for 6 weeks. All animals were maintained in a controlled environmental condition of temperature and humidity, were fed a standard pellet diet and had water available *ad libitum*. Blood samples after 6 weeks of injections were obtained in both groups. Hereafter, the animals were sacrificed

with an overdose of pentobarbital and hearts were excised for further histological examination. The perfused hearts were fixed overnight in 4% paraformaldehyde and transferred in 70% ethanol until embedded in paraffin. Subsequently, 5 µm thick sections were cut and stored at room temperature until staining. Residual tissue of the left ventricle was crushed to a fine powder, immediately frozen in liquid nitrogen and stored at -80°C.

3.3.3 Conventional echocardiographic measurements

Transthoracic echocardiography was performed under 2% isoflurane in all animals at baseline and at 6 weeks post-injection with a Vivid*i* ultrasound machine (GE Vingmed Ultrasound) using a 10 MHz linear array transducer. A standard parasternal long axis image and short-axis views at mid-ventricular level were acquired at a temporal resolution of ≈ 200 frames per second. Conventional echocardiographic parameters (*e.g*. LV end-diastolic diameter (LVEDD), LV end-systolic diameter (LVESD), posterior wall thicknesses (PWT) and anterior wall thicknesses (AWT)) were obtained from the B-mode images at midpapillary level in the parasternal short-axis view. End-systolic volumes (ESV) and end-diastolic volumes [209] were calculated by $\pi*D_M^2*B/6$, where D_M indicates the systolic/diastolic diameter of the ventricle in mid-ventricular short-axis view and B is LV length on parasternal long-axis image. Subsequently, ejection fraction (EF) was measured as (EDV–ESV)/EDV, and expressed in %. The end-diastolic sphericity index (SI) was calculated by dividing the EDV by the volume of a sphere whose diameter was equal to the major end-diastolic LV long axis. The LV long axis was obtained from the 2D dataset as the longest distance between the center of the mitral annulus and the endocardial apex.

3.3.4 Strain and strain rate by speckle tracking imaging

STI data analysis was performed on an EchoPAC workstation (GE Vingmed Ultrasound, version 7.0.1, Horten, Norway), as described previously [204]. Briefly, measurements of circumferential strain (S_{circ}) and circumferential strain rate (SR_{circ}) at midventricular level were performed on selected best-quality two-dimensional images. The endocardium was manually traced in an optimal frame, from which a speckle tracking region of interest was automatically selected. The region of interest width was adjusted as needed to fit the wall thickness from

endocardium to epicardium. The software detected and tracked the speckle pattern subsistent to the standard two-dimensional echocardiography after segmenting the ventricular silhouette into 6 segments. The tracking quality was then visually inspected, and, if satisfactorily for at least five segments, the tracing was accepted. As registration of the electrocardiogram was not always feasible in these animals, end systole and end diastole were therefore defined as the minimum and maximum LV short-axis area, respectively.

3.3.5 Fibrosis measurement

Sections of 5 μm thick were obtained at cardiac midventricular level and stained using the Masson trichrome staining method. Myocardial fibrosis was assessed in all animals and quantified in 8 randomly chosen fields per section, as previously described [210]. The area of collagen deposition indicated by blue staining was outlined and quantified by an automated image analysis program (Carl Zeiss, AxioVision 4.6, Zaventem, Belgium). Blood vessels were excluded. The ratio of the area of collagen deposition to the global area was calculated and expressed as percent collagen deposit.

3.3.6 Assessment of glucose, sRAGE, CML and AGEs levels

Plasma levels of total AGEs (MyBiosource, San Diego, CA, USA) and sRAGE (Aviscera bioscience, Santa Clara, CA, USA) were determined using enzyme-linked immunosorbent assay (ELISA). Serum levels of CML were measured using ELISA (MyBiosource, San Diego, CA, USA). Glucose concentration after 6 weeks of injections was measured using Analox GM7 (Analis SA, Suarlée, Belgium).

3.3.7 Western blot

Protein concentrations of the LV tissues were determined by the BCA protein assay kit (Thermo Fisher, Erembodegem, Belgium). Samples containing equal amount of proteins were separated on a 12% SDS-PAGE gel with a mini protean 3 electrophoresis system (Bio-rad Laboratories, Temse, Belgium), transferred to a polyvinylidene fluoride (PVDF) membrane and subsequently, blocked for 2 hours with 5% BSA in Tris-buffered solution containing 0.1% Tween-20 (TBS-T) followed by incubation overnight at 4°C in the presence of a specific RAGE primary antibody (1/1000, goat polyclonal IgG, Santa cruz, sc-8230, Heidelberg

Germany), AGEs antibody (1/500, mouse monoclonal IgG, Sopachem, 6D12, Eke, Belgium) or lysyl oxidase (LOX) antibody (1/1000, rabbit polyclonal IgG, Abcam, ab31238, Cambridge, United Kingdom). Horseradish peroxidase-conjugated secondary antibodies (DAKO, Belgium) at a dilution of 1/2000 were used. Both primary and secondary antibodies were diluted in 2% BSA-TBS-T. RAGE, AGEs and LOX were visualized with the enhanced chemiluminescence [209] technique using the Pierce ECL Plus Western blotting Substrate (Thermo Fisher, Erembodegem, Belgium).

3.3.8 Real-time PCR

Total ribonucleic acid (RNA) was extracted from LV tissue using RNeasy fibrous tissue kit (Qiagen, Antwerpen, Belgium) following the manufacturer's guidelines. The concentration and purity of RNA was assessed with the NanoDrop 2000 spectrophotometer (Isogen life science, Temse, Belgium). cDNA was synthesized using high capacity cDNA reverse transcription kit (Invitrogen, Merelbeke, Belgium). The expression of TNF-α (forward primer: GTC-TGT-GCC-TCA-GCC-TCT-TC, reverse primer: CCC-ATT-TGG-GAA-CTT-CTC-CT), RAGE (forward rimer: ATG-GAA-ACT-GAA-CAC-AGG-AAG-GA, reverse primer: TCC-GAT-AGC-TGG-AAG-GAG-GA) and IL-6 (forward primer: TAG-TCC-TTC-CTA-CCC-CAA-CTT-CC, reverse primer: TTG-GTC-CTT-AGC-CAC-TCC-TTC) were studied. Real-time PCR was carried out in an optical 96-well plate using the StepOnePlus (Applied Biosystems, Belgium). SYBR Green (Invitrogen, Merelbeke, Belgium) chemistry-based qPCR was performed [211]. Gene expression data were analyzed with MIQE guidelines taken into account [212]. The most stable reference genes, TATA Box Binding Protein (Tbp, forward primer: TGG-GAT-TGT-ACC-ACA-GCT-CCA, reverse primer: CTC-ATG-ATG-ACT-GCA-GCA-AAC-C) and tyrosine 3-monooxygenase/tryptophan 5-monooxygenase activation protein zeta (YWAHZ, forward primer: GAT-GAA-GCC-ATT-GCT-GAA-CTT-G, reverse primer: GTC-TCC-TTG-GGT-ATC-CGA-TGT-C) for this experimental set-up were determined by geNorm analysis and normalization of the data was performed using qBase software (Biogazelle, Zwijnaarde, Belgium).

3.3.9 Statistical analysis

Values are expressed as median [75th percentile; 25th percentile]. Comparisons were performed using Mann-Whitney U test or Wilcoxon matched pairs test for paired data. Simple linear regression models were applied to assess the relationship between different parameters. A value of $p<0.05$ was considered statistically significant and analyses were performed using GraphPad Prism (GraphPad Software, San Diego, CA, USA).

3.4 Results

3.4.1 HMW-AGEs injections in healthy rats lead to LV dysfunction

The protein patterns of control (BSA alone), BSA-derived AGEs (*i.e.* HMW-AGEs)) and a commercially available AGEs sample (positive control) were characterized on a SDS-PAGE gel, stained with Coomassie blue (Figure 3.1A). HMW-AGEs (lane 3) and the commercially available positive control (lane 4) were characterized by the smear of high molecular weight proteins. It is worth noticing that in lane 3 (HMW-AGEs), no band was observed at 66 kDa indicating that most BSA of our sample underwent modifications related to the glycation. Fluorescence intensities of HMW-AGEs as prepared in-house or purchased from an external source were comparable and were significantly higher than in unmodified BSA, further confirming the presence of fluorescent glycated products in our HMW-AGEs sample (Figure 3.1B).
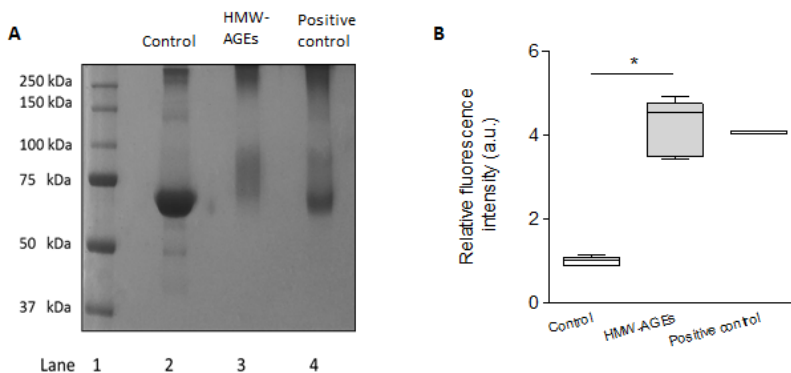
Figure 3.1 Characterization of HMW-AGEs. (A) SDS-PAGE stained with Coomassie blue. Lane 1, molecular mass marker; lane 2, BSA (7 mg/ml) incubated for 5 days at 37°C (Control); lane 3, BSA (7 mg/ml) incubated with glycolaldehyde (90 mM) for 5 days at 37°C (HMW-AGEs), lane 4: positive control. (B) Median, 75th percentile, 25th percentile, minimum and maximum relative fluorescence intensity of the samples, determined at an excitation and emission wavelength of 370 and 460 nm respectively. * denotes $p < 0.05$.

HMW-AGEs were subsequently injected in healthy rats. Despite daily injection of glycated products for 6 weeks, circulating glucose levels remained comparable and within the normal physiological range in HMW-AGEs injected animals as compared to the control group (Figure 3.2A). As expected, circulating total AGEs levels were significantly higher after 6 weeks in the HMW-AGEs group (Figure

3.2B). but this increase was not related to an increase in CML, a major member of the LMW-AGEs family (Figure 3.2C). Cardiac function at baseline and 6 weeks post-injections was evaluated in control and HMW-AGEs injected animals. Conventional echocardiographic characteristics of both groups are summarized in Table 3.1.
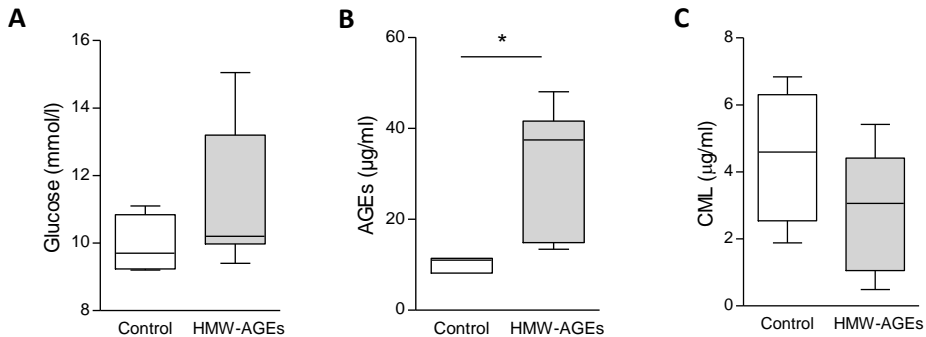
Figure 3.2 Effect of 6 weeks HMW-AGEs injection on circulating glucose, total AGEs and CML levels. Plasma glucose (A), plasma AGEs (B) and serum carboxylmethyllysine (CML) (C) in HMW-AGEs injected animals compared to control animals after 6 weeks injections. Data are shown as median, 75th percentile, 25th percentile, minimum and maximum. * denotes p < 0.05.

After 6 weeks of injections, HMW-AGEs animals displayed a change in LV morphology with signs of hypertrophy (AWT and PWT increased by 40%) associated with increased LV diameters within the same range. LV volumes, EDV and ESV, were significantly higher in HMW-AGEs injected animals compared to baseline (respectively, 192[357;182] µl vs 158[166;129] µl and 56[127;40] µl vs 38[46;27] µl, p<0.05).

Table 3.1 Conventional echocardiographic characteristics.

	Control		HMW-AGEs	
Parameters	**Baseline**	**6 weeks**	**Baseline**	**6 weeks**
HR (bpm)	425[452;409]	403[420;394]	401[413;396]	398[406;373]
LVEDD (mm)	4.9[5.3;4.7]	5.4[6.1;4.8]	5.0[5.3;4.6]	5.9[7.5;5.8]†
LVESD (mm)	3.2[3.4;3.1]	3.6[4.0,3.1]	2.9[3.1;2.5]	3.5[4.9;3.1]†
AWT (mm)	1.38[1.41;1.34]	1.53[1.58;1.46]	1.26[1.29;1.25]	1.85[1.94;1.74]†*
PWT (mm)	1.55[1.59;1.53]	1.69[1.79;1.58]	1.52[1.63;1.47]	2.03[2.09;1.85]†*
EDV (µL)	153[170;136]	202[271;146]	158[166;129]	192[357;182]†
ESV (µL)	51[54;49]	69[88;53]	38[46;27]	56[127;40]†
SV (µL)	101[122;82]	133[184;93]	110[120;90]	153[211;135]†
CO (mL/min)	42[52;35]	55[73;41]	43[47;36]	57[85;56]†
SI	0.19[0.20;0.17]	0.18[0.20;0.16]	0.18[0.19;0.16]	0.30[0.34;0.26]†*
EF (%)	65[71;60]	67[68;66]	74[76;70]	70[77;66]

HR, heart rate; LVEDD, left ventricular end-diastolic diameter; LVESD, left ventricular end-systolic diameter; AWT, anterior wall thickness; PWT, posterior wall thickness; EDV, end diastolic volume; ESV, end systolic volume; SV, stroke volume; CO, cardiac output; SI, sphericity index; EF, left ventricular ejection fraction in HMW-AGEs injected and control animals. Data are presented as median [75th percentile, 25th percentile]. *denotes $p<0.05$ *vs* Control. † denotes $p<0.05$ *vs* corresponding baseline.

Furthermore, SI, as a measure of heart geometry, was significantly higher in the treated animals compared to baseline (0.30[0.34;0.26] *vs* 0.18[0.19;0.16], p<0.05). However, no changes were observed for EF for both groups over the course of the study.
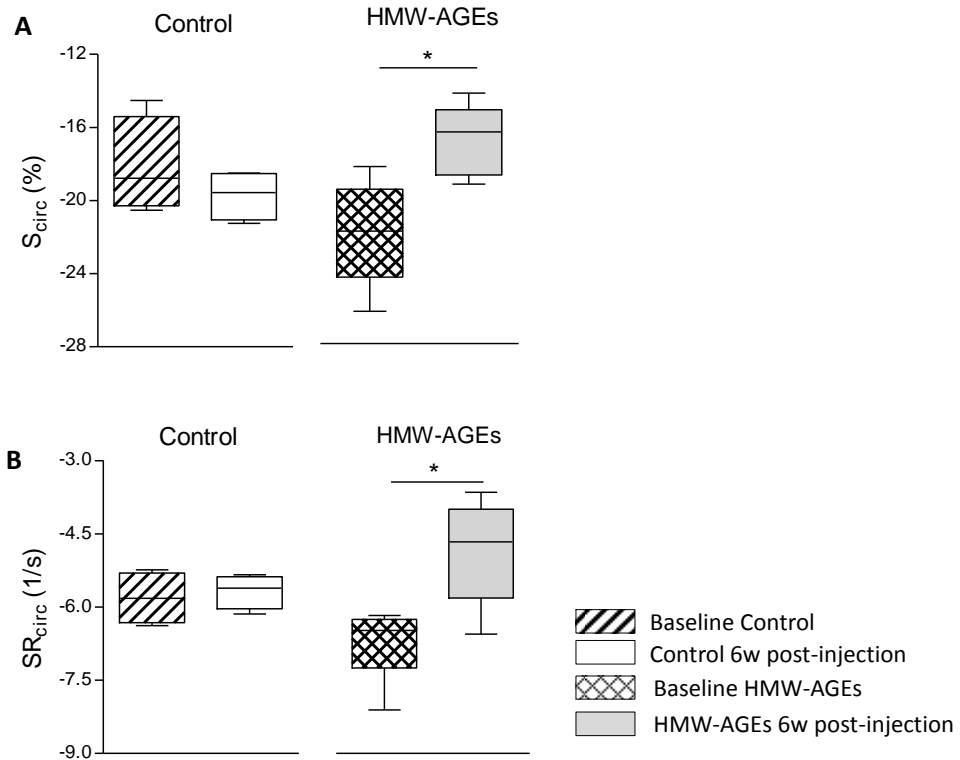
Figure 3.3 STI-derived deformation parameters at baseline and 6 weeks post-injection. Circumferential strain (S_{circ}) (A), circumferential strain rate (SR_{circ}) (B) measured at baseline and after 6 weeks of injections in the control group and HMW-AGEs injected animals. Data are shown as median, 75th percentile, 25th percentile, minimum and maximum. * denotes p < 0.05.

After 6 weeks injections, deformation parameters such as S_{circ} (Figure 3.3A) and SR_{circ} (Figure 3.3B) were significantly decreased in the AGEs group but not in control animals (respectively, -16[-15;-18]% *vs* -22[-20;-24]% and -4.6[-4;-5.5] 1/s *vs* -6.7[-6.3;-6.8] 1/s, p<0.05).

3.4.2 Cardiac dysfunction induced by HMW-AGEs is not mediated through RAGE activation

Figure 3.4A is an example of Western blot for RAGE and β-actin from LV samples. Full length RAGE protein level was not different in both groups (Figure 3.4B, left panel). This result was confirmed by the unchanged gene expression for RAGE, as shown in Figure 3.4B, right panel.
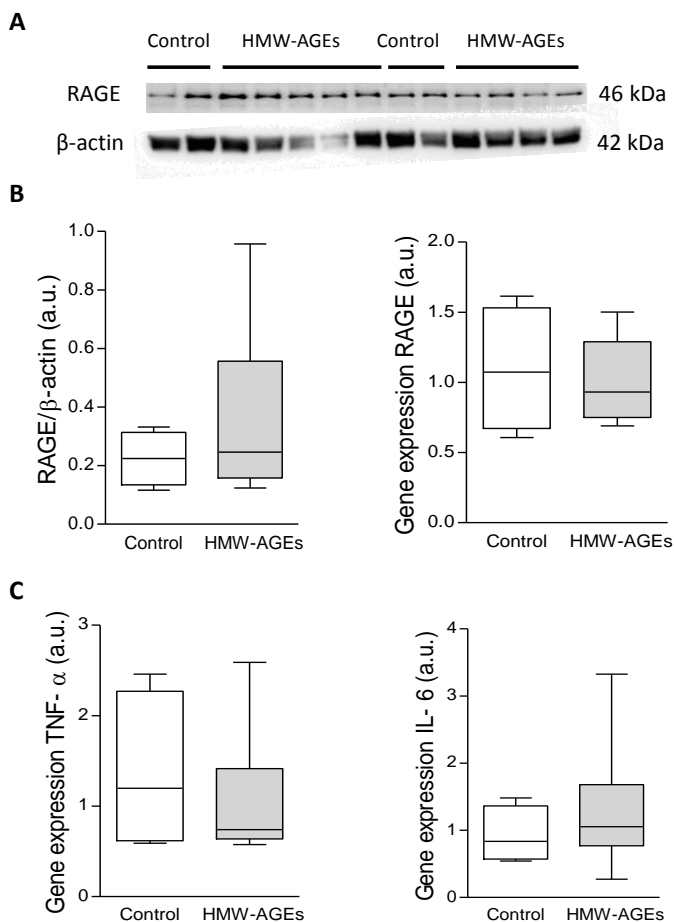
Figure 3.4 Expression of RAGE, TNF-α and IL-6. (A) Representative Western blot for RAGE and β-actin in the control animals and the HMW-AGEs injected animals. (B) Quantitative analysis of RAGE protein expression normalized to β-actin and RAGE mRNA expression. (C) Gene expression of TNF-α and IL-6 in HMW-AGEs injected and control animals. Data are shown as median, 75th percentile, 25th percentile, minimum and maximum in both groups.

Gene expression of the downstream effectors of RAGE were also evaluated. As shown in Figure 3.4C, gene expression of TNF-α and IL-6 were comparable in both groups, confirming the absence of activation of RAGE signaling pathway.
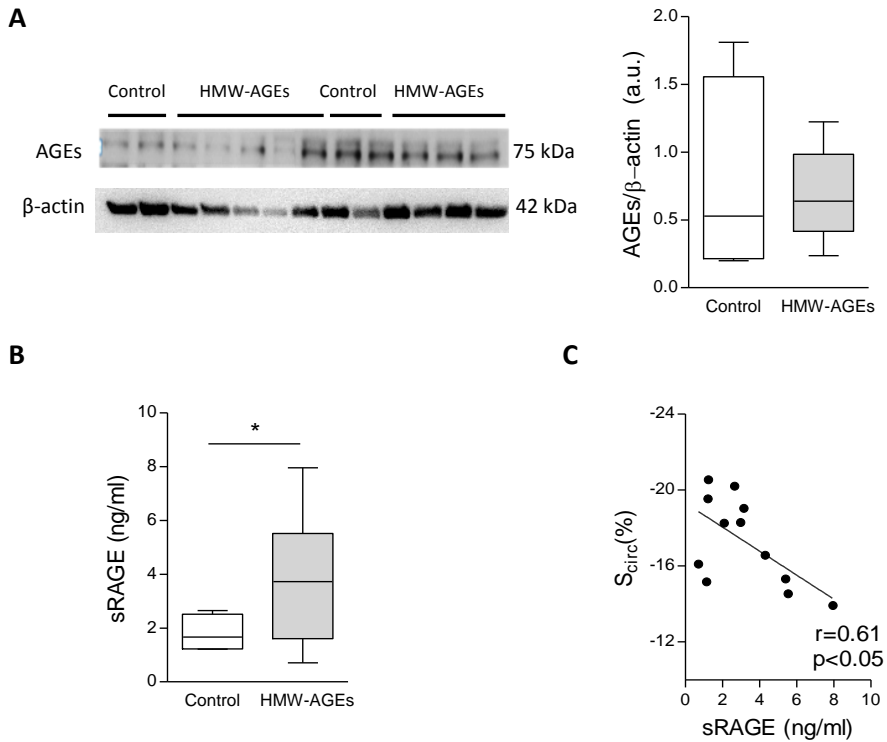
Figure 3.5 Expression of AGEs and increased plasma sRAGE levels which correlates with strain. (A) Representative Western blot for AGEs and β-actin in the control animals and the HMW-AGEs injected animals. Quantitative analysis of AGEs tissue expression normalized to β-actin. (B) Plasma levels of sRAGE in HMW-AGEs injected animals and in control animals. (C) Circumferential strain (S_{circ}) expressed as a function of sRAGE levels. Data are shown as median, 75th percentile, 25th percentile, minimum and maximum. * denotes p < 0.05.

As shown in Figure 3.5A, AGEs levels in LV tissue samples were comparable in both groups, indicating no specific accumulation of glycated products in cardiac tissue. Interestingly, plasma sRAGE levels, the circulating form of RAGE, were significantly higher in the HMW-AGEs injected animals compared to control (Figure 3.5B), and inversely correlated with S_{circ} (r=0.61, p<0.05, Figure 3.5C).

3.4.3 HMW-AGEs induce prominent fibrosis

Representative examples of the myocardial fibrosis in LV sections from both groups are shown in Figure 3.6A. After 6 weeks of injections, the HMW-AGEs group displayed a significantly larger myocardial collagen deposition compared to control animals (Figure 3.6B). This increase was accompanied with a higher LOX expression in the HMW-AGEs injected group (Figure 3.6C). In addition, the increase in collagen content correlated with changes in SI (r=0.78, p<0.05; Fig 3.6D left panel) and S_{circ} (r=0.72, p<0.05, Fig 3.6D right panel), as measures of ventricular morphology and function.
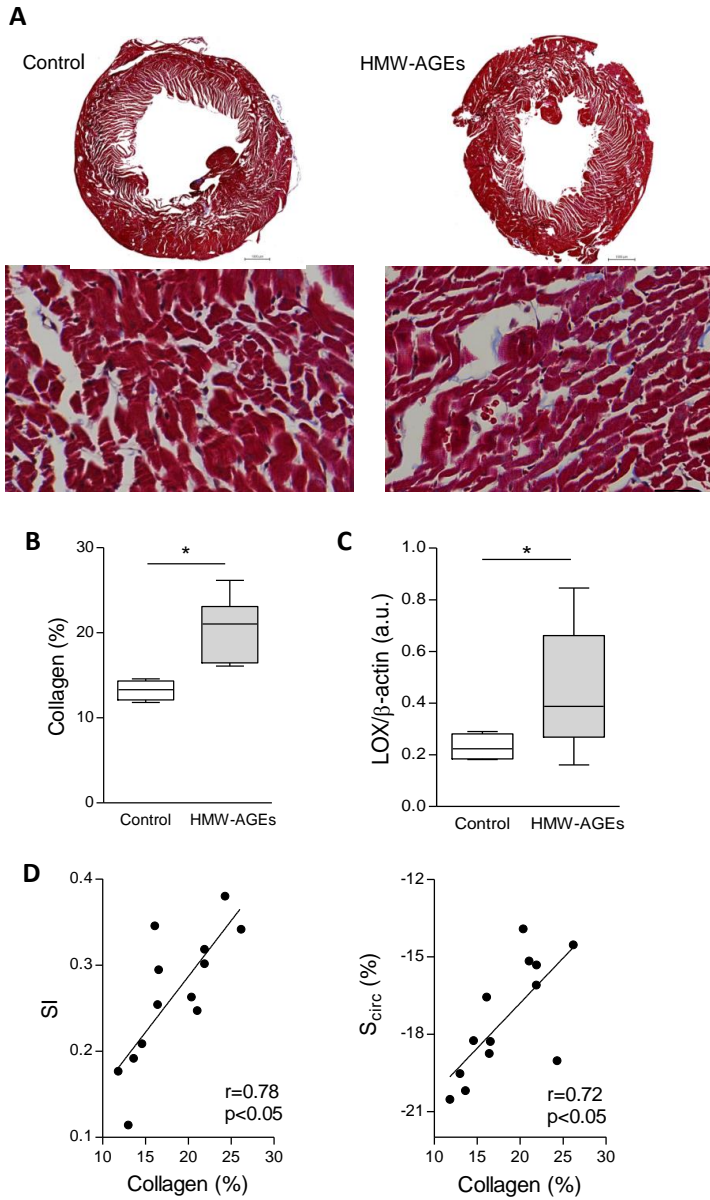
Figure 3.6 HMW-AGEs lead to myocardial fibrosis. (A) Typical Masson trichrome staining in transverse sections of LV taken at the level of the papillary levels. Arrows display typical interstitial myocardial fibrosis. (B) Quantification of total collagen from the sections in HMW-AGEs injected animals and control animals. (C) Quantitative Western blot of LOX expression normalized to β-actin. (D) Sphericity index (SI) and circumferential strain (S_{circ}) expressed as a function of total collagen in both groups. Data are shown as median, 75th percentile, 25th percentile, minimum and maximum. * denotes $p<0.05$.

3.5 Discussion

In this study, we show that HMW-AGEs have an important causative role in the pathophysiology of cardiac dysfunction, independent of other confounding factors such as diabetes or other cardiovascular pathologies. In addition, we show that the nature of the dysfunction is likely to be attributed to collagen cross-linking rather than activation of the receptor RAGE.

3.5.1 Increased circulating AGEs level is a cause for cardiac dysfunction

From studies conducted in diabetic patients or animal models, it remains unclear whether the increase in AGEs levels is a cause or a consequence of the dysfunction, independent or not to diabetes. Most studies examining AGEs have been conducted in patients or animal models with high circulating glucose [125, 213]. Despite daily injections of glycated products, signs of hyperglycaemia were not observed in our study. Recent studies confirm our results and demonstrate that increased AGEs levels are not necessarily correlated to diabetes [22, 214, 215]. Accordingly, the implication of AGEs and the binding to their receptor RAGE in non-diabetic HF patients as well as in animal models with increased oxidative stress, ischemia-reperfusion or myocardial infarction has been recently emphasized [22, 81, 214]. In this study, we demonstrate that elevated circulating AGEs levels are responsible for cardiac dysfunction, characterized by wall hypertrophy and increased SI. However, interestingly, no changes in EF were observed, while deformation parameters were significantly decreased. In that context, growing evidence shows that changes in conventional echocardiographic systolic parameters, such as EF, occur later in the disease process and may not be sensitive enough to unmask subtle changes in LV structure and global function. In addition, it has been previously demonstrated that strain and strain rate are more robust measures of contractility which are less influenced by changes in cardiac load and structure and accurately reflect (regional) myocardial contractility in rodents [216]. Our data indicate that the use of deformation parameters for early detection of subtle cardiac remodeling is a reliable tool to be used in animal models and in the clinical setting.

3.5.2 HMW-AGEs are as deleterious as the well characterized LMW-AGEs

Due to methodological issues, a limited number of AGEs have been examined and reported [217]. LMW-AGEs (*e.g.* CML and pentosidine) are the most frequently measured AGEs and as a consequence, are associated to the severity of various cardiovascular disease phenotypes [26, 217]. However, there is raising evidence that not only LMW-AGEs but also HMW-AGEs have important physiological effects [129]. Many studies have shown that CML levels indeed correlate with the severity of the phenotype in diabetic as well as in non-diabetic chronic HF patients [140, 141]. It is commonly admitted that CML, and LMW-AGEs in general, contribute to abnormal Ca^{2+} handling, contractile protein alterations and altered energy metabolism [142]. In our study, however, changes at the cardiomyocyte level and potential alterations of Ca^{2+} handling were not explored and further experiments need to be conducted for a better understanding of the cellular mechanisms involved (see chapter 3). Concerning the involvement of AGEs in cardiac stiffness, electron microscopy studies failed to demonstrate the association of CML with collagen fibrils remodeling [142]. Because CML is not a cross-linking structure, it is therefore unlikely to induce cardiac stiffness, suggesting the involvement of other members of the AGEs family in the development of cardiac dysfunction [143]. Therefore, distinguishing LMW-AGEs from HMW-AGEs may be essential in understanding the role of AGEs in the pathogenesis of cardiac stiffness and cardiovascular diseases in general. Takeushi *et al.* have demonstrated that both HMW-AGEs and LMW-AGEs coexist in sera of diabetic patients [143]. They report that in fact, total AGEs, but not CML, correlate with the severity of the diabetic phenotype or with the different stages of diabetic complications [145]. As a consequence, examining CML levels might not be the best marker to predict the worse outcome in diabetes, myocardial infarction or ischemia-reperfusion. In that context, our data suggest that HMW-AGEs might be of importance and should be taken into account in the clinical setting.

3.5.3 Mechanism of action of HMW-AGEs

From previous studies, the mechanism of action of AGEs and of LMW-AGEs in particular, is believed to be either through the activation of the receptor for AGEs (*i.e.* RAGE) or through an increased protein cross-linking. In our study, we demonstrate that HMW-AGEs do not alter RAGE expression neither at the

protein nor at the mRNA level. Because no change in expression does not necessarily mean an unchanged function, we also checked a potential activation of downstream effectors of RAGE. No activation of the downstream effectors of the RAGE pathway such as TNF-α and IL-6 was observed. From our data, there is no evidence for activation of the RAGE signaling pathway, indicating that the effect of HMW-AGEs is unlikely to be mediated through the activation of the receptor. Additionally, we show that myocardial fibrosis is significantly increased in the HMW-AGEs group and is associated with changes in global cardiac architecture and function. These changes are comparable to what is observed in diabetes where the increase in circulating AGEs is associated with diastolic dysfunction, also via increased myocardial fibrosis and stiffness [78]. In addition, we observe a significant increase in protein levels of LOX. LOX is a protein involved in the cross-linking of collagen fibrils. The role of LOX has been demonstrated previously in animals and patients with enhanced myocardial stiffness [99, 218, 219]. López *et al.* reported a correlation between LOX and collagen cross-linking and between cross-linking and LV stiffness in chronic HF patients [99, 220]. Authors also suggest that LOX plays a role in the adverse structural remodeling in remote myocardial infarction, which contributes to HF of ischemic origin [99]. Our data indicate that the observed increased stiffness is a consequence of the elevated HMW-AGEs level that is associated with increased fibrosis and LOX expression. In this study, however, the direct measure of collagen cross-linking (such as soluble/insoluble collagen ratios) was not performed. Nevertheless, our data strongly suggest that the observed cardiac dysfunction is likely to be caused by an increased collagen cross-linking mediated through LOX.

3.5.4 Limitations

There are several limitations that should be noted. Hemodynamic measurements in order to assess LV pressure, were not performed. However, the current study demonstrates that HMW-AGEs *per se* lead to cardiac dysfunction in non-pathological settings, as evidenced by higher LV volumes, reduced contractility and significant myocardial collagen accumulation. In addition, strain and strain rate deformation parameters were measured only in the circumferential direction. Radial strain components could theoretically be assessed from the

acquired parasternal short-axis images. However, several studies have demonstrated that radial strain assessment by speckle tracking is less accurate and reproducible, probably due to the smaller area and hence the total number of speckles available for analysis. Similarly, no longitudinal strain data have been obtained in the current study, since the anatomical position of the rodent heart impedes acquiring data from an apical view. Moreover, the additional value of measuring longitudinal function in rodents may be questioned as it has been previously demonstrated that the long-axis contribution to heart function is relatively small in these animals.

No identification of the chemical structure of HMW-AGEs has been performed. To date, because of the diversity of the several classes of AGEs, there are still no established methods to identify AGEs but in the context of targeted therapy in patients, a better knowledge of the nature of the HMW-AGEs would be useful and requires further investigation. Finally, in our study, the total levels of circulating sRAGE were measured by ELISA. However, circulating sRAGE could be generated from cleavage of cell-surface RAGE (cRAGE) or novel splice variants of RAGE (esRAGE), which are known to have a different physiological function.

In conclusion, our data demonstrate that rather than via activation of AGEs/RAGE signaling pathway, the deleterious effects of HMW-AGEs are likely mediated via an increased collagen cross-linking responsible for the observed cardiac dysfunction. In addition, the prominent cardiac fibrosis is associated with an increased LOX expression.

4

Mechanistic insight into glycated proteins (HMW-AGEs) and cardiac dysfunction

4.1 Abstract

Background. High molecular weight advanced glycation end products (HMW-AGEs) are known to play a key role in the development of cardiac dysfunction (Chapter 3). However whether the dysfunction is driven by remodeling at the cellular level remains unknown.

Methods. Adult rats were randomly assigned to daily intraperitoneal injection for 6 weeks with either HMW-AGEs (20 mg/kg/day, n=25) or a control solution (n=19). Echocardiographic and hemodynamic measurements were performed at sacrifice. Single cardiomyocytes from the left ventricle were obtained by enzymatic dissociation through retrograde perfusion of the aorta. Unloaded cell shortening, time to peak and time to 50% relaxation were measured during field stimulation and normalized to diastolic length. L-type Ca^{2+} current density (I_{CaL}) and steady-state inactivation of I_{CaL} were measured during whole-cell ruptured patch clamp. Protein expression was determined using Western blot. Finally, myofilament functional properties were measured in membrane-permeabilized cardiomyocytes.

Results. After 6 weeks of HMW-AGEs injection, rats displayed *in vivo* cardiac dysfunction. At the cellular level, single cardiomyocytes were significantly wider. Unloaded cell shortening was significantly reduced in HMW-AGEs and was associated with slower kinetics. Peak I_{CaL} density was significantly decreased in HMW-AGEs and L-type Ca^{2+} channel inactivation was significantly shifted towards more negative potentials. Finally, HMW-AGEs altered intrinsic properties of the myofilaments.

Conclusion. Rats subjected to high circulating HMW-AGEs display *in vivo* as well *as in vitro* structural and functional remodeling. In that context, our data indicate that HMW-AGEs induce changes observed at the organ level that are related to cellular structural and functional remodeling.

4.2 Introduction

One of the most common diseases experienced by our ageing Western population are cardiovascular diseases (CVDs). Heart failure (HF) is the final stage of many cardiovascular diseases characterized by the inability of the heart to pump blood to meet the energy demand of the body. The development of HF is a complex process related to a series of physiological and molecular factors, characterized by structural and functional disorders that still remain incompletely understood [3]. Advanced glycation end products (AGEs) are important components of our western diet that might contribute to CVDs development and progression. Over the past few year, there is more evidence that advanced glycation end products (AGEs) contribute to the development and progression of cardiovascular dysfunction [33, 221]. In Chapter 3, we have shown that high molecular weight AGEs (HMW-AGEs), as opposed to the well-characterized low molecular weight AGEs (LMW-AGEs) are responsible for cardiac dysfunction. While the majority of the studies available focus on the LMW-AGEs, very little is reported on HMW-AGEs. However, their importance in cardiac pathophysiology is rising [222]. Whether the cardiac dysfunction seen *in vivo* is the result of profound remodeling at the cellular level remains to date unknown. Therefore the goal of this project was to investigate cardiomyocyte properties in the setting of chronic exposure to HMW-AGEs. We hypothesize that HMW-AGEs chronically induce changes in the contractile properties of adult rat cardiomyocytes. In depth, we will investigate whether altered myofilament properties, alterations in the excitation-contraction coupling (ECC), increased oxidative stress or decreased Ca^{2+} influx contribute to changes in contractile properties.

4.3 Materials and Methods

4.3.1 Animal model

Male Sprague Dawley rats (Charles River Laboratories, Lyon, France) of ±150 grams were used. The animal protocol was approved by the Local Ethical Committee (Ethische Commissie Dierproeven, UHasselt, Diepenbeek, Belgium). The animals were daily injected intraperitoneal (*i.p.*) for 6 weeks with HMW-AGEs (20 mg/kg/day) (n=25) or a control solution (n=19). HMW-AGEs were prepared as described in chapter 3 [63]. All animals were maintained in a controlled environmental condition of temperature and humidity, were fed a standard pellet diet and had water available *ad libitum*. Blood samples and echocardiographic measurements after 6 weeks of injections were obtained in both groups. After 6 weeks of daily injection, invasive hemodynamic measurements were performed. Finally, the heart was harvested and adult single cardiomyocytes were isolated.

4.3.2 Conventional echocardiographic measurements

Transthoracic echocardiography was performed under 2% isoflurane in all animals at baseline and at 6 weeks post-injection with a Vivid*i* ultrasound machine (GE Vingmed Ultrasound) using a 10 MHz linear array transducer. A standard parasternal long axis image and short-axis views at mid-ventricular level were acquired at a temporal resolution of ≈ 200 frames per second. Conventional echocardiographic parameters (*e.g.* LV end-diastolic diameter (LVEDD), LV end-systolic diameter (LVESD), posterior wall thicknesses (PWT) and anterior wall thicknesses (AWT)) were obtained from the B-mode images at midpapillary level in the parasternal short-axis view. End-systolic volumes (ESV) and end-diastolic volumes [209] were calculated by $\pi * D_M^2 * B/6$, where D_M indicates the systolic/diastolic diameter of the ventricle in mid-ventricular short-axis view and B is LV length on parasternal long-axis image. Subsequently, ejection fraction (EF) was measured as (EDV–ESV)/EDV, and expressed in %. The end-diastolic sphericity index (SI) was calculated by dividing the EDV by the volume of a sphere whose diameter was equal to the major end-diastolic LV long axis. The LV long axis was obtained from the 2D dataset as the longest distance between the center of the mitral annulus and the endocardial apex.

4.3.3 Hemodynamic measurements

At sacrifice, hemodynamic measurements were conducted in anesthetized rats with 3% isoflurane supplemented by oxygen. Functional cardiac parameters were measured via the right carotid artery into the LV. Left ventricular pressure (LVP) and peak time derivatives maximum dP/dt and minimum dP/dt were measured with the SPR 320 Rat Pressure Catheter (AD Instruments, Germany) during 10 minutes to ensure stability of the results. Left ventricular end diastolic pressure (LVEDP), left ventricular end systolic pressure (LVESP) and time constant of LV pressure decay during isovolumetric relaxation period (Tau) was calculated with LabChart 7 software (AD instruments, Germany).

4.3.4 Cardiomyocyte isolation

After 6 weeks of injection, rats were injected with heparin (1000 u/kg *i.p.*) and sacrificed with an overdose of Dolethal (150 mg/kg *i.p.*). Hearts were dissected and weighted. Single adult cardiomyocytes from the LV were obtained by enzymatic dissociation through retrograde perfusion of the aorta. The hearts were perfused with normal Tyrode (NT) (in mM: NaCl 137, KCl 5.4, $MgCl_2$ 0.5, $CaCl_2$ 1, Na-HEPES 11.8, glucose 10 and taurine 20, pH 7.35) on a Langendorff setup at 37°C. After perfusion with a Ca^{2+} free solution (in mM: NaCl 130, KCl 5.4, KH_2PO_4 1.2, $MgSO_4$ 1.2, Hepes 6, glucose 20, pH 7.2), the tissue was perfused with an enzyme solution (Ca^{2+} free solution, collagenase type II (1.5 g/l; Worthington, Lakewood, USA) and protease type XIV (0.06 g/l; Sigma, Diegem, Belgium)), followed by a low Ca^{2+} solution (0.1 mM). The digested LV tissue was minced and subsequently filtered with a mesh of 300 µm. Part of the freshly isolated cells were used to assess fractional cell shortening or electrophysiology measurements. Experiments were performed at room temperature within 6 hours of cell isolation. Remaining cells were stored at -80°C and used for protein expression and experiments on the myofilaments function.

4.3.5 Unloaded cell shortening

Isolated cardiomyocytes were placed into a perfusion chamber with NT, on the stage of an inverted microscope (Nikon Diaphot). Cardiomyocyte length and width were measured in ± 25 cells per animal. Unloaded cell shortening of intact

cardiomyocytes was measured with a video-edge detector (Crescent Electronics, USA). Field stimulation was done with pulses of constant voltage, using platinum electrodes. Steady-state stimuli were applied at frequencies of 1, 2 and 4 Hz. Unloaded cell shortening was normalized to diastolic cell length (L/L$_0$) and presented as % (*i.e.* fractional shortening). Time to peak of contraction (TTP, ms) and time to half-relaxation (RT$_{50}$, ms) were measured to assess kinetics of cell shortening. Fractional cell shortening was also measured before and after isoproterenol (ISO; 300 nM) or N-acetyl-L-cysteine (NAC; 5 mM) application.

4.3.6 Electrophysiological measurements

The L-type Ca^{2+} current (I$_{CaL}$) was measured during whole-cell voltage-clamp and was normalized to cell capacitance, as a measure of cell surface. Patch pipettes (2-3 MOhm) were filled with a pipette solution containing (in mM: 120 KAsp, 20 KCl, 10 HEPES, 5 MgATP, 10 EGTA, 10 NaCl, pH 7.2). I$_{CaL}$ was measured by a single depolarizing step of 150 ms from -70 mV to +10 mV. To assess the rate of inactivation of I$_{CaL}$, voltage inactivation component was derived by using biexponential fitting of I$_{CaL}$ inactivation. Current-voltage relationship of I$_{CaL}$ was measured during 10 mV depolarisation steps ranging from -40 mV to +60 mV. The voltage-dependence of the steady-state inactivation and activation were determined with a classical two-steps protocol [223]. In brief, inactivating pre-pulses of 400 ms were applied from a holding potential of -70 mV to various potentials. The amplitudes of the peak inward current during the test pulse (I) at 0 mV were normalized to their respective maximum value (I$_{max}$) and were plotted as a function of the inactivating potential. Steady-state activation plot was generated by dividing peak I$_{Ca}$ measured at a given potential by the difference between measured and reversal potential. The amplitudes of the channel conductance during the test pulse (G) were normalized to their respective maximum value (G$_{max}$) and were plotted as a function of the activating potential. Steady-state kinetic parameters were determined by fitting steady-state activation and inactivation data to Boltzmann equations (curves were fitted between 0 and 1) to calculate the half-activating and half-inactiving potential (V50) as decribed by Vornanen *et al* [224].

4.3.7 Myocyte skinning and measurement of isometric force

Single skinnend myocytes were prepared from the frozen cell pellets. The pellet was first thawed in a Ca^{2+}-free relaxing solution containing (in mM: 6 Na_2ATP, 6 $MgCl_2$, 2 EGTA, 140 KCl, 10 imidazole, pH 7.0). The thawed cardiomyocytes were incubated for 5 minutes in the same solution with 0.5% Triton X-100 to permeabilize and remove lipid membranes. Isometric force was measured in the skinned cardiomyocytes fixed between a piezoelectric motor and a force transducer at 15°C. Absolute forces were normalized to the cross-sectional area of the cardiomyocytes and expressed as developed tension (in kN/m^2). The passive force (F_{pass}) was measured at different sarcomere length in Ca^{2+}-containing relaxing solution (in mM: 5.89 Na_2ATP, 6.48 MgCl, 4.76 Kprop, 100 BES, 7 $Ca^{2+}EGTA$ and 14.5 creatininephosphate) by slackening the myocyte by 30% of its length. Active tension (F_{act}) was calculated as $F_{act} = F_{total} - F_{pass}$. Rate of force redevelopment (k_{tr}) was determined using a slack-re-stretch. In brief, after steady state force was reached, cardiomyocytes were allowed to shorten to 30% of their original length and then were re-stretched to the original length. K_{tr} was derived from a single exponential fitting of force redevelopment.

4.3.8 Protein expression

BCA protein kit (Thermo Fisher, Erembodegem, Belgium) was used to assess protein concentrations of LV cells of both groups. By using a 12% SDS-PAGE gel with a mini protean 3 electrophoresis system (Bio-rad Laboratories, Temse, Belgium), equal amounts of proteins were separated. Gels were transferred to a polyvinylidene fluoride (PVDF) membrane. Blocking was performed during 2 hours with 5% milk in Tris-buffered solution containing 0,1% Tween-20 (TBS-T). Membranes were incubated overnight at 4°C in the presence of specific primary antibodies (SERCA, 1/4000, mouse anti-rat IgG, Santa Cruz, sc-376235, Heidelberg, Germany; PLN, 1/1000, goat anti-rat IgG, Santa Cruz, C-21923, Heidelberg, Germany; NCX, 1/1000, rabbit anti-rat IgG, Santa Cruz, sc-32881, Heidelberg, Germany; PLN S16, 1/1000, rabbit anti-rat IgG; Badrilla, A010-12, Leeds, UK; PLN T17, 1/1000, rabbit anti-rat IgG, Badrilla, A010-12AP, Leeds, UK; CS, 1/4000, rabbit anti-rat IgG, Abcam, ab129095, Cambridge, UK). All primary antibodies were diluted in 5% milk-TBS-T. Horseradish peroxidase-conjugated secondary antibodies were used and diluted 1/2000 in 5% milk-TBS-

T. Proteins were visualized with the enhanced chemiluminscence (ECL) technique using Pierce ECL Plus Western blotting Substrate (Thermo Fisher, Erembodegem, Belgium). Data were normalized to β-actin protein expression (1/1000, mouse anti-rat IgG, Santa Cruz, sc-47778, Heidelberg, Germany). Densitometry of the protein bands was quantified via the ImageQuant TL software.

4.3.9 Citrate synthase activity

Protein extract samples from frozen cardiomyocytes were used to assess citrate synthase (CS) activity. CS was measured according to the manufacturer's protocol (Citrate Synthase assay kit, CS0720, Sigma-Aldrich, Diegem, Belgium). CS activity, as evaluated by absorbance value monitored at wavelengths of 412 nm at 20 seconds intervals for a period of 3 minutes was assessed by using a plate reader (FLUOstar OPTIMA Microplate Reader, BMG LABTECH, Belgium). CS activity was normalized to baseline CS activity, measured without the component oxaloacetic acid (OAA). Data are reported in units (µmol/ml/min).

4.3.10 Statistical analysis

Statistical analysis was performed with Prism (Graphpad software, USA). All data are expressed as mean ± standard error of the mean (SEM). The parametric tests which were used to compare the HMW-AGEs and control group are unpaired t-tests. Paired t-tests were used to evaluate both groups before and after application of ISO and NAC. In addition, two-way ANOVA test was used when appropriate. A value of $P<0.05$ was considered statistically significant.

4.4 Results

4.4.1 HMW-AGEs alter global LV function *in vivo*

Hemodynamic parameters are summarized in Table 4.1. Peak rate of pressure rise (dP/dt_{max}), used as a measure of ventricular contractility, was significantly decreased while ventricular relaxation, as assessed by peak rate of pressure decline (dP/dt_{min}) was significantly increased after 6 weeks HMW-AGEs injection ($P<0.05$). Other parameters such as EDP, mean pressure and Tau remained comparable between the groups (Table 4.1).

Table 4.1 Characteristics of hemodynamic measurements.

Parameters	6 weeks post-injections	
	Control	HMW-AGEs
HR (BPM)	367.08 ± 6.38	363.62 ± 9.07
Max pressure (mmHg)	94.72 ± 3.29	89.42 ± 3.41
EDP (mmHg)	3.57 ± 1.69	5.35 ± 2.69
Mean pressure (mmHg)	36.49 ±2.09	37.03 ± 2.72
dP/dt_{max} (mmHg/s)	7356.10 ± 405.93	6282.96 ± 286.02 *
dP/dt_{min} (mmHg/s)	-6387.12 ± 266.26	-5426.406 ± 262.89 *
Tau (s)	0.064 ± 0.015	0.046 ± 0.015

Max pressure, maximal LV pressure; EDP, end-diastolic pressure; dP/dt_{max} , maximum peak time of pressure rise; dP/dt_{min}, minimum peak time pressure decline; Tau, time constant of LV pressure decay during isovolumetric relaxation period. LV pressure measurement parameters were evaluated 6 weeks post-injections in control (n=12) and HMW-AGEs (n=10) injected animals. Data are presented as mean ± SEM. * denotes P<0.05.

4.4.2 HMW-AGEs induce morphological remodeling

As shown in Figure 4.1, HW/BW and HW/TL ratios were significantly increased in HMW-AGEs animals indicating increased heart mass. This increase was further confirmed by the increased AWT and PWT assessed by conventional echocardiographic and previously described in chapter 3.
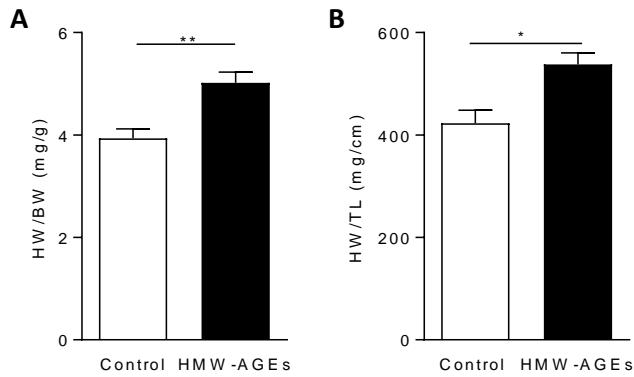
Figure 4.1 Effect of 6 weeks HMW-AGEs injection on heart weight. Heart weight/body weight (HW/BW; mg/g) (left) and HW/tibia length (HW/TL; mg/cm) (right) in control (n=16) and HMW-AGEs (n=17). Data are expressed as mean ± SEM. ** denotes P<0.01 and * denotes P<0.05.

Figure 4.2A are representative pictures of isolated cardiomyocytes from both groups. As summarized in Figure 4.2B and Figure 4.2C, there were no obvious differences in appearance of the sarcomeres of the myocytes from both groups. While cell length was not increased, cell width was significantly increased in HMW-AGEs (25.4 ± 0.4 µm *vs* 24.7 ± 0.6 µm in control, P<0.05; Figure 4.2B). Distribution of cell width and length is shown in Figure 4.2C.

A

B

C
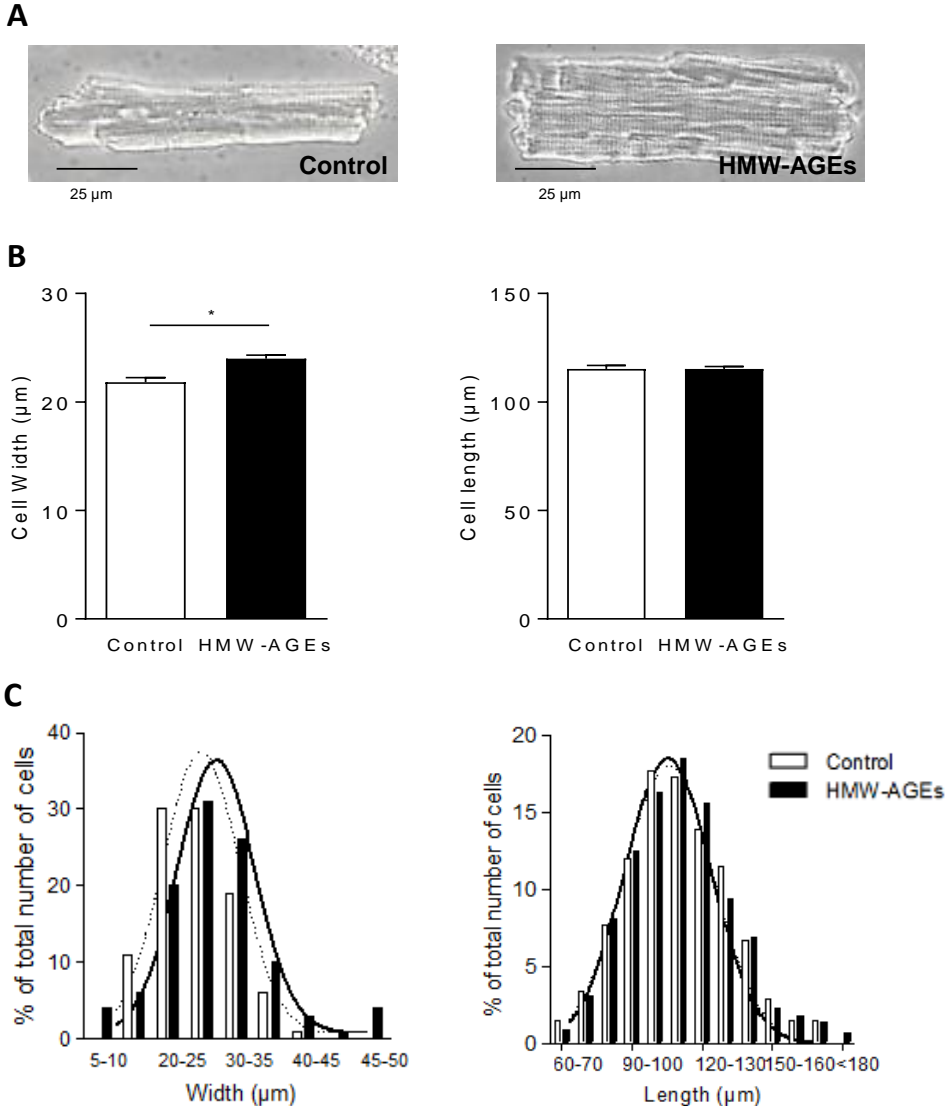
Figure 4.2 Morphology of isolated LV cardiomyocytes. (A) Representative transmitted light image of a single LV cardiomyocyte isolated from control (left) or HMW-AGEs (right) injected animals. (B) Analysis of cardiomyocyte width (μm) and length (μm) in control (n_{cells}= 203) and HMW-AGEs (n_{cells}= 436). (C) Frequency distribution of cardiomyocyte width and length in both groups. Data are expressed as mean ± SEM. * denotes P<0.05.

4.4.3 HMW-AGEs cause contractile impairment

A representative example of fractional cell shortening during field stimulation at 1 Hz in both groups is shown in Figure 4.3A. Unloaded fractional cell shortening at 1 Hz was significantly reduced in the HMW-AGEs group (Figure 4.3B).
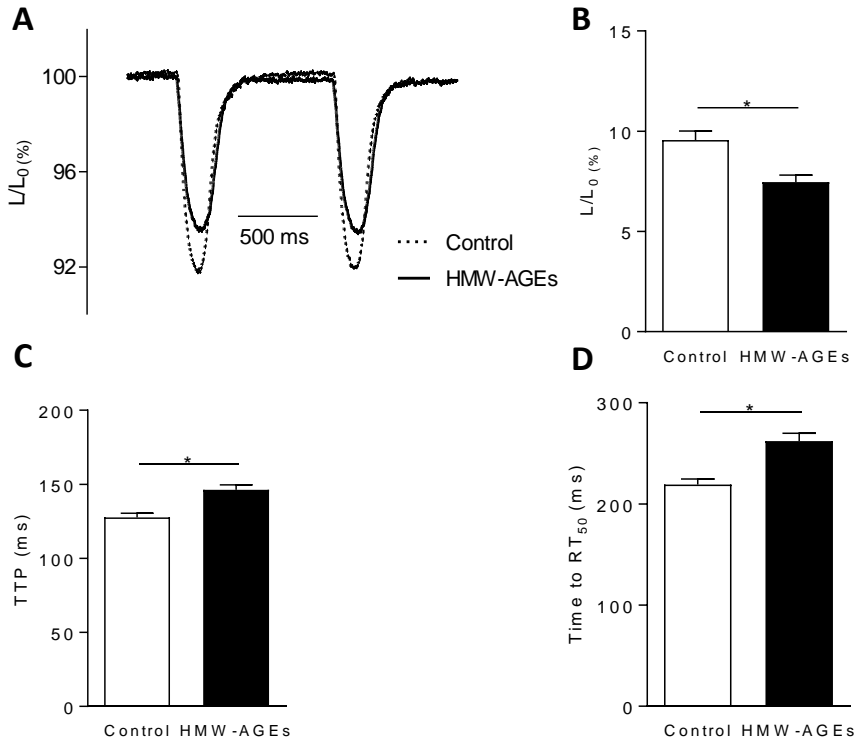
Figure 4.3 Cell shortening during field stimulation. (A) Representative example of unloaded cell shortening during field stimulation at 1 Hz in control and HMW-AGEs cardiomyocytes. (B) Fractional cell shortening normalized to cell length (L/L$_0$, %), (C) time to peak of contraction (TTP, sec) and (D) time to half-relaxation (Time to RT$_{50}$, sec) in cardiomyocytes derived from control (n$_{cells}$=64) or HMW-AGEs (n$_{cells}$=104) injected animals. Data are expressed as mean ± SEM. * denotes P<0.05.

TTP and time to RT$_{50}$ at 1 Hz were both significantly increased in HMW-AGEs compared with control (P<0.05; Figure 4.3C and 4.3D) indicating a reduced contraction associated with slower kinetics. Smaller and slower contractions were also seen at higher frequencies, *i.e.* 2 and 4 Hz (Figure 4.4).
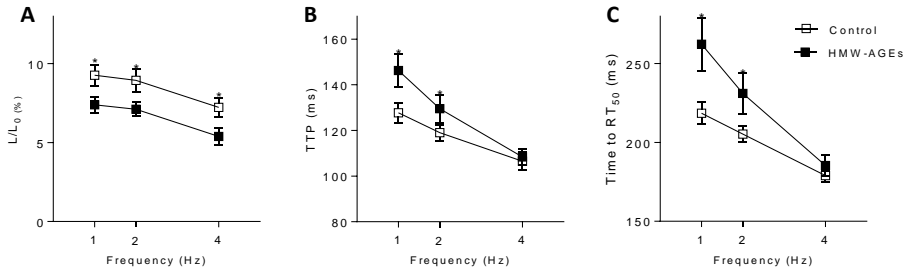
Figure 4.4 Frequency dependency of cell shortening during field stimulation. (A) Frequency dependency of fractional cell shortening normalized to cell length (L/L_0, %) (left), (B) time to peak of contraction (TTP, sec) (middle) and (C) time to half-relaxation (Time to RT_{50}, sec) (right) at 1, 2 and 4 Hz in cardiomyocytes derived from control (n_{cells}=64) or HMW-AGEs (n_{cells}=104) animals. Data are expressed as mean ± SEM. *denotes P<0.05.

To test for a possible altered contractile reserve, unloaded cell shortening was measured before and after application of 300 nM ISO. ISO is a full agonist of β-adrenergic receptors (β-AR) and is structurally similar to adrenaline. In normal cardiomyocytes, binding of ISO to β-AR activates a stress signal which causes increased and faster contractions. If the β-adrenergic response is altered, ISO will not have effects on contractility and contractile reserve is affected [225]. As shown in Figure 4.5A and as expected, ISO application increased fractional cell shortening at 1 Hz in control cells. The related increased shortening observed with ISO was comparable in both groups, indicating an unaltered contractile reserve in HMW-AGEs treated animals.

Kinetics of contraction after ISO application (i.e. TTP) significantly decrease in both groups (Figure 4.5B). Additionally, RT_{50} tended to decrease in both groups but data did not reach significance (Figure 4.5C). Altogether, data indicate that adrenergic response in single cells was not altered by HMW-AGEs. Cardiomyocytes did not response different to stress situations after application to HMW-AGEs.
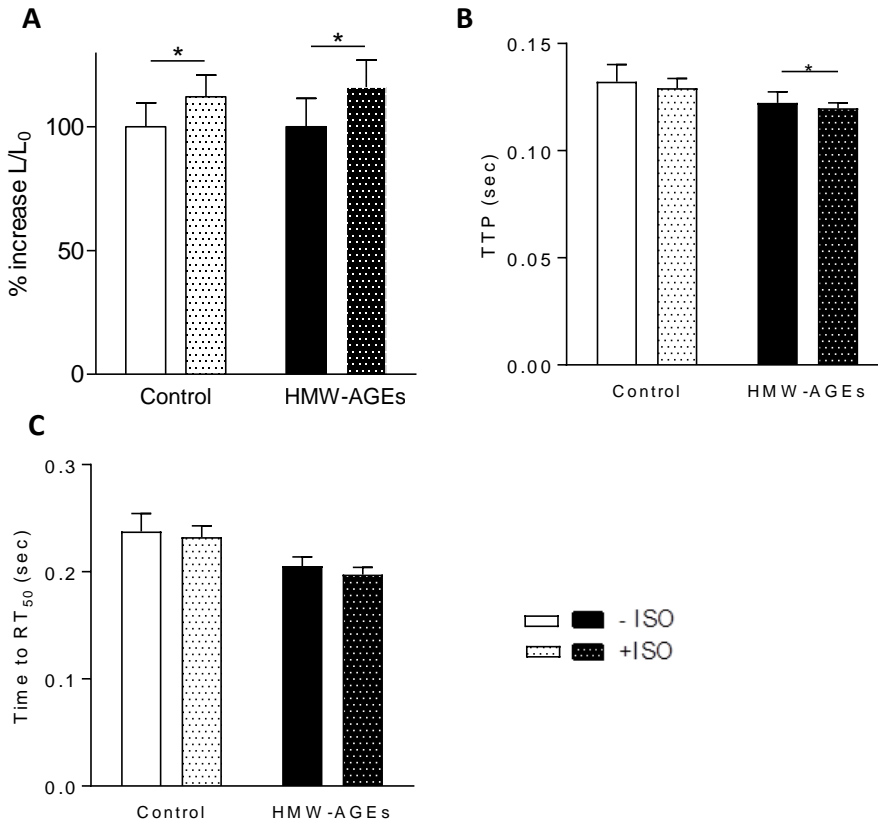
Figure 4.5 Effect of isoproterenol on unloaded cell shortening at 1 Hz. (A) Relative change in fractional cell shortening normalized to cell length (L/L_0, %), (B) time to peak of contraction (TTP, sec) and (C) time to half-relaxation (time to RT_{50}, sec) at 1 Hz before and after isoproterenol (ISO) application in cardiomyocytes derived from control (n_{cells}=13) or HMW-AGEs (n_{cells}=18) injected animals. Data are expressed as mean ± SEM. – ISO = before ISO, + ISO = after ISO. * denotes P<0.05.

To further unravel underlying mechanisms resulting in impaired cardiomyocyte relaxation, we examined protein levels of SERCA, PLN and NCX. As shown in Figure 4.6, protein levels of SERCA, PLN or NCX were comparable between groups. In addition, phosphorylated forms of phospholamban (PLN) *i.e.* PLN serine 16 (PLN S16) and PLN threonine 17 (PLN T17) were not altered. The ratio
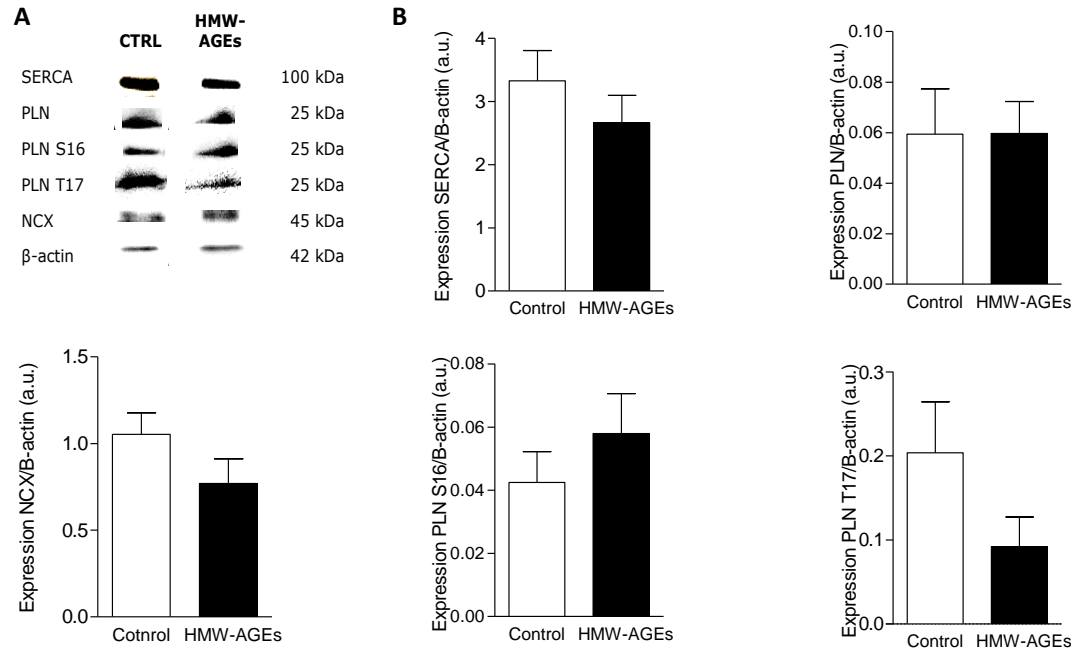
Figure 4.6 Expression of proteins involved in the excitation-contraction coupling. (A) Representative Western blot for different excitation-contraction coupling (ECC) proteins in control (CTRL) and HMW-AGEs. (B) Quantitative analysis of different ECC proteins normalized to β-actin in control (n=7) and HMW-AGEs (n=11) injected animals. SR Ca^{2+} ATPase (SERCA), phospholamban (PLN), Na^+/Ca^{2+} exchanger (NCX), phosphorylated isoform of PLN on serine 16 (PLN S16) and phosphorylated isoform of PLN on threonine 17 (PLN T17). Data are expressed as mean ± SEM.

SERCA/PLN, an important determinant for cell relaxation, was also not changed (data not shown).

To further investigate the reduced contractile function seen in cardiomyocytes, we examined intrinsic properties of the myofilaments in skinned myocytes.

As shown in Figure 4.7A, passive force was significantly reduced in HMW-AGEs compared to control at all sarcomere lengths. Maximal Ca^{2+}-activated active force tended to be reduced in HMW-AGEs (17.97 ± 1.98 kN/m² in control *vs* 13.28 ± 1.38 kN/m² in HMW-AGEs, p = 0.06, Figure 4.7B). Finally, rate of force redevelopment (K_{tr}) was significantly decreased in HMW-AGEs (Figure 4.7C).
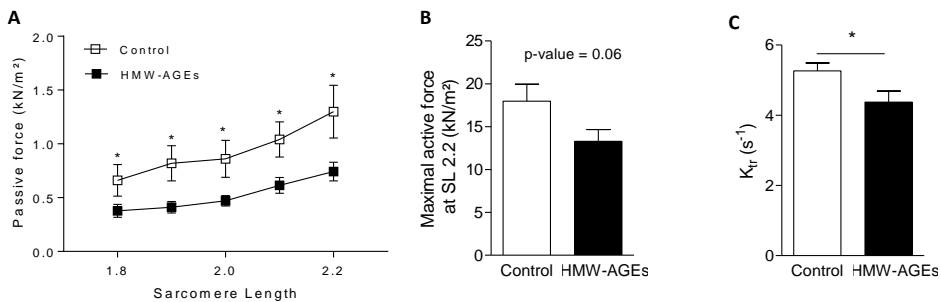
Figure 4.7 Force development in skinned single myocytes. (A) Passive force at different sarcomere lengths normalized to cross-sectional area in control and HMW-AGEs. (B) Active force developed per cross-sectional area at sarcomere length 2.2 µm in control and HMW-AGEs. (C) The rate of force redevelopment, K_{tr} in control and HMW-AGEs. Data are expressed as mean ± SEM in $n_{cells}=25$ in control and $n_{cells}=24$ in HMW-AGEs. * denotes P<0.05.

4.4.4 HMW-AGEs alter L-type Ca^{2+} channel properties

A representative current recording elicited by a depolarizing step to +10 mV is shown in Figure 4.8A. The peak I_{CaL} density was significantly smaller in HMW-AGEs cells compared to control. Changes in slow inactivation of Ca^{2+} current (voltage-dependent, τ_{slow}) were not statistically different (Figure 4.8B). As summarized in Figure 4.8C, voltage-dependence of I_{CaL} remained bell-shaped with HMW-AGEs and peak L-type Ca^{2+} current density (I_{CaL}) was significantly smaller in HMW-AGEs.
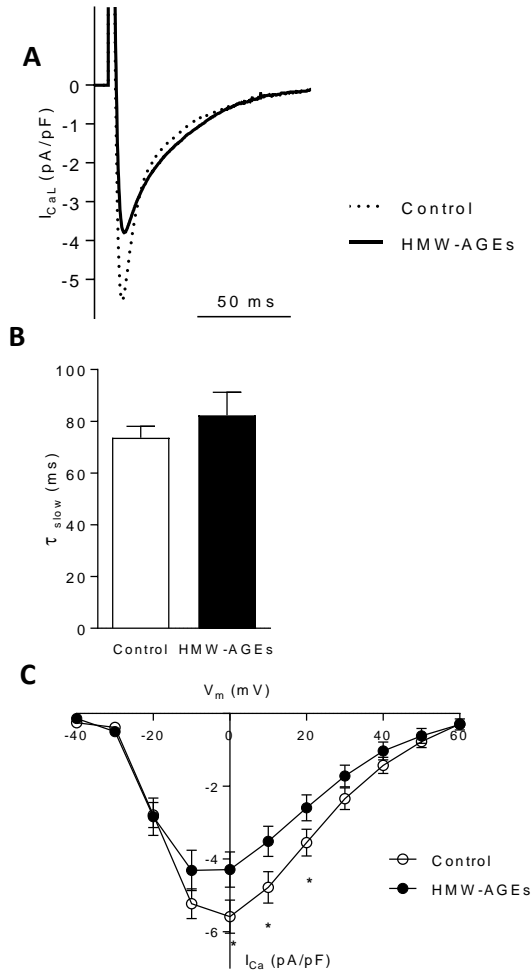
Figure 4.8 L-type Ca^{2+} current density. (A) Representative example of L-type Ca^{2+} current (I$_{CaL}$) density elicited by a depolarizing step to +10 mV in control (n$_{cells}$=26) and HMW-AGEs (n$_{cells}$=20) cardiomyocytes. (B) Slow time (τ$_{slow}$, ms) constant in control (n$_{cells}$=21) and HMW-AGEs (n$_{cells}$=24) derived cardiomyocytes. (C) Voltage-dependence of I$_{CaL}$ in both groups. Data are expressed as mean ± SEM. * denotes P<0.05.

To further investigate potential changes in the intrinsic properties of L-type Ca^{2+} channels, steady-state inactivation and steady-state activation of I$_{CaL}$ were evaluated (Figure 4.9). The voltage protocol for measuring steady-state activation and inactivation of I$_{CaL}$ and a representative current recording is shown in Figure 4.9A en B respectively.
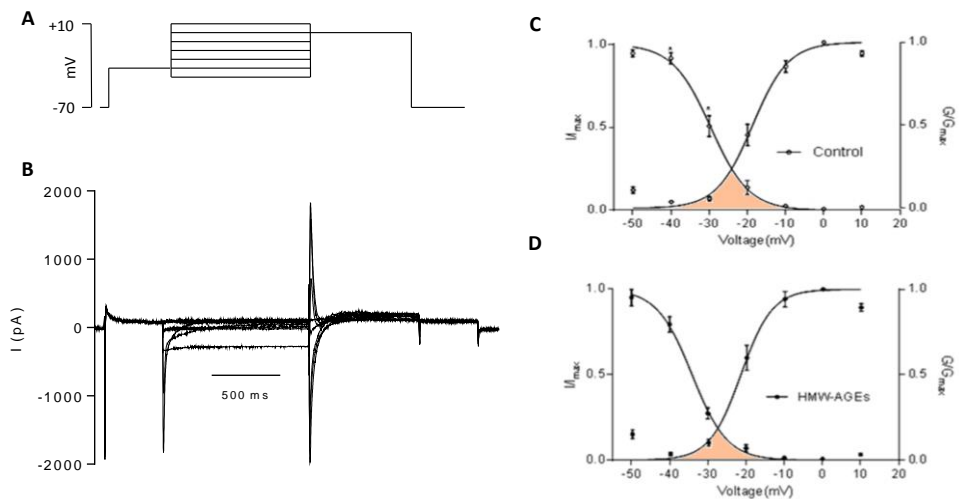
Figure 4.9 Steady-state inactivation and activation curves of the L-type Ca^{2+} current. (A) Voltage protocol used to measure steady-state activation and inactivation. (B) Representative current recording from a ventricular cardiomyocyte subjected to the voltage protocol given in A. (C) Steady-state activation and inactivation of the L-type Ca^{2+} current (I_{CaL}) in control (n_{cells}=12) cardiomyocytes. Amplitudes of the peak inward current during the test pulse (I) were normalized to their respective maximum value (I_{max}) and are plotted as a function of the inactivating potential. The activation window is indicated in color. (D) Steady-state activation and inactivation of I_{CaL} in HMW-AGEs (n_{cells}=8) derived cardiomyocytes. Amplitudes of channel conductance during the test pulse (G) were normalized to their respective maximum value (G_{max}) and are plotted as a function of the activating potential. The activation window is indicated in color. Data are expressed as mean ± SEM. * denotes P<0.05.

As shown in Figure 4.9C and D, HMW-AGEs led to a shift towards more negative potentials of steady-state inactivation of I_{CaL}, a measure of channel availability. Steady-state activation of I_{CaL}, a measure of channel conductance was not significantly different between the groups. Activation of I_{CaL} was half maximal (V50) at -18.7±0.5 mV in control cells compared to -21.6±0.7 mv in treated cells. Inactivation of I_{CaL} was half maximal (V50) at -29.6±0.5 mV in control cells compared to -34.2±0.5 mV in treated cells. These data indicate that inactivation properties of Ca^{2+} channels are impaired. As a result of overlap between activation and inactivation curves, the activation window was smaller in

the HMW-AGEs cardiomyocytes compared to the activation window of the control cells.

4.4.5 Action potential duration tended to be prolonged in HMW-AGEs

Action potential duration (APD) was measured during whole-cell current-clamp mode (Figure 4.10). Resting membrane potential (V_m) was comparable in both cell types. AP duration at 50% (APD_{50}) and at 90% (APD_{90}) repolarization tended to be increased in the HMW-AGEs group compared with the control group. However, data did not reach statistical significance, probably due to the low number of cells.
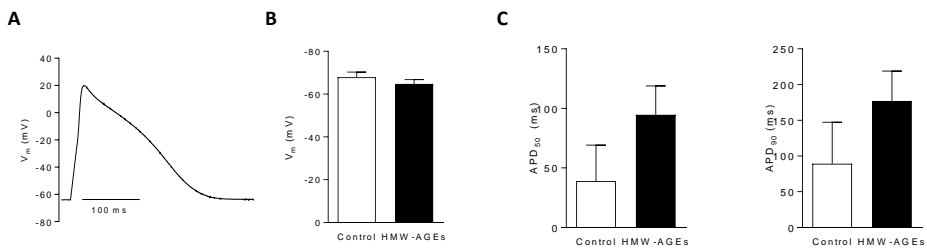
Figure 4.10 Action potential characteristics. (A) Representative example of an action potential at 1 Hz (B) Resting membrane potential (V_m) and (C) action potential duration at 50% (APD_{50}) and at 90% (APD_{90}) repolarization in control (n_{cells}=5) and HMW-AGEs (n_{cells}=9) derived cardiomyocytes. Data are expressed as mean ± SEM.

4.4.6 Changes in mitochondrial activity do not seem to be involved in altered excitation-contraction coupling

Alterations in mitochondrial properties could be a cause for altered ECC and contraction. As a measure for mitochondrial mass, neither CS protein expression (Figure 4.11A and B) nor CS activity (Figure 4.11C) were different in control and HMW-AGEs samples, suggesting unaltered mitochondria mass.
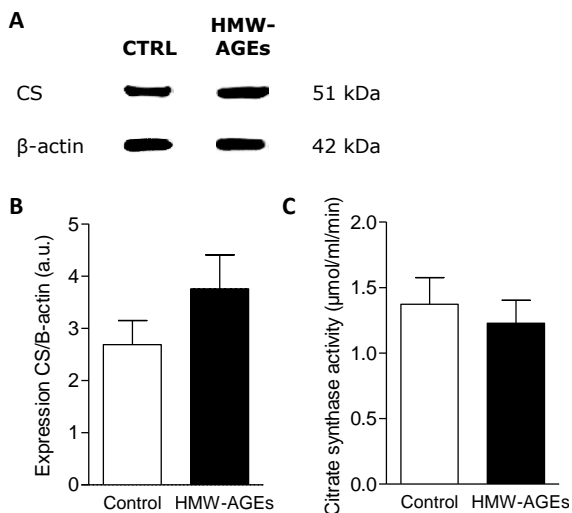
Figure 4.11 Protein expression of citrate synthase and citrate synthase activity.
(A) Representative Western blot for citrate synthase (CS). (B) Quantitative analysis of CS protein expression in control (n=7) and HMW-AGEs (n=12) injected animals. (C) Quantitative analysis of citrate synthase activity in control (n=7) and HMW-AGEs (n=12) injected animals. Data are expressed as mean ± SEM.

In cardiomyocytes NADPH-dependent ROS production is a substantial source of ROS. To test for potential increased ROS levels in HMW-AGEs responsible for the reduced contraction, unloaded cell shortening was assessed in the presence of a ROS scavenger NAC (5 mM). As summarized in Figure 4.12, amplitude and kinetics of contraction in both groups were comparable after NAC application. Data suggest that the reduced cardiomyocyte contractile properties are unlikely to be mediated through increased ROS levels.
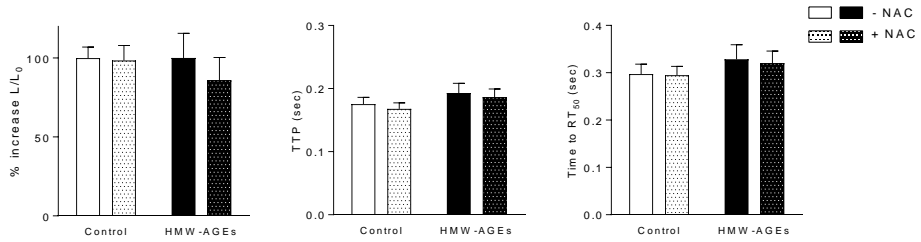
Figure 4.12 Effect of N-acetyl-L-cysteine (NAC) on unloaded cell shortening at 1 Hz during field stimulation. (A) Fractional cell shortening normalized to cell length (L/L$_0$, %), (B) time to peak of contraction (TTP, ms) and (C) time to half-relaxation (time to RT$_{50}$) at 1 Hz before and after N-acetyl-L-cysteine (NAC) application in control (n$_{cells}$=7) or HMW-AGEs (n$_{cells}$=8) cardiomyocytes. Data are expressed as mean ± SEM. – NAC = before NAC, + NAC = after NAC application.

4.5 Discussion

In this study, we show that cardiac dysfunction *in vivo*, induced by HMW-AGEs is the result of profound cardiomyocyte remodeling, including cell hypertrophy, reduced contractile and myofilament properties associated with altered Ca^{2+} handling.

4.5.1 Morphological remodeling and cardiomyocyte hypertrophy

As for Chapter 3, *in vivo* hypertrophy was observed in HMW-AGEs injected animals as shown by increased AWT and PWT. The increase in heart mass was confirmed by the increase in HW/BW ratio and HW/TL ratio. In addition, at the cellular level, cardiomyocytes undergoing high levels of HMW-AGEs were significantly wider. As shown also by others [226], our model displayed concentric hypertrophy, characterized by an increase in wall thickness and cardiac mass, with a small reduction in chamber volume. In our study, isolated cardiomyocytes were wider, indicating hypertrophy at the cellular level. Such LV remodeling at the cardiomyocyte level was also shown by Gerdes *et al* [227]. They reported that concentric hypertrophy is characterized by cardiomyocytes that only grow in a transverse direction while keeping cell length constant, which is in line with our results.

A potential trigger for the altered cell hypertrophy in our study could be the increase in mechanical load. Cross-linking of extracellular matrix (ECM) components by AGEs are known to cause alterations in tissue stiffness, tissue mechanical properties and ultimately increased mechanical load subjected to cardiomyocytes [172]. In addition, increased mechanical load, due to cross-linking in our study, can activate collagen and ECM protein synthesis in fibroblasts to induce fibrosis. As shown in Chapter 3, an increased interstitial myocardial fibrosis is observed in our animal model. Additionally, in response to mechanical load, cardiomyocytes are subjected to many factors such as angiontensin II (Ang II), endothelin 1 (ET-1), insulin-like growth factor 1 (IGF1) which will activate intracellular signaling pathways leading to cell growth [228]. In our study, however, potential additional changes in circulating ANgII, ET-1 and IGF-1 were not investigated but would require further attention. Signaling cascades and

proteins responsible for cardiac growth and hypertrophy are complex and are summarized in Figure 4.13.
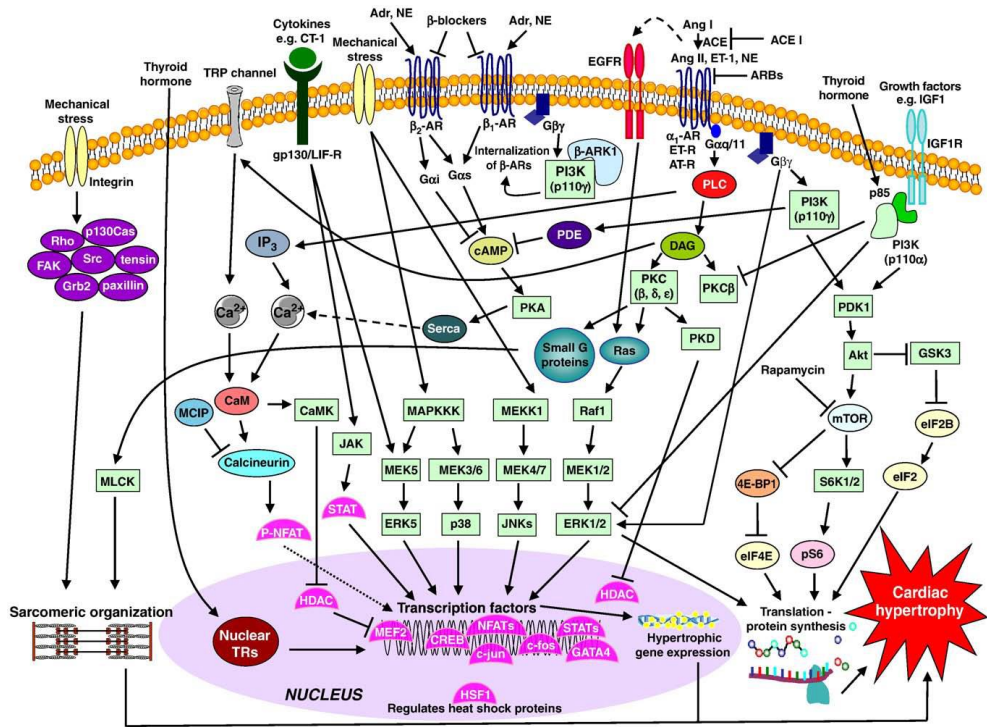
Figure 4.13 A schematic overview of the major signaling pathways involved in cardiac hypertrophy. [228]

4.5.2 Altered contractile properties are related to altered myofilament properties and reduced Ca^{2+} current

We observed *in vivo* no changes in CO and EF, however as already discussed in chapter 3, CO and EF are global parameters and are not sensitive enough to detect small changes. Nevertheless, at cellular level a profound remodeling was observed, characterized by decreased unloaded shortening of intact cardiomyocytes associated with slower kinetics. The observed changes at the cellular level corroborate data *in vivo* where a significant altered dP/dt$_{max}$ was observed, indicating reduced ventricular contractility in the rats treated with HMW-AGEs. One possible cause for the reduced contraction could be a reduced Ca^{2+} influx through L-type Ca^{2+} channels. Indeed, during ECC, Ca^{2+} is transported into the cytosol via L-type Ca^{2+} channels which are located in the

transverse tubules (T-tubules). This Ca^{2+} influx through I_{CaL} causes Ca^{2+}-induced-Ca^{2+}-release (CICR). High levels of Ca^{2+} are transported out of the SR into the cytosol to activate myofilaments and cause activation of the ECC resulting in cardiomyocyte contraction [68]. A reduced I_{CaL} will result in a reduced CICR and smaller induced contraction [229]. In our model as for other studies for diabetes [230-233], cardiomyocytes isolated from treated animals displayed lower I_{CaL}, suggesting that the reduced Ca^{2+} influx could be one cause for the reduced contractile function. The reduced Ca^{2+} influx could be related to altered structural morphology. Indeed, several animal and human studies have shown alterations in the T-tubule network characterized by decreased T-tubule density or disruption of the structure [234-238]. These changes are a cause for altered Ca^{2+} influx via I_{CaL}. T-tubules have a high density of LTCC, which was confirmed by Brette *et al.*. They reported that ± 75% of the L-type Ca^{2+} current flows across the T-tubules [239, 240]. A loss of T-tubules would disproportionately decrease I_{CaL} density. In our study, we do observe hypertrophy and reduced I_{CaL}. Whether this is the result of reduced T-tubules high density or disorganization remains to be elucidated. In addition, our data indicate that the intrinsic properties of the LTCC were altered by HMW-AGEs. Steady-state inactivation of the L-type Ca^{2+} channel, as a measure for channel availability, was significantly decreased in HMW-AGEs cells indicating that the LTCCs in HMW-AGEs animals are less available and inactivated more rapidly, compared to controls. Therefore, less Ca^{2+} can be transported in the cytosol resulting in a reduced I_{CaL}. In line with our results, LTCC inactivation is also shown to be reduced in a diabetic setting [241]. However, the exact underlying mechanism on HMW-AGEs induced Ca^{2+}-channel properties changes remains currently unexplained. Whether the change in LTCC properties is mediated through RAGE activation is unlikely. Indeed, as previously mentioned and further confirmed in chapter 3, we have shown that HMW-AGEs mechanism of action is not mediated through RAGE activation [63]. Besides changes in LTCC properties, a change in LTCC structure namely an increase in LTCC cross-linking could be an explanation for the reduced I_{CaL}. Indeed, others have shown that cross-linking of Ca^{2+} release channels (RyR) by AGEs was a cause for altered channel function [74]. Additional to reduced Ca^{2+} influx, impaired myofilament properties have been shown to be responsible for a reduced unloaded cell shortening [242, 243]. In our animal model, active force development

tended to be reduced (p=0.06). As also shown by others, a reduced CICR related to reduced Ca^{2+} influx will be the primary cause for the impaired Ca^{2+} availability to bind on the myofilaments [242, 243]. Additionally, we observed a reduced rate of tension activation characterized by a significant decrease in maximal k_{tr}. A possible mechanism for the observed decreased k_{tr} could be a shift in myosin heavy chain (MHC) expression toward the slow β isoform in the myofilaments in HMW-AGEs injected animals. The expression of MHC-α and MHC-β, two functionally distinct cardiac MHC isoforms, is tightly controlled by developmental and hormonal factors [244, 245]. The β-isoform is characterized by a lower filament sliding velocity compared to the α-isoform and it is capable to generate force with a higher economy of energy consumption. However, decreased contractile function can promote disease progression and therefore outweigh the benefits of preserved energy consumption [246]. Such a change in MHC-β levels has been observed during cardiac hypertrophy in a mice model with a null mutation of α-MyHC [247]. A shift in MHC-β isoform could be the underlying molecular mechanism of the decreased k_{tr} observed in the HMW-AGEs animals. However, it remains to be confirmed in our model.

Cardiomyocytes from HMW-AGEs displayed slower kinetics with slower contraction and relaxation times. It is known from literature that AGEs can cross-link SR Ca^{2+} regulatory proteins (*e.g.* SERCA pump and RyR), therefore altering their function [30]. In normal cardiomyocytes, SERCA pumps Ca^{2+} back into the SR to reduce the intracellular Ca^{2+} concentration, causing cardiomyocyte relaxation [68]. Reduced SERCA activity would lead to slower cardiomyocyte relaxation [248]. A reduced activity of SERCA can be due to the decreased SERCA, PLN and/or NCX expression.

In diabetic animal models, it is widely shown that SERCA expression is decreased and PLN expression is increased causing arrhythmias and diabetic cardiomyopathy [249-251] while others failed to report these findings [252]. Petrova *et al.* investigated specifically the effect of AGEs on SERCA, PLN and NCX protein expression. Fetal mouse cardiomyocytes were exposed to AGEs for 24 hours. Protein expression of these players involved in ECC were not affected by AGEs [95]. These data are in line with the results obtained in our experiments. In our

study, SERCA, PLN and their phosphorylated forms (T17 and S16) and NCX remained unchanged in HMW-AGEs treated animals.

Our data are somehow different from what others have previously described in diabetes [249, 250]. Whether the observed unchanged protein levels are true or whether there is a trend, remains to be further elucidated. Another possible explanation could be a reduced protein activity due to cross-linking. Indeed, as shown by previous studies, an unchanged expression does not necessarily mean an unchanged protein activity that could, in addition to altered ECC, contribute to the altered contractile function. This specific aspect would require experiments to identify whether not only protein expression but also protein activity of SERCA, PLN and NCX are altered by HMW-AGEs and thereby also contribute to impaired relaxation.

Finally, passive tension was determined in skinned cardiomyocytes. Cardiomyocyte passive forces play an important role in cardiac muscle as it is part of the diastolic wall tension that determines the extent of filling of the heart [253]. In our study, we observed a significantly decreased passive force in cardiomyocytes from the treated animals. This was also observed in humans with chronic atrial fibrillation and patients with dilated cardiomyopathy (DCM) where the decreased passive tension is explained by a switch in titin isoforms [254, 255]. In cardiac tissue, two main isoforms of titin are known, *e.g.* N2B (3000 kDa) and N2BA (3200 to 3350 kDa). The different-length isoforms are a result from alternative splicing. A switch towards more compliant titin-isoforms, seen by an increased N2BA/N2B ratio, could cause an increased cellular compliance that may help in cardiomyocyte survival, possibly in response to stiffening of the heart by increased fibrosis [256]. Whether this mechanism is also responsible for the decreased passive force in our model, needs to be investigated.

4.5.3 Limitations

There are several limitations that should be noted. We did not investigate the amount and structure of T-tubuli and the localization of LTCC. Measurements of intracellular Ca^{2+} in order to assess diastolic Ca^{2+} handling, were not performed but would require further investigation to determine the extent of Ca^{2+} disturbance. In addition, to explain the reduced active and passive forces,

amount of contractile material per cross-sectional area in the cardiomyocytes should be evaluated but are missing in this study.

An important aspect is the electrical remodeling, in particular changes in NCX and K^+-currents in the setting of high levels of HMW-AGEs that were not investigated in this study but would require further evaluation.

Finally, despite negative preliminary data on changes in mitochondrial mass and activity in our model, the potential deleterious role of ROS in the reduced I_{CaL}, altered SERCA2a activity, RyR carboxylation and nitrosylation, all contributing to altered ECC, should be further investigated.

To conclude, rats subjected to high circulating HMW-AGEs display *in vivo* as well *as in vitro* structural and functional remodeling. In that context, our data indicate that HMW-AGEs induce changes observed at the organ level that are related to cellular remodeling. As a consequence, our data suggest that targeting the deleterious effects of HMW-AGEs could be the clue to improve cardiac outcome.

5

Acute exposure of HMW-AGEs reduces cardiomyocyte contractile capacity

5.1 Abstract

Background. Sustained elevated levels of high molecular weight advanced glycation end products (HMW-AGEs) are known to promote cardiac dysfunction. Recent data suggest that acutely elevated AGEs levels occur in situations of increased oxidative stress. Whether this acute increase might have detrimental effects on cardiac function remains unknown. In this study, we investigated whether acute HMW-AGEs exposure affected cardiomyocyte function.

Methods. Single cardiomyocytes from the left ventricle of adult male rats were obtained by enzymatic dissociation through retrograde perfusion of the aorta. L-type Ca^{2+} current density was evaluated during whole cell patch-clamp in the presence or absence of HMW-AGEs (200 µg/ml). Expression of RAGE, janus kinase (JNK) and phosphorylated JNK (pJNK) were assessed by Western blot. Experiments were performed at room temperature. Data are expressed as mean±SEM.

Results. After 4 minutes HMW-AGEs application, unloaded cell shortening was significantly reduced. This impaired contractile function was related to reduced Ca^{2+} current, i.e. I_{CaL}. Finally, effects on contraction and I_{CaL} were not mediated through RAGE signaling pathway activation.

Conclusion. Our study demonstrates that acute exposure to HMW-AGEs results in irreversible cardiomyocyte dysfunction.

5.2 Introduction

The deleterious effects of advanced glycation end products (AGEs) on cardiac performance have been mainly attributed to indirect mechanisms mediated through enhanced coronary artery disease, inflammation and increased fibrosis, rather than a direct effect on cardiomyocyte function [201]. In Chapter 3, we have demonstrated that a sustained increase in circulating high molecular weight AGEs (HMW-AGEs) levels is a cause and not only a consequence of cardiac dysfunction *in vivo* [257]. Indeed, we have shown that a chronic increase in circulating HMW-AGEs is a cause for prominent cardiac dysfunction, characterized by wall hypertrophy, increased heart sphericity, reduced strain and strain rate with preserved ejection fraction. In addition, animals treated with HMW-AGEs displayed increased myocardial fibrosis but no signs of activation of the receptor for advanced glycation end products (RAGE). In Chapter 4, we investigated the effects of HMW-AGEs more in depth on the level of the cardiomyocytes. We observed a profound remodeling on the cellular level seen by cell hypertrophy, reduced contractile properties and myofilament properties with altered Ca^{2+} handling.

Acute effects of increased AGEs have been less intensively studied. Nevertheless, few reports indicate that increased AGEs levels have deleterious effects already in an acute setting. Indeed, in a small group of intensive care unit patients, higher circulating AGEs levels were reported, possibly reflecting an acute increase in oxidative stress [214]. In addition, acute application of AGEs in bovine endothelial cells led to Ca^{2+} leak, possibly via IP_3 receptor activation, resulting in overall reduced intracellular Ca^{2+} levels within few minutes [258]. However, in that study, it is unclear whether LMW- or HMW-AGEs are the AGEs responsible for the altered function observed in endothelial cells. Taken together, sparse data indicate that AGEs could potentially alter excitation-contraction coupling acutely and directly. In this project, we investigated how cardiomyocyte function is affected after acute exposure to increased HMW-AGEs levels.

5.3 Materials and methods

5.3.1 Animal

Healthy male Sprague dawley rats (Charles River Laboratories, Lyon, France) of ± 150 grams were used. This investigation conforms to the EU Directive 2010/63/EU for animal experiments and was approved by a local ethical committee (Ethische Commissie Dierproeven, UHasselt, Diepenbeek, Belgium). The animals for the *in vitro* experiments were sacrified with an overdose of Dolethal (150 mg/kg).

5.3.2 Cardiomyocyte isolation

Single adult cardiomyocytes from the LV were obtained by enzymatic dissociation through retrograde perfusion of the aorta. The hearts were perfused with normal Tyrode (NT) (in mM: NaCl 137, KCl 5.4, $MgCl_2$ 0.5, $CaCl_2$ 1, Na-HEPES 11.8, glucose 10 and taurine 20; pH 7.35) on a Langendorff setup at 37°C. After perfusion with a Ca^{2+} free solution (in mM: NaCl 130, KCl 5.4, KH_2PO_4 1.2, $MgSO_4$ 1.2, Hepes 6, glucose 20, pH 7.2), the tissue was perfused with an enzyme solution (Ca^{2+} free solution, collagenase type II (1.5 g/l; Worthington, Lakewood, USA) and protease type XIV (0.06 g/l; Sigma, Diegem, Belgium)), followed by a low Ca^{2+} solution (0.1 mM $CaCl_2$). The digested LV tissue was minced and subsequently filtered with a mesh of 300 µm. Part of the freshly isolated cells were used to assess fractional cell shortening or electrophysiology measurements. Experiments were performed at room temperature within 6 hours of cell isolation. Cells were incubated for 4 minutes with either HMW-AGEs (200 µg/ml) or BSA (used as a control, 200 µg/ml). Remaining cells were frozen -80°C and used for protein expression experiments.

5.3.3 Unloaded cell shortening

Unloaded cell shortening of intact cardiomyocytes was measured with a video-edge detector, as previously described, at 1 Hz [242] (Crescent Electronics, USA). Cell shortening was normalized to diastolic cell length (L/L_0) and presented as % (fractional cell shortening). Time to peak of contraction (TTP) and time to half time relaxation (time to RT_{50}) were measured to assess kinetics of cell shortening. Fractional cell shortening was measured before and after HMW-AGEs (200 µg/ml) application for 4 minutes.

5.3.4 Electrophysiological recordings

L-type Ca^{2+} current (I_{CaL}) was measured during whole-cell voltage-clamp and was normalized to cell capacitance, as a measure of cell surface, before and after HMW-AGEs (200 µg/ml) application. Patch pipettes (2-3 MOhm) were filled with a pipette solution containing (in mM: 120 KAsp, 20 KCl, 10 HEPES, 5 MgATP, 10 EGTA, 10 NaCl, pH 7.2). I_{CaL} was measured by a single depolarizing step of 150 ms from -70 mV to +10 mV. Current-voltage relationship of I_{CaL} was measured during 10 mV steps ranging from -50 mV to +60 mV [259].

5.3.5 Western blot

BCA protein kit (Thermo Fisher, Erembodegem, Belgium) was used to assess protein concentrations of LV cells of both groups. By using a 12% sodium dodecyl sulphate polyacrylamide gel electrophoresis (SDS-PAGE) gel with a mini protean 3 electrophoresis system (Bio-rad Laboratories, Temse, Belgium), equal amounts of proteins were separated. Gels were transferred to a polyvinylidene fluoride (PVDF) membrane. Blocking was performed during 2 hours with 5% milk in Tris-buffered solution containing 0,1% Tween-20 (TBS-T). Membranes were incubated overnight at 4°C in the presence of specific primary antibodies (RAGE, 1/1000, Santa Cruz, sc-8230, Heidelberg, Germany; janus kinase (JNK), 1/1000, 9295, Cell Signaling Technology, Danvers, USA; phosphorylated janus kinase (pJNK), 1/1000, 9251, Cell Signaling Technology, Danvers, USA). All primary antibodies were diluted in 5% milk-TBS-T. Horseradish peroxidase-conjugated secondary antibodies were used and diluted 1/2000 in 5% milk-TBS-T. Proteins were visualized with the enhanced chemiluminscence (ECL) technique using Pierce ECL Plus Western blotting Substrate (Thermo Fisher, Erembodegem, Belgium). Data were normalized to β-actin protein expression (1/1000, mouse anti-rat IgG, Santa Cruz, sc-47778, Heidelberg, Germany). Densitometry of the protein bands was quantified via the ImageQuant TL software.

5.3.6 Statistical analysis

Statistical analysis was performed with Prism (Graphpad, software, USA). All data are expressed as mean ± standard error of the mean (SEM). Unpaired t-

test, paired t-test or two-way ANOVA was used when appropriate. $P<0.05$ was considered statistically significant.

5.4 Results

5.4.1 Acute exposure of HMW-AGEs reduces Ca^{2+} current resulting in a reduced cell shortening

Figure 5.1A is a representative example of unloaded cardiomyocyte shortening over time at baseline, HMW-AGEs exposure and during wash-out. As summarized in Figure 5.1B (left panel), acute exposure to HMW-AGEs led to a reduced unloaded cardiomyocyte shortening of 25%. Kinetics of contraction and relaxation (respectively TTP and RT$_{50}$) remained unchanged (Figure 5.1B, middle and right panel). Washout of HMW-AGEs for 10 minutes did not reverse the decreased cardiomyocyte function.
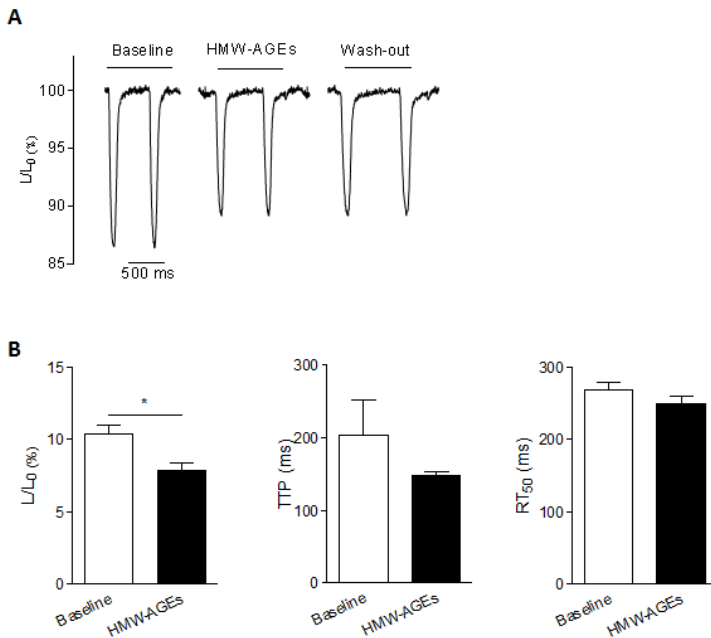
Figure 5.1 HMW-AGEs impair cardiomyocyte contractile properties. (A) Representative example of unloaded cell shortening over time before and after HMW-AGEs application. (B) Fractional cell shortening normalized to cell length (L/L$_0$, %) (left), time to peak of contraction (TTP, ms) (middle) and time to half-relaxation (time to RT$_{50}$, ms) (right) measured at baseline and after acute exposure to HMW-AGEs (n$_{Cells}$ = 31). Data are expressed as mean ± SEM. * denotes p<0.05.

Figure 5.2A is a representative example of I$_{CaL}$ density during whole-cell voltage-clamp elicited by a depolarizing step to +10 mV before and after HMW-AGEs exposure. The peak I$_{CaL}$ density was significantly smaller after HMW-AGEs

(-5.2±0.6 pA/pF *vs* -7.8±1.1 pA/pF at baseline, p<0.05). As shown in the current-voltage relationship summarized in Figure 5.2B, the reduced I_{CaL} was present at most membrane potentials.
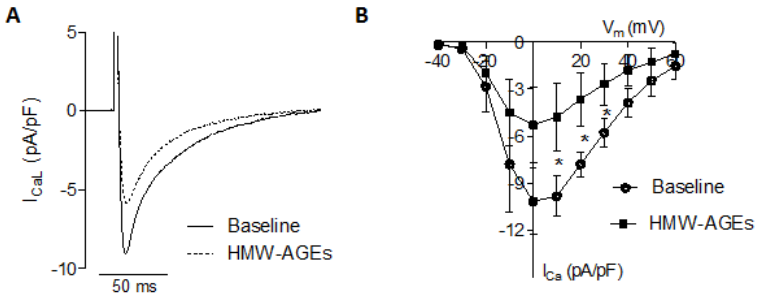
Figure 5.2 Electrophysiological properties of L-type Ca^{2+} current. (A) Representative example of L-type Ca^{2+} current (I_{CaL}) density (pA/pF) recording elicited by a single depolarizing step of 150 ms from -70 to + 10 mV. (B) Current-voltage relationship of I_{CaL} before and after HMW-AGEs (n_{cells} = 12). Data are expressed as mean ± SEM.

5.4.2 The altered cardiomyocyte contractile properties are not mediated through activation of RAGE signaling pathway

Figure 5.3A is a representative Western blot for RAGE, JNK/pJNK ratio and β-actin from cardiomyocytes incubated with or without HMW-AGEs. As shown in Figure 5.3B, expression of RAGE did not differ with exposure to HMW-AGEs. Furthermore, JNK, pJNK and JNK/pJNK ratio remained comparable in treated and untreated cardiomyocytes.
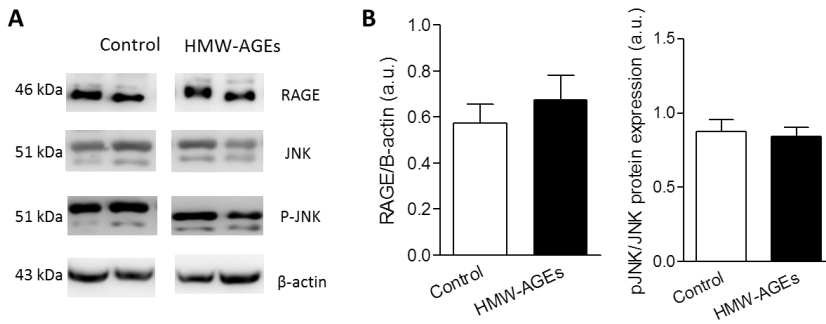
Figure 5.3 RAGE signaling activation is not responsible for the observed contractile changes. (A) Representative Western blot of RAGE, janus kinase (JNK), phosphorylated janus kinase (pJNK) in control cell (not exposured to HMW-AGEs) and cells exposured to HMW-AGEs. (B) Quantitative analysis of the protein expression normalized to β-actin (n = 5 in each group). Data are expressed as mean ± SEM.

5.5 Discussion

In this study, we show that acute exposure of ventricular cardiomyocytes to HMW-AGEs reduces I_{CaL} resulting in reduced unloaded cell shortening, independent of the activation of the AGEs/RAGE signaling pathway.

HMW-AGEs have been shown to be deleterious for cardiac function when chronically elevated [63]. Whether an acute increase in HMW-AGEs would have detrimental effects on cardiomyocyte function is currently unknown. However, some studies report increased AGEs levels in a small group of patients hospitalized in the intensive care unit. In order to offer optimal healthcare for these patients, it is essential to understand the deleterious effect of acutely elevated AGEs levels on cardiac function. The experiments were performed in the presence or absence of HMW-AGEs (200 μg/ml). Serum AGEs levels obtained from ELISA measurements reported to range between 1.6 μmol/l and 2.8 μmol/l in heart failure patients [33]. In our study, HMW-AGEs sample concentration is 2.8 μmol/l, which corresponds to the concentration of 200 μg/ml, therefore justifying the clinical relevance of the chosen concentration used in our study.

A recent study by Yan *et al.* has reported a decreased Ca^{2+} transient in neonatal cardiomyocytes after 8 hours of AGEs exposure [97]. This was further confirmed by Petrova *et al.* who demonstrated an impaired SR Ca^{2+} recycling after 24 hours AGEs exposure of foetal cardiomyocytes [95]. Our study demonstrates that acute and short exposure (4 minutes) of adult cardiomyocytes to HMW-AGEs reduces substantially their contractile capacities, due to a reduced Ca^{2+} influx via L-type Ca^{2+} channels. In our experimental settings, it appeared that the decrease in contractile and electrophysiological function occurred very rapidly (after already 2-3 minutes), was at steady-state after 4 minutes, remained unchanged up to 8 minutes (data not shown) and was not reversible. Such a rapid deleterious effect was also reported by others. Indeed, Naser et *al.* have demonstrated a depletion of Ca^{2+} from the intracellular store in bovine aortic endothelial cells, resulting in overall reduced intracellular Ca^{2+} levels within 5 minutes exposure [258]. However, it is unclear which subtype of AGEs (HMW-AGEs or their low molecular weight counterparts LMW-AGEs) were responsible for the altered endothelial function. In our study, application of HMW-AGEs led to reduced unloaded shortening without affecting its kinetics. Such changes were previously reported by Ma *et*

al. where a decrease in cell shortening in mice cardiomyocytes exposed for 2 hours with methylglyoxal-AGEs was observed. Additionally, they observed significantly longer contractions with slower kinetics. In their study, these alterations were counterbalanced by application of small interfering RNA for RAGE or an anti-RAGE antibody, suggesting that AGEs/RAGE interaction was essential for the observed deleterious effects [96]. In our study however, we could not show changes in I_{CaL} kinetics (data not shown), suggesting the involvement of other possible pathways. It is known that JNK and pJNK are effector molecules of the RAGE signaling pathway that are activated rapidly. Indeed, treatment of human alveolar epithelial cells A549 with methylglyoxal-AGEs for 7 minutes cause an increased pJNK expression, confirming the activation of the RAGE pathway [260]. However, in our experiments, application of HMW-AGEs for 4 minutes did not activate pJNK, suggesting a direct mechanism on cardiomyocytes and Ca^{2+} channels rather than RAGE-mediated deleterious mechanisms. This result is in accordance with what was previously reported on HMW-AGEs mechanism of action [63]. Furthermore, Yan *et al.* demonstrated that blocking RAGE with anti-RAGE IgG was shown to be able to restore AGEs-induced SR Ca^{2+} content reduction and Ca^{2+} transient amplitude. However, exposure time in their study was a lot longer (8 hours) compared to our study (4 minutes) likely involving other signaling pathways and explaining this discrepancy [97].

There are some limitations that should be stated. Whether HMW-AGEs indeed do bind RAGE to activate such signaling pathway or whether exposure time was too short to activate this pathway remains to be clarified. In addition, how HMW-AGEs affect Ca^{2+} channel properties is unknown and remains to be further investigated.

In conclusion, our study demonstrates that acute exposure to HMW-AGEs leads to irreversible cardiomyocyte dysfunction.

6

Pyridoxamine improves survival and limits cardiac dysfunction after MI

6.1 Abstract

Background. Advanced glycation end products (AGEs) play a key role in the progression of heart failure. Whether treatments limiting AGEs formation would prevent adverse left ventricular remodeling after myocardial infarction (MI) remain unknown. We investigated whether pyridoxamine (PM) could limit adverse cardiac outcome in MI.

Methods. Rats were divided into MI, MI+PM and Sham. Echocardiography and hemodynamic parameters were used to assess cardiac function 8 weeks post-surgery. Total interstitial collagen, collagen I and collagen III were quantified using Sirius Red and polarized light microscopy.

Results. PM improved survival following left anterior descending (LAD) coronary artery occlusion. Pre-treatment with PM significantly decreased the plasma AGEs levels. MI rats treated with PM displayed reduced left ventricular end-diastolic pressure and tau compared to untreated MI rats. Deformation parameters were also improved with PM. The preserved diastolic function was related to the reduced collagen content, in particular in the highly cross-linked collagen type I, mainly in the peri-infarct region, although not via TGF-β1 pathway.

Conclusion. Our data indicate that PM treatment prevents the increase in AGEs levels and reduces collagen levels in a rat model of MI, resulting in an improved cardiac phenotype. As such, therapies targeting formation of AGEs might be beneficial in the prevention and/or treatment of maladaptive remodeling following MI.

6.2 Introduction

Heart failure (HF) remains a leading cause of mortality and morbidity worldwide and is defined as the inability of the heart to meet the energy demand of the body. The development of HF is a complex process related to a series of physiological and molecular factors, characterized by structural and functional disorders that still remain incompletely understood [3]. Despite successful acute treatment strategy for coronary events, adverse left ventricular (LV) remodeling following myocardial infarction (MI) often evolves into HF, resulting in cardiac pump failure and development of lethal arrhythmias [261]. Several clinical and experimental studies support the view that advanced glycation end products (AGEs) might have a significant role in cardiac dysfunction [7, 214, 262]. AGEs are proteins and lipids that become non-enzymatically glycated and oxidized after persistent contact with aldose sugar and/or a high degree of oxidative stress. Increased circulating levels and tissue accumulation of AGEs have been extensively reported in patients with diabetes and are associated with adverse outcome and survival, suggesting a possible contribution of AGEs to the increased prevalence of HF in these conditions [7]. Whether the increase in circulating AGEs levels is only a consequence of hyperglycemia remains unclear. Recently, we have demonstrated that a marked elevation in circulating AGEs levels in healthy rats occurs independently of circulating glucose levels. In that setting, animals exhibit diastolic dysfunction with increased cardiac stiffness and collagen deposition [63]. Recent studies corroborate the involvement of AGEs in other pathological conditions than diabetes, such as ischemia-reperfusion, enhanced states of oxidative stress and MI [22, 263]. Additionaly Blackburn et al. reported that AGEs contribute to negative cardiac remodeling and dysfunction in a mice model for MI [264].

AGEs-lowering therapies, targeting either the formation of AGEs and/or their downstream effects such as protein cross-linking or activation of the receptor for advanced glycation end products (RAGE), appear to be very promising. Indeed, treatment of senescent or diabetic rats with pyridoxamine (PM, a natural form of vitamin B6 that inhibits the formation of AGEs) or with ALT-711 (a cross-link breaker) reduced myocardial stiffness, decreased myocardial collagen and limited oxidative stress, improving overall cardiac function [171, 265-268]. Some of these "anti-AGEs" therapies are currently undergoing clinical trials

but results regarding their beneficial effects are still under debate or even not addressed [66, 269, 270]. Indeed, to date, little evidence provide a clear answer on the potential effect of supplemental amounts of PM, alone or with other vitamin supplements, to reduce the risk or severity of cardiovascular disease. In particular, the effect of PM in the setting of MI is unknown. Therefore, the purpose of this study was to investigate whether prevention of AGEs formation, using PM, would limit adverse LV remodeling related to MI. Accordingly, rats subjected to left anterior descending (LAD) coronary artery ligation were treated or not with PM for 9 weeks. The effect of the PM treatment on cardiac function was assessed, using conventional and speckle tracking echocardiography complemented with hemodynamic measurements. Identification of the nature of the remodeling was assessed by *in vitro* measurements using molecular tools.

6.3 Materials and methods

This investigation conforms to the EU Directive 2010/63/EU for animal experiments and was approved by the local Ethical Committee for Animal Experiments of Hasselt University, Belgium.

6.3.1 Experimental protocol

35 Sprague-Dawley male rats (175-200 g) (Charles River Laboratories, L'Arbresle, France) were randomly assigned into 3 groups (Sham, MI, MI+PM). PM treatment (1g/L in drinking water) or placebo (drinking water alone) was started 1-week prior to surgery. After 1 week, rats were subjected to LAD ligation or Sham surgery. Additionally, 7 animals were pre-treated with PM and underwent Sham-surgery. In brief, a left thoracotomy was performed in the intercostal space between the third and fourth rib and the heart was exposed. After opening the pericardium, the LAD was occluded with 6/0 Prolene suture. Successful occlusion of the LAD was confirmed by observation of LV pallor immediately post-ligation. The chest was closed, the lungs re-inflated and the endotracheal tube was gently retracted after restoration of spontaneous respiration. Sham-operated rats underwent identical surgery without LAD ligation. All animals were maintained in a controlled environmental condition of temperature and humidity, were fed a standard pellet diet and had water available *ad libitum*. At the time of sacrifice (8 weeks post-surgery), non-invasive echocardiographic and invasive hemodynamic measurements were performed. Only animals showing clear myocardial dysfunction during echocardiographic examination eight weeks post-surgery were further included in the current study. Finally, the hearts were harvested and transversal sections of the LV were fixed in 4% paraformaldehyde (PFA) overnight and embedded in paraffin. Subsequently, 8 µm thick paraffin sections were cut and stored at room temperature until staining. Residual tissue of the left ventricle was crushed to a fine powder, immediately frozen in liquid nitrogen and stored at -80°C for further protein or gene expression analysis.

6.3.2 Echocardiography

Conventional echocardiographic measurements

As described previously [63], transthoracic echocardiography parameters were assessed 8 weeks post-surgery with a Vivid*i* ultrasound machine (GE Vingmed Ultrasound) using a 10 MHz linear array transducer under 2% isoflurane anesthesia. A standard parasternal long axis image and short-axis views at mid-ventricular level were acquired at a temporal resolution of ≈ 200 frames per second. Conventional echocardiographic parameters (*e.g.* LV end-diastolic diameter (LVEDD), LV end-systolic diameter (LVESD), posterior wall thicknesses (PWT) and anterior wall thicknesses (AWT)) were obtained from the B-mode images at midpapillary level in the parasternal short-axis view. End-systolic volumes (ESV) and end-diastolic volumes (EDV) were calculated by $\pi * D_M^2 * B/6$, where D_M indicates the systolic/diastolic diameter of the ventricle in mid-ventricular short-axis view and B is LV length on parasternal long-axis image. Subsequently, ejection fraction (EF) was measured as (EDV–ESV)/EDV, and expressed in %. End-diastolic shericity index (SI) was calculated by dividing the EDV by the volume of a sphere whose diameter was equal to the major end-diastolic LV long axis. The LV long axis was obtained from the 2D dataset as the longest distance between the center of the mitral annulus and the endocardial apex.

Speckle tracking imaging echocardiography

STI data analysis was performed on an EchoPAC workstation (GE Vingmed Ultrasound, version 7.0.1, Horten, Norway), as described previously [216]. Briefly, measurements of radial and circumferential strain (S_{rad}, S_{circ} respectively) together with radial and circumferential strain rate (SR_{rad} and SR_{circ} respectively) at midventricular level were performed on selected best-quality two-dimensional images. The endocardium was manually traced in an optimal frame, from which a speckle tracking region of interest was automatically selected. The region of interest width was adjusted as needed to fit the wall thickness from endocardium to epicardium. The software detected and tracked the speckle pattern subsistent to the standard two-dimensional echocardiography after segmenting the ventricular silhouette into 6 segments. The tracking quality was then visually inspected, and, if satisfactorily for at least five segments, the

tracing was accepted. End systole and end diastole were defined as the minimum and maximum LV short-axis area, respectively. LV twist was defined as the angular displacement of the LV around its central axis in the short-axis image and was expressed in units of degrees (°). Counterclockwise LV rotation as seen from the apex was expressed as a positive value. LV UR was expressed in degrees per second (°/s).

6.3.3 Hemodynamic measurements

Pressure measurements were performed in all animals with a 2F microtip high-fidelity (Millar Inc, Houston, USA) catheter advanced into the LV via the right carotid artery. A quad-bridge amplifier and PowerLab26T module (AD Instruments, Oxford, United Kingdom) was used to transfer the pressure transducer data to LabChart v7.3.7 software (AD Instruments).

6.3.4 Sirius red staining and polarization microscopy

A Sirius red/Fast Green staining kit (Chondrex, USA) was used to detect total interstitial collagen. After staining, sections were mounted in DPX mounting medium. Images were acquired using a Zeiss Axioplan microscope with an Axiocam HrC camera and 2 polarizing filters. Polarization microscopy was performed to visualize collagen type I and III. The total amount of Sirius red staining and collagen type I and III were quantified using the Axiovision software analysis program. Quantification was averaged from 3-4 regions either located next to the infarct (*i.e.* peri-infarct) or in the LV remote region. Blood vessels were excluded. Data were normalized to global viable area and expressed as percent collagen deposit. Data were analyzed by two independent operators who were blinded for the analysis.

6.3.5 Western blot

Protein concentrations of the LV tissues were determined by the BCA protein assay kit (Thermo Fisher, Erembodegem, Belgium). Proteins were separated on a 12% sodium dodecyl sulfate polyacrylamide gel electrophoresis (SDS-PAGE) gel with a mini protean 3 electrophoresis system (Bio-rad Laboratories, Temse, Belgium), transferred to a polyvinylidene fluoride (PVDF) membrane. The membranes were blocked for 2 hours with 5% milk in Tris-buffered solution

containing 0.1% Tween-20 (TBS-T) followed by overnight incubation at 4°C with a specific lysyl oxidase (LOX) antibody (1/1000, rabbit polyclonal IgG, Abcam, ab31238, Cambridge, United Kingdom). Horseradish peroxidase-conjugated secondary antibodies (DAKO, Belgium) at a dilution of 1/2000 were used. Both primary and secondary antibodies were diluted in 2% milk-TBS-T. LOX was visualized with the enhanced chemiluminescence (ECL) technique using the Pierce ECL Plus Western blotting Substrate (Thermo Fisher, Erembodegem, Belgium). Data were normalized to β-actin protein levels.

6.3.6 Real-time PCR

Total ribonucleic acid (RNA) was extracted from LV tissue using RNeasy fibrous tissue kit (Qiagen, Antwerpen, Belgium) following the manufacturer's guidelines. The concentration and purity of RNA was assessed with the NanoDrop 2000 spectrophotometer (Isogen life science, Temse, Belgium). cDNA was synthesized using high capacity cDNA reverse transcription kit (Invitrogen, Merelbeke, Belgium). The expression of tumor necrosis factor α (TNF-α, forward primer: GTC-TGT-GCC-TCA-GCC-TCT-TC, reverse primer: CCC-ATT-TGG-GAA-CTT-CTC-CT), RAGE (forward primer: ATG-GAA-ACT-GAA-CAC-AGG-AAG-GA, reverse primer: TCC-GAT-AGC-TGG-AAG-GAG-GA), interleukin-6 (IL-6, forward primer: TAG-TCC-TTC-CTA-CCC-CAA-CTT-CC, reverse primer: TTG-GTC-CTT-AGC-CAC-TCC-TTC) and transforming growth factor β1 (TGF-β1, forward primer: GTG-GAC-CGC-AAC-AAC-GCA-ATC-T, reverse primer: CGG-GAC-AGC-AAT-GGG-GGT-TCT) were studied. Real-time PCR was carried out in an optical 96-well plate using the StepOnePlus (Applied Biosystems, Belgium). SYBR Green (Invitrogen, Merelbeke, Belgium) chemistry-based qPCR was performed [211]. Gene expression data were analyzed with MIQE guidelines taken into account [212]. The most stable reference genes, TATA Box Binding Protein (Tbp, forward primer: TGG-GAT-TGT-ACC-ACA-GCT-CCA, reverse primer: CTC-ATG-ATG-ACT-GCA-GCA-AAC-C) and tyrosine 3-monooxygenase/tryptophan 5-monooxygenase activation protein zeta (YWAHZ, forward primer: GAT-GAA-GCC-ATT-GCT-GAA-CTT-G, reverse primer: GTC-TCC-TTG-GGT-ATC-CGA-TGT-C) for this experimental set-up were determined by geNorm analysis and normalization of the data was performed using qBase software (Biogazelle, Zwijnaarde, Belgium).

6.3.7 Assessment of CML and AGEs levels

Plasma levels of total AGEs (MyBiosource, San Diego, CA, USA) and carboxyethyllysine (CEL, MyBiosource, San Diego, CA, USA) were determined using enzyme-linked immunosorbent assay (ELISA).

6.3.8 Statistical analysis

Values are expressed as median [75th percentile; 25th percentile]. Comparisons were performed using non-parametric Mann-Whitney U test or Kruskal-Wallis test with an additional Dunns post-hoc analysis when appropriate. Simple linear regression models were applied to assess the relationship between different parameters. Survival rate was analyzed using the Kaplan-Meier method and log-rank test. Analyses were performed using GraphPad Prism (GraphPad Software, San Diego, CA, USA). A value of $p < 0.05$ was considered statistically significant.

6.4 Results

6.4.1 Pyridoxamine pre-treatment improves survival following MI

Figure 6.1A summarizes survival in all groups. As shown in the Kaplan-Meier plot, all 5 Sham-operated animals survived the surgery. Of the 16 animals untreated that underwent LAD ligation, 7 survived, resulting in a survival rate of 44%. Pre-treatment with PM increased this survival rate to 78%. When observed, mortality occurred within 24 hours after surgery. To evaluate whether a change in circulating AGEs levels was responsible for the improved survival, we checked total circulating AGEs one week after pre-treatment with PM, just before performing the surgery, in the animals that survived the surgery. As shown in Figure 6.1B, animals pre-treated with PM displayed significantly reduced circulating AGEs levels compared to animals receiving placebo.
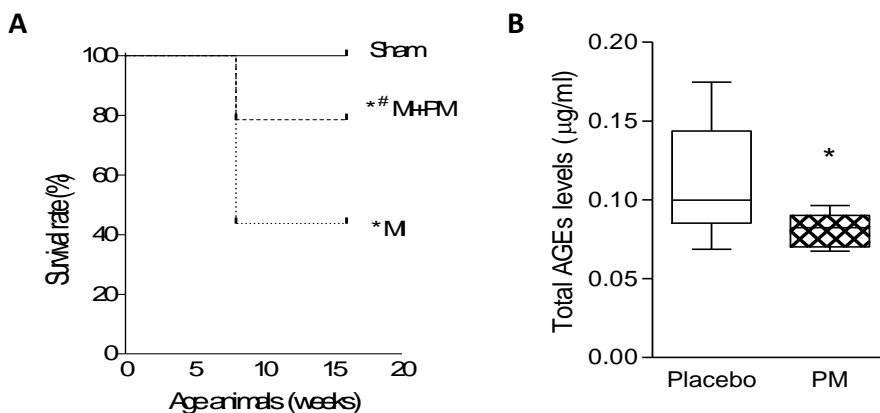
Figure 6.1 Reduced total AGEs levels improves survival post-MI. (A) Kaplan-Meier plot of survival rate in Sham-operated animals (Sham), animals undergoing LAD ligation (MI) and animals undergoing LAD ligation pre-treated with pyridoxamine (MI+PM). N=5, 16 and 14 initially for Sham, MI and MI+PM respectively. (B) Total AGEs levels measured just before surgery, after 1 week PM pre-treatment in Sham (N=5), MI (N=7) and MI+PM (N=11). Data are shown as median [75th percentile; 25th percentile]. * denotes p<0.05 *vs* Sham, # denotes p<0.05 *vs* MI.

6.4.2 Pyridoxamine limits diastolic function in MI but does not prevent hypertrophy

Animals with MI displayed an increased LV mass as demonstrated by the marked increase in heart weight/body weight ratio (HW/BW, Figure 6.2A) and LV weight to body weight ratio (Figure 6.2B). PM pre-treatment was unable to prevent this increased LV mass. Conventional echocardiographic characteristics of the animals are summarized in Table 6.1 Eight weeks post-surgery.
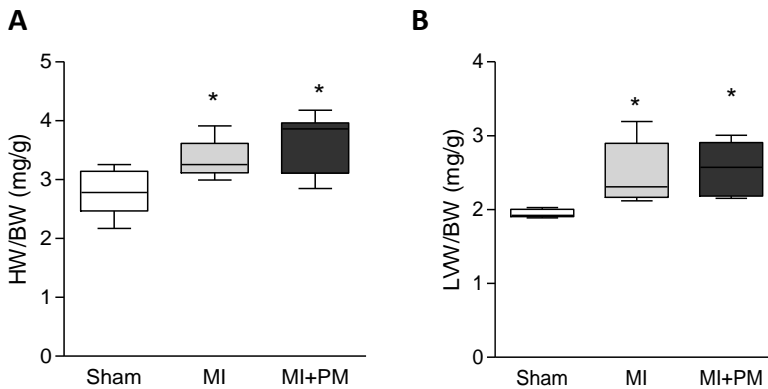
Figure 6.2 Pyridoxamine does not limit increased LV mass. (A) Heart weight to body weight ratio (HW/BW) and (B) LV weight to body weight ratio (LVW/BW). Data are shown as median [75th percentile; 25th percentile] in Sham (N=5), MI (N=5) and MI+PM (N=6). * denotes p<0.05 *vs* Sham

EF, a parameter for global cardiac function, was significantly reduced after MI but not improved in animals undergoing pre-treatment with PM. Furthermore, MI animals displayed changes in LV morphology with signs of wall thinning associated with increased LV diameters and volumes, typical for animals with large MI. PM treatment did not significantly improve these parameters. Finally, SI, a measure for heart geometry, was significantly higher in MI compared to Sham and remained unchanged in the treated animals. However, it is worth noticing that most values, particularly diastolic parameters show a trend towards improved values, indicating a somehow beneficial effect of PM on cardiac parameters.

To identify more subtle changes in cardiac function, speckle tracking imaging (STI)-derived deformation parameters were investigated. As summarized in Table 6.2, strain and strain rate were significantly impaired with MI and improved with PM treatment (Table 6.2). Furthermore, twist and untwist rate (UR), early markers of respectively LV ejection and LV filling, were significantly improved with PM (Table 6.2).

Table 6.1 Effect of pyridoxamine on global conventional echocardiographic parameters.

Parameters	Sham	MI	MI + PM
HR (bpm)	357[365;346]	365[365;342]	358[388;340]
LVEDD (mm)	6.5[6.6;6.4]	8.9[9.1;7.8]*	7.9[8.7;7.4]*
LVESD (mm)	4.2[4.2;4.1]	6.2[6.5,6.0]*	6.4[6.8;6.0]*
AWT (mm)	1.52[1.55;1.47]	0.98[0.98;0.93]*	1.02[1.06;0.98]*
PWT (mm)	1.69[1.74;1.61]	1.33[1.42;1.25]*	1.51[1.77;1.32]
EDV (µL)	288[311;269]	570[599;439]*	451[537;384*]
ESV (µL)	94[100;91]	229[266;216]*	248[289;212]*
SI	0.25[0.26;0.25]	0.42[0.43;0.31]*	0.36[0.42;0.30]*
EF (%)	67[68;67]	48[60;39]*	46[47;45]*

HR, heart rate; LVEDD, left ventricular end-diastolic diameter; LVESD, left ventricular end-systolic diameter; AWT, anterior wall thickness; PWT, posterior wall thickness; EDV, end diastolic volume; ESV, end systolic volume; SI, sphericity index; EF, left ventricular ejection fraction;. Data are shown as median [75th percentile, 25th percentile] in Sham (N=5), MI (N=5) and MI+PM (N=6). * denotes p<0.05 *vs* Sham.

Table 6.2 Effect of pyridoxamine on cardiac deformation parameters.

Parameters	Sham	MI	MI + PM
S_{rad} (%)	42.1[42.2;31.3]	12.3[16.8;9.9]*	16.8[17.8;15.4]*
SR_{rad} (1/s)	8.9[10.2;8.1]	3.8[4.0;3.3]*	4.7[4.8;4.4]*#
S_{circ} (%)	-23.5[-21.7;-23.9]	-10.5[-7.5,-11.1]*	-10.2[-8.3;-12.3]*
SR_{circ} (1/s)	-6.7[-6.5;-6.7]	-2.9[-2.8;-4.4]*	-3.5[-2.9;-4.1]*
LV twist (°)	12.5[13.5;10.3]	5.1[6.5;4.6]*	8.7[9.5;6.8]*#
UR (°/s)	-244[-224;247]	-111[-110;-122]*	-158[-151;-166]*#

S_{rad}, radial strain; SR_{rad}, radial strain rate; S_{circ}, circumferential strain; SR_{circ}, circumferential strain rate. LV twist, left ventricular twist; UR, untwist rate. Data are shown as median [75th percentile, 25th percentile] in Sham (N=5), MI (N=5) and MI+PM (N=6). * denotes $p < 0.05$ *vs* Sham, # denotes $p < 0.05$ *vs* MI.

PM pre-treatment did not improve peak rates of pressure rise and decline (dP/dt_{max} and dP/dt_{min} respectively) (Figure 6.3A). Cardiac diastolic function, evaluated with left ventricular end-diastolic pressure (LVEDP) (Figure 6.3B) and relaxation time constant (*i.e.* tau) (Figure 6.3C), was improved with PM pre-treatment.
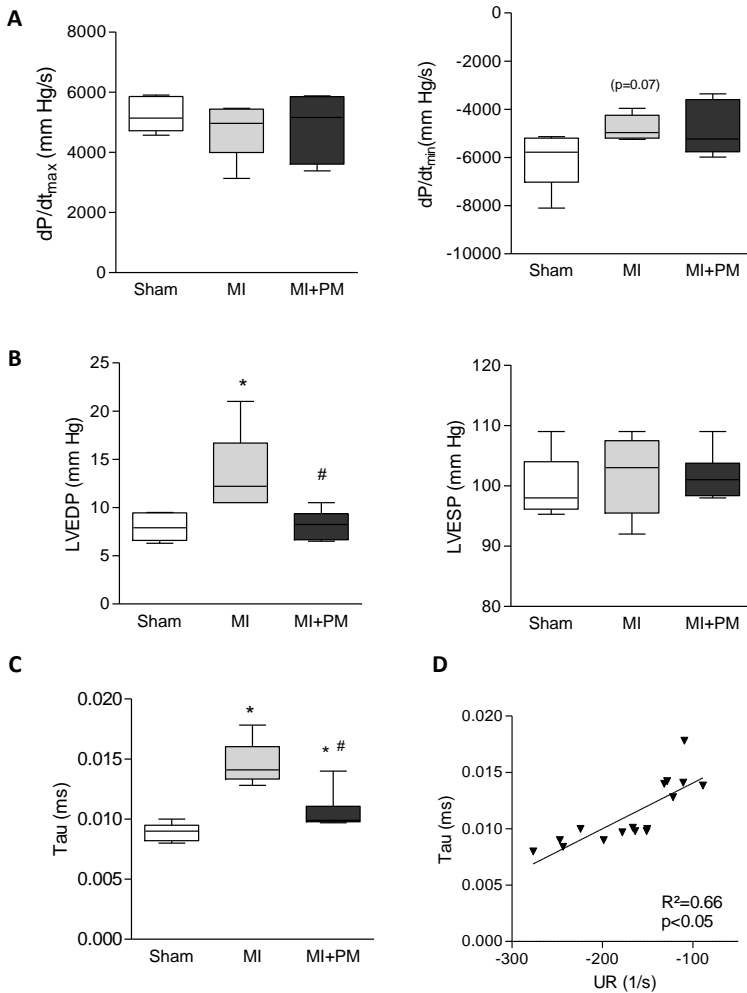
Figure 6.3 Pyridoxamine limits diastolic dysfunction. (A) Peak rate of pressure rise (*i.e.* dP/dt_{max}, left panel) and decline (*i.e.* dP/dt_{min}, right panel). (B) LV end-diastolic (LVEDP, left panel) and LV end-systolic (LVESP, right panel) pressure. (C) Relaxation time constant (*i.e.* tau) and (D) correlation between relaxation time constant (*i.e.* tau) and untwist rate (*i.e.* UR). Data are shown as median [75th percentile; 25th percentile] in Sham (N=5), MI (N=5) and MI+PM (N=6). * denotes p<0.05 *vs* Sham, # denotes p<0.05 *vs* MI.

Left ventricular end-systolic pressure (LVESP) remained however unchanged with PM pre-treatment (Figure 6.3B). In addition, the correlation between tau and untwist rate (UR), parameters obtained independently, further confirmed the improvement of diastolic dysfunction observed *in vivo* with PM pre-treatment (Figure 6.3D). Overall, data indicate an improvement of diastolic but not systolic function in animals pre-treated with PM.

6.4.3 The reduced LOX expression is responsible for the improved diastolic function

As shown in Figure 6.4A, LOX levels were significantly increased in MI. Pre-treatment with PM normalized LOX levels to Sham levels. The increase in LOX levels positively correlated with the increased tau values obtained *in vivo* (Figure 6.4B), confirming the involvement of collagen cross-linking in the stiffness of the LV in the setting of MI. Examination of mRNA levels of TGF-β1 revealed that the modulation of LOX levels was not mediated by TGF-β1 signaling pathway (Figure 6.5C).

To further identify the underlying mechanisms responsible for the dysfunction *in vivo*, we examined collagen levels in the peri-infarct region in the 3 groups. Typical examples of Sirius Red/Fast green staining together with their corresponding pictures obtained with polarized light microscopy in the different groups are shown in Figure 6.5A. As expected, total interstitial collagen was significantly increased in MI, in particular in the peri-infarct area. Pre-treatment with PM significantly reduced total collagen levels in this region (Figure 6.5B).
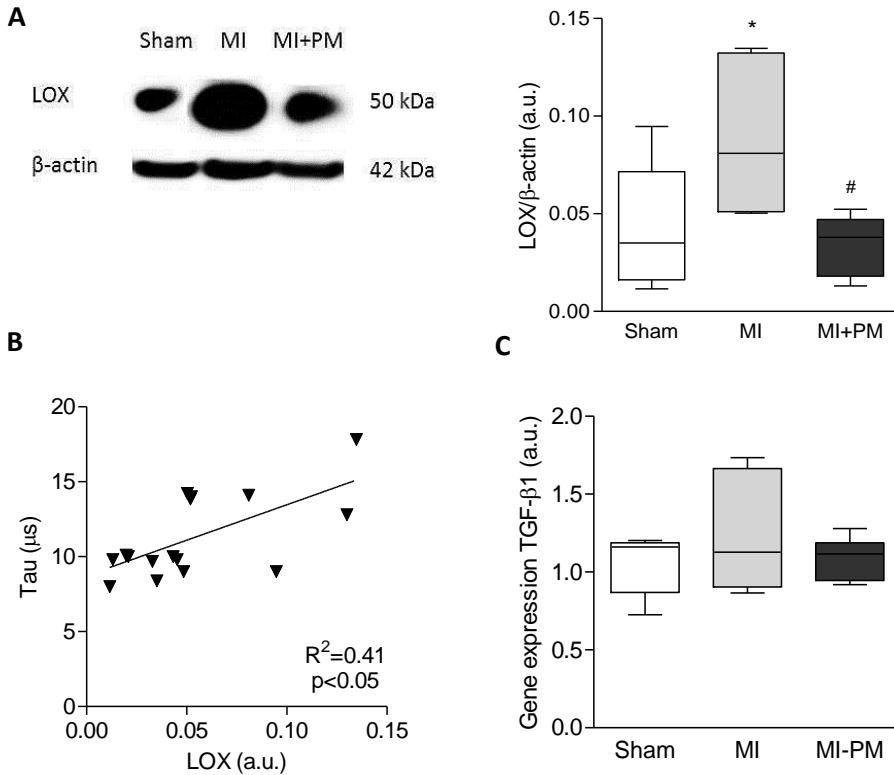
Figure 6.4 The decreased LOX protein expression correlates to the improved relaxation. (A) Representative example and quantitative Western blot of LOX expression normalized to β-actin. (B) Correlation between LOX levels and relaxation time constant (*i.e.* tau). (C) mRNA levels of TGF-β1 in the 3 experimental groups. Data are shown as median [75th percentile, 25th percentile] in Sham (N=5), MI (N=5) and MI+PM (N=6). * denotes p<0.05 *vs* Sham, # denotes p<0.05 *vs* MI.

This reduction was associated with a decrease in highly cross-linked collagen type I (Figure 6.5C, left panel) and a reduced immature collagen type III (Figure 6.5C, right panel). The same trend was observed in the remote region where total interstitial collagen, collagen type I and collagen type III were increased in MI and slightly reduced with PM (data not shown).

Scale bars represent 50 μm
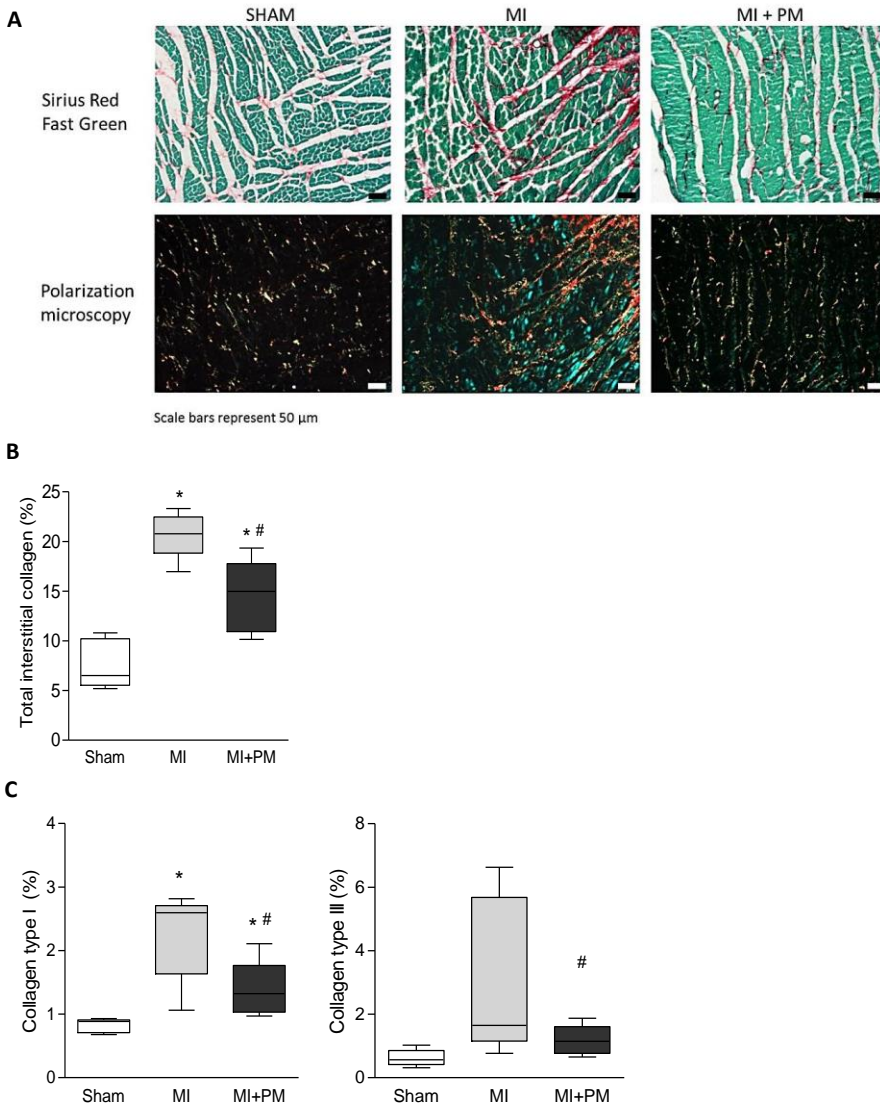
Figure 6.5 Pyridoxamine reduces collagen content. (A, upper panel) Representative images of interstitial collagen obtained with Sirius red/Fast Green in the peri-infarct area. (A, lower panel) Representative images of collagen type I and type III, under polarized light microscopy. The red color indicates the highly cross-linked collagen type I, the green color indicates immature collagen type III. (B) Total interstitial collagen quantification in the peri-infarct area. (C) Collagen type I (left panel) and collagen type III (right panel) quantification in the peri-infarct region. Data are shown as median [75th percentile; 25th percentile] in Sham (N=5), MI (N=5) and MI+PM (N=6). * denotes $p<0.05$ *vs* Sham, # denotes $p<0.05$ *vs* MI.

Finally, to gain further mechanistic insights in the improved survival and improved phenotype, we examined levels of CEL and RAGE in the 3 experimental groups.
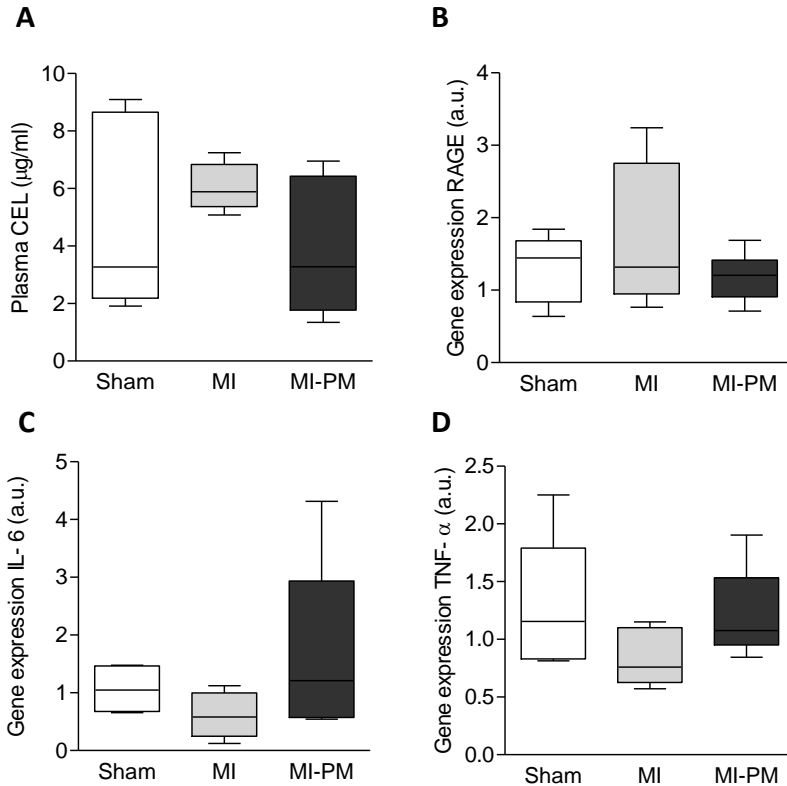
Figure 6.6 RAGE and its downstream effectors are not modulated by pyridoxamine. (A) Plasma N(epsilon)-(carboxyethyllysine (CEL) levels measured 8 weeks post-surgery. Gene expression of RAGE (B), IL-6 (C), TNF-α (D) in the experimental groups. Data are shown as median [75th percentile; 25th percentile] in Sham (N=5), MI (N=5) and MI+PM (N=6).

As shown in Figure 6.6A, CEL levels tended to be increased in MI, and normalized to Sham levels with PM. mRNA levels of RAGE, a potential target for CEL, remained comparable in the groups (Figure 6.6B). Unchanged levels of IL-6 and TNF-α (Figure 6.6C and D), downstream effectors of RAGE, further confirmed the activation of a RAGE-independent pathway by PM.

6.4.4 Pre-treatment with PM has a minor impact on cardiac function in Sham-operated animals

As expected, 9 weeks PM treatment in Sham-operated animals did not lead to measurable physiological cardiac hypertrophy, nor to detectable changes in cardiac function (Table 6.3). However, total interstitial collagen was significantly reduced by 44% in Sham-operated treated animals (6.5 [9.6; 5.9] *vs* 4.3 [5.2; 3.6], p<0.05).

Table 6.3 Effect of pyridoxamine on cardiac parameters in Sham-operated animals.

Parameters	Sham	Sham + PM
HR (bpm)	357[365;346]	365[403;355]
EF (%)	67[68;66]	72[74;67]
AWT (mm)	1.52[1.55;1.47]	1.59[1.67;1.54]
LVEDD (mm)	6.54[6.64;6.37]	6.41[6.69;6.26]
LVEDP (mmHG)	7.9[9.4;6.9]	8.3[9.5;7.4]
Tau (ms)	0.009[0.009;0.008]	0.009[0.009;0.008]
HW/BW (mg/g)	2.78[3.03;2.77]	3.09[3.36;2.91]

HR, heart rate; EF, left ventricular ejection fraction; AWT, anterior wall thickness; LVEDD, left ventricular end-diastolic diameter; LVEDP, left ventricular end-diastolic pressure; Tau, relaxation time constant; HW/BW, heart weight to body weight ratio. Data are shown as median [75th percentile, 25th percentile] in Sham (N=5) and Sham + PM (N=7).

6.5 Discussion

In this study, we show that PM improves survival and limits the adverse cardiac outcome related to MI. The associated improved diastolic function is attributed to a reduced LOX expression resulting in lower level of highly cross-linked collagen type I.

In our study, animals treated with PM displayed a better survival following LAD occlusion compared to untreated littermates. This result is in accordance with other studies examining the underlying mechanisms related to survival in a rat model of diabetes, subjected *ex vivo* to ischemia-reperfusion. Indeed, in this model, the improved survival was attributed to reduced CEL levels and restoration of the signaling pathways counter-acting ischemia and apoptosis by PM [271]. In our model, CEL levels tended to be higher in MI compared to Sham and normalized in MI animals treated with PM. In that context, one would expect that RAGE levels and their downstream effectors (*e.g.* IL-6 and TNF-α) would be modulated by PM, resulting in a better survival and cardiac outcome, as they are known to modulate the response to hypoxic injury, possibly via the activation of JNK and Akt pathways [272].

In our study, gene expression levels of RAGE, IL-6 and TNF-α were comparable in the different groups. These data suggest that in our model, the beneficial effects of the PM treatment on survival are independent of RAGE pathway activation. However, one cannot exclude any potential alterations of RAGE at the protein level as only mRNA of RAGE levels were examined. In addition, IL-6 and TNF-α are cytokines that are also regulated in a RAGE-independent manner. Consequently, further studies are needed to clearly identify the role of RAGE and the underlying pathways involved in this process, such a janus kinase (JNK) and Akt pathways, their phosphorylation status and Bcl-2/Bax ratio as suggested by others [271].

In their study, Almeida *et al*. attribute the improved phenotype to the anti-oxidant and scavenger properties of PM [271]. This hypothesis was also confirmed by Muellenbach *et al.* where PM was shown to improve insulin-resistance in obese pre-diabetic Zucker rats [273]. In our study, however, the potential anti-oxidant properties of PM were not investigated but would require further attention to determine whether the beneficial effect of PM is limited to reduced

infarct size and collagen content. Indeed, a possible explanation for the improved survival rate with PM could be attributed to a decreased infarct size and/or reduced incidence of lethal arrhythmias. Similar hypotheses were drawn in a rat model of cardiac ischemia in which the animals were treated 2 days prior to surgery with pyridoxal 5-phosphate (PLP), a downstream active metabolite of PM [274, 275]. In these studies, authors postulate that the beneficial effect of PLP is mediated through a decreased SR calcium transport activity defect and by a blockade of purinergic receptors. In our study, PM concentration was somehow higher than the concentration used in the study of Dhalla *et al.,* but comparable to others [271, 274]. To date, a direct correlation between PM levels and infarct size is lacking. In our study, infarct size was estimated from the histological sections. We have seen that in treated animals, infarct size tended to be smaller compared to the untreated counterparts (respectively, 22±4% *vs* 32±3% LV mass, p>0.05). In fact, these values are actually an underestimation of the beneficial effect of PM on infarct size since animals with a large MI are likely to be the ones that did not survive the surgery. It has been extensively described that mechanical load is known to determine the extent of remodeling in both peri-infarct and remote regions [276]. In our model, AWT and PWT were reduced in MI, indicating wall thinning, feature typical for a large MI. However, wall thickness in the remote area (*i.e*. PWT) was preserved in the PM treated animals. Our data suggest that mechanical load subjected to the remote area, as a surrogate for infarct size, was reduced in the treated animals, suggesting a somehow reduced infarct size with PM. However, a precise quantification of infarct size using triphenyl tetrazolium chloride (TTC) staining in all animals included in the study was not performed and would deserve further confirmation. Despite this limitation, it is reasonable to think that PM could contribute to an increased survival rate by restricting the infarct size and as a consequence, reducing occurrence of lethal arrhythmias. Whether the increased survival rate is directly correlated to the reduced incidence of arrhythmias or to a blockade of purinergic receptors by PM as suggested by others[275], remains to be elucidated.

Overall, cardiac diastolic function in rats treated with PM was better compared to untreated animals. However, in our hands, most conventional echocardiographic parameters remained comparable between treated and

untreated MI animals. It is currently admitted that changes in conventional echocardiographic parameters occur later in the disease process and may not be sensitive enough to unravel changes in cardiac structure and function. In that context, speckle tracking echocardiography has become a valuable tool to evaluate early and/or subtle changes in cardiac function. Because this imaging modality is less influenced by changes in load and structure, the evaluation of strain, strain rate, twist and untwist rate were shown to accurately reflect (regional) myocardial contractility in patients as well as in rodents [216, 277-279]. Indeed, it has been previously shown that changes in LV rotation, (twist and untwist rates) correlate to diastolic function [280]. In our model, changes in tau correlated with changes in UR, further corroborating the altered diastolic function. PM was able to improve tau and deformation parameters such as SR, twist and untwist rates. Together with the improved LVEDP, our data indicate a beneficial effect of PM on diastolic function in rats with severe cardiac failure.

Circulating AGEs levels are known to be elevated in patients after MI [281, 282]. AGEs contribute to the development of cardiovascular dysfunction by 2 major mechanisms: binding to their cell surface receptor RAGE or cross-linking of intra and/or extracellular proteins [7, 30]. As stated earlier, our data do not indicate the activation of RAGE, meaning that despite the reduced circulating AGEs levels with PM, the observed beneficial effects are not unlikely to be mediated through the modulation of AGE-RAGE pathway. In the other hand, we observed an increase in LOX protein expression after MI which was normalized to Sham values with PM. The involvement of LOX in detrimental remodeling following MI was also confirmed by others in a mouse model of MI [283] and in a rat model of aortocaval fistula-induced volume overload [284]. LOX is a protein involved in the cross-linking of collagen fibrils which contributes to decreased vascular elasticity and myocardial flexibility and hence promoting vascular and myocardial stiffness [99, 285-287]. In their study, Gonzáles-Santamaría conclude that inhibiting LOX could be a potential therapeutic strategy to limit post-MI injury [283]. In our study, we show that indeed, a decrease in LOX protein level correlates with the improved tau measured *in vivo.* These data are also in agreement with studies conducted in chronic HF patients as well as in rats with diastolic dysfunction demonstrating a direct correlation between collagen cross-linking and cardiac stiffness [99, 257].

Accordingly, we also show that total interstitial collagen is increased in both the peri-infarct and remote area [99, 286]. We attribute this increase to higher collagen type I and collagen type III levels, mainly in the peri-infarct region, but also, to a smaller extent, in the remote region. Remarkably, PM reduced, but not completely normalized, collagen levels in the LV. The concomitant reduction in collagen content and LOX expression suggests a reduced collagen cross-linking, resulting in an increased tissue compliance and improved diastolic function. Our data are in line with other studies conducted in animal models of diabetes or in senescent rats [267, 269, 288, 289]. LOX expression is regulated via TGF-β1 by either the PI3K/Akt, Smad3 or mitogen-activated protein kinase (MAPK) signaling pathway [290]. Increased mRNA and protein expression of TGF-β1 has been shown in 1 week old scar and within the peri-infarct region after MI and is associated with increased synthesis of pro-collagen type I [291]. This is due to the activation of TGF-β-R1 which promotes fibroblast differentiation and pro-collagen type I, III and LOX secretion [283, 292]. Once LOX has entered the extracellular matrix, it is activated by periostin and/or osteopontin and leads to cross-linking of collagen type I, stiffening of the myocardium and ultimately diastolic dysfunction [220, 293, 294]. Therefore, one could speculate that the beneficial effect of PM on LOX and as a consequence on interstitial fibrosis, could be mediated via the TGF-β1 pathway. However, in our study, mRNA levels of TGF-β1 revealed no significant difference between PM treated and non-treated groups indicating no marked increase in TGF-β1 synthesis. However, the role of TGF-β1 should not be excluded entirely since it is stored in the extracellular matrix of normal myocardium as a latent protein complex. After activation, the latent binding protein (LTBP) is sequestered from TGF-β1 switching it to a functional growth factor promoting fibroblast differentiation and LOX secretion [295]. Several molecules could be held responsible for activation of latent TGF-β1 but the mechanism is not well-known. Some studies report that increased ROS release due to oxidative stress promotes latent TGF-β1 activation [296]. Since PM has been shown to exhibit anti-oxidant effects [165, 297], we hypothesize that PM decreases LOX expression indirectly through reduction in ROS production and a concomitant decrease in latent TGF-β1 activation. This would result in either a decrease in fibroblast activation and reduction in collagen and LOX secretion. In fact, changes in TGF-β1 are generally also associated with changes in pro-

inflammatory markers, and as mentioned previously, IL-6 and TNF-α levels were not changed in our study. Further investigation is therefore needed to unravel this aspect, examining a broad range of potential candidates and alternative pathways. For instance, it has been previously shown that LOX expression is tightly regulated by the pro-fibrotic cytokine connective tissue growth (CTGF). In addition, the small RhoGTPase Rac 1 is known to regulate CTGF expression in cardiac fibroblasts [298]. On the other hand, angiotensin II (Ang II) is known to be upregulated in cardiac remodeling post-MI and has been shown to activate Rac. How PM interferes in this signaling pathway remains unclear and would deserve attention.

There is a specific limitation in our study that should be acknowledged, being the lack of evaluation of cardiomyocyte remodeling in both peri-infarct and remote area. Due to the beneficial remodeling of the extracellular matrix and the trend towards the reduced infarct size, one would expect that the mechanical load subjected to the viable myocardium would be reduced with PM, leading to a somehow beneficial effect on cardiomyocyte function. In that context, the impact of PM on cardiomyocyte contractility and intracellular calcium handling requires therefore further evaluation.

To conclude, our data indicate that PM treatment reduces circulating AGEs and tissue collagen levels in a rat model of MI, resulting in an improved cardiac phenotype. PM might be a useful supplement to prevent and/or limit adverse remodeling related to ischemic injury.

7

Several clinical and experimental studies support the view that advanced glycation end products (AGEs) might have a significant role in many pathological situations, in particular in cardiac failure [32, 33, 264, 299]. AGEs accumulation is a normal process that occurs with aging, when the turnover rate of protein for glycoxidation is reduced [61]. Increased circulating AGEs levels and tissue accumulation have been reported to occur early in lifetime in patients with diabetes and are associated with adverse outcome and survival. Additionally, AGEs are also linked to play a role in cardiovascular diseases [30, 200]. AGEs are proteins or lipids that become glycated and oxidized after persistent contact with reducing sugars or short-chain aldehydes [10, 25]. Based on their molecular weight, AGEs can be categorized in two classes: low molecular weight AGEs (LMW-AGEs) and high molecular weight AGEs (HMW-AGEs). There is growing evidence reporting that HMW-AGEs contribute to the development and progression of cardiovascular dysfunction *in vivo*. In this thesis, we aimed at characterizing the cardiac dysfunction induced by HMW-AGEs. First, we focused on *in vivo* characteristics by means of echocardiography and hemodynamic measurements **(Chapters 3 and 4)**. Thereafter, we went deeper to unravel the underlying mechanisms and investigated the functional changes at the cellular level after chronic HMW-AGEs application **(Chapter 4)**. As an acute increase in AGEs levels can occur in intensive care patients, we also assessed the effects of HMW-AGEs acutely on cardiomyocyte function **(Chapter 5)**. Finally, the effect of blocking AGEs formation by pyridoxamine (PM) was investigated in a rat model of myocardial infarction (MI) **(Chapter 6)**.

7.1 The chronic effects of HMW-AGEs on cardiac function

In **Chapter 3**, we have demonstrated that animals displayed a sustained increase in circulating total AGEs without hyperglycaemia. HMW-AGEs injections induced cardiac dysfunction characterized by wall hypertrophy, increased heart sphericity, reduced strain and strain rate with preserved ejection fraction. Rather than via activation of AGEs/RAGE signaling pathway, the deleterious effects of HMW-AGEs on heart function are likely mediated via an increased collagen cross-linking. In addition, the prominent cardiac fibrosis is associated with an increased LOX expression.

In **Chapter 4**, we investigated the effects of HMW-AGEs on the cellular level. We show that single cardiomyocytes were significantly wider. We also demonstrated that unloaded cell shortening was significantly reduced in HMW-AGEs and was associated with slower kinetics. Peak I_{CaL} density was significantly decreased in HMW-AGEs and LTCC inactivation was significantly shifted towards more negative potentials, meaning that LTCCs are less available and inactivated more rapidly, compared to controls. Therefore, less Ca^{2+} can be transported in the cytosol resulting in a reduced I_{CaL}. However, the exact underlying mechanism of HMW-AGEs induced Ca^{2+}-channel properties changes remains currently unexplained. Whether the change in LTCC properties is mediated through RAGE activation is unlikely. Indeed, as previously mentioned and further confirmed in **Chapter 3**, we have shown that HMW-AGEs mechanism of action is not mediated through RAGE activation. Additional to reduced I_{CaL}, impaired myofilament properties have been shown to be responsible for a reduced unloaded cell shortening. Finally, passive tension was determined in skinned cardiomyocytes. Cardiomyocyte passive forces play an important role in cardiac muscle as it is part of the diastolic wall tension that determines the extent of filling of the heart [253]. In our study, we observed a significantly decreased passive force in cardiomyocytes from the treated animals. However, the exact mechanism how HMW-AGEs change the properties of the myofilaments are at the moment unknown.

All these findings indicate that rats subjected to high circulating HMW-AGEs display structural and functional remodeling.

7.2 Differences between acute and chronic effects of HMW-AGEs

Acutely, we observed that HMW-AGEs reduce Ca^{2+}-current resulting in a reduced cell shortening, independent of the activation of the AGEs/RAGE signaling pathway **(Chapter 5)**. One uncertainty relies on the fact that we are not sure whether HMW-AGEs can interact with RAGE within 4 minutes incubation. Co-immunoprecipitation experiments, with different incubation times, are needed to answer this question. However, previous functional data in a more chronic setting indicate that the RAGE pathway is not activated in the presence of HMW-AGEs suggesting that the effect of HMW-AGEs is not mediated through a direct binding of HMW-AGEs to RAGE. As opposed to our data, Chen et al. have shown

in rat kidney fibroblasts that 200 µg/ml LMW-AGEs led to RAGE activation as shown by the increased JNK phosphorylation within few minutes [300]. In our current data, JNK and JNK phosphorylation levels were not increased after 4 minutes HMW-AGEs, suggesting that RAGE signaling was not activated after HMW-AGEs application. The fact that after 4 minutes, I_{CaL} was reduced and that the effect remained stable and irreversible further suggests that HMW-AGEs bind on L-type Ca^{2+} channels with a high affinity. Additional data demonstrated no changes in intrinsic properties of Ca^{2+} channels (e.g. voltage-dependence inactivation of I_{CaL}). Consequently, we hypothesize that the observed decreased I_{CaL} in our study could be caused by a decreased amount of Ca^{2+} ions that could pass the channel pore, through binding of HMW-AGEs to L-type Ca^{2+} channels. Upon binding HMW-AGEs would block the channel pore. To further confirm this hypothesis, co-immunoprecipitation experiments between HMW-AGEs and DHP-receptor α-subunit should be performed in future studies.

In the chronic setting, we show that cardiac dysfunction *in vivo*, induced by HMW-AGEs, is the result of profound cardiomyocyte remodeling, including cell hypertrophy, reduced contractile and myofilament properties associated with altered Ca^{2+} current without any sign of AGEs/RAGE activation **(Chapter 3)**.

In **Chapter 4**, at the cellular level a remodeling was observed characterized by decreased unloaded shortening of intact cardiomyocytes associated with slower kinetics, which may be caused by a reduced Ca^{2+} influx through L-type Ca^{2+} channels. These findings are already discussed in **point 7.1**.

To conclude, it is difficult to compare the results obtained from the acute study with the chronic study since one is an *in vitro* study and the other an *in vivo*. Further studies with other experimental designs should be performed in order to answer this question.

7.3 Effect of PM as pre-treatment in myocardial infarction

In **chapter 6**, we show that PM improves survival and limits the adverse cardiac outcome related to MI. The associated improved diastolic function is attributed to a reduced LOX expression resulting in lower levels of highly cross-linked collagen type I.

PM was able to improve tau and deformation parameters such as SR, twist and untwist rates. Together with the improved LVEDP, our data indicate a beneficial effect of PM on diastolic function in rats with severe cardiac failure. We also observed an increase in LOX protein expression after MI which was normalized to Sham values with PM. The involvement of LOX in detrimental remodeling following MI was also confirmed by others in a mouse model of MI [283] and in a rat model of aortocaval fistula-induced volume overload [284]. LOX is a protein involved in the cross-linking of collagen fibrils which contributes to decreased vascular elasticity and myocardial flexibility and hence promoting vascular and myocardial stiffness [99, 285-287]. In **Chapter 6**, we show that indeed, a decrease in LOX protein level correlates with the improved Tau measured *in vivo.* These data are also in agreement with studies conducted in chronic HF patients as well as in rats with diastolic dysfunction demonstrating a direct correlation between collagen cross-linking and cardiac stiffness [99, 257].

7.4 Limitations of this work

The limitations of each chapter are already discussed. However, there are some general limitations that should be added.

7.4.1 Physiological relevance of our HMW-AGEs

We injected healthy animals with HMW-AGEs prepared by incubating bovine serum albumin (BSA) with glycolaldehyde. Glycolaldehyde formed either as a fragmentation product in the Maillard reaction or as a result of the myeloperoxidase-hydrogen peroxide-chloride (MPO) reaction can also react with proteins which result in the formation of AGEs.[44] The reaction between glycolaldhyde and amino acids can lead to the formation of AGEs such as CML and glycolaldehyde-pyridine (GA-pyridine) [56]. Several reports showed increased levels of these AGEs in diabetes patients and therefore indicating a role for modification of proteins with aldehydes in a diabetic setting [56, 59, 60]. Additionally, the presence of GA-pyridine has been found in human atherosclerotic fibrotic lesions and in glomerular mesangium in renal diseases, indicating their involvement in pathological situations [301, 302]. However, until now, no data have been available on the effect of glycolaldehyde-derived AGEs in the human heart *in vivo* as well as *in vitro*. Furthermore, Takeuchi *et al*. developed non-

carboxymethyllysine anti-AGE antibodies that recognize serum proteins modified by short chain sugars or aldehydes (*e.g.* glyceraldehyde and glycolaldehyde) and dicarbonyl compounds (*e.g.* methylglyoxal and glyoxal). They show in their study that glycolaldehyde derived AGEs are present in serum from diabetic patients [303]. These results confirm the physiological relevance of glycolaldehyde-derived AGEs. Finally, immunoblotting of serum protein samples from diabetic patients with glycolaldehyde-derived AGEs antibodies showed a high immunoreactivity around 200 kDA, indicating the presence of HMW glycolaldehyde-derived AGEs in diabetic patients [303]. However, we did not perform these experiments on our own HMW-AGEs in order to proof their physiological relevance.

In our study, we valilated our sample by comparing it with a commercial available glycolaldehyde-derived AGEs sample by means of fluorescence spectroscopy and coomassie blue staining **(Chapter 3)**. These data demonstrated the presence of fluorescent AGEs and AGEs with a high molecular weight. Finally, we measured also some AGEs molecules with ultra-performance liquid chromatography tandem mass spectrometry (UP-LC/MS/MS) and found 131 µmol/l N-carboxymethyllysine (CML), 6.1 µmol/l carboxyethyllysine (CEL) and 7.2 µmol/l methylglyoxal-derived hydroimidazoline (MG-H1) in our sample [304-307]. However, these molecules only respresent a small fraction of total AGEs present in our sample. Furthermore, we do not know the degree of cross-linking. However, the presence of high molecular weight proteins in the SDS-PAGE gel gives an indication of high degree of cross-linking.

Regarding HMW-AGEs, we do not know the exact composition of the glycolaldehyde-derived AGEs samples we used. Despite this limitation, data indicate that (1) the AGEs have a HMW, (2) UP-LC/MS/MS can detect CML, CEL and MG-H1, (3) fluorescent AGEs are present in our sample and (4) the used ELISA kit (see material and methods chapter 2) commercially available was able to detect our HMW-AGEs. Additionally, future experiments are necessary to proof their physiological relevance in humans.

7.4.2 General limitations

It is important to keep in mind that the work presented in this thesis was conducted in rats and translation to humans is not always easy. However, the use of a rodent animal models has provided a valuable insight into the human cardiac physiology and disease. Small rodents are easier to handle and house, have a shorter gestation time and have lower maintenance cost than larger animals models [308]. These characteristics make small rodent models logistically and economically the most used model for cardiac physiology. Additionally, it is possible to link *in vivo* cardiac parameters (such as echocardiography, pressure-volume loops, *etc*) with *in vitro* and *ex vivo* functional studies [309, 310].

The overall anatomical structure in rodents and humans is comparable. However, at the physiological level there are important differences that translate into different underlying mechanisms, the most important to mention is the very high heart rate in rats compared to humans. In rats, a rapid systolic contraction and diastolic filling is necessary for maintaining their cardiac output. As a consequence, the action potential duration in rodents is much shorter compared with humans [311-313]. Additionally, during relaxation Sarcoplasmic reticulum Ca^{2+} ATPase (SERCA) is responsible for resequestration of 90-92% of calcium in rats while in humans it accounts for 76% [229, 314, 315]. In other words, the contribution of Na^+/Ca^{2+} exchanger (NCX) in the removal of calcium during diastole is much larger in humans compared to rodents and has been shown to be further increased in pathological situations [316].

7.5 Future perspectives

Future experiments are already discussed in each research chapter. However, there are some general future perpectives that should be stated.

7.5.1 Effect of HMW-AGEs on the vasculature

This thesis focuses only on the acute and chronic effects of HMW-AGEs on the global heart function and more in depth on the cardiomyocytes. However, as already mentionned, AGEs have also deleterious effects on the vasculature leading to decreased vascular elasticity and promotion of vascular stiffness. To date, there is no data available on the effect of HMW-AGEs specific on the vasculature. A broader knowledge on the effects of HMW-AGEs on the

vasculature would be interesting to get a broader view of the deleterious effects of HMW-AGEs on cardiovascular function.

7.5.2 Involvement of PM in neutralizing HMW-AGEs

In this thesis, we evaluate the effects of PM treatment on global AGEs levels, without making a distinction between LMW-AGEs and HMW-AGEs. Whether PM targets specifically HMW-AGEs remains unknown. Therefore, combining pre-treatment of PM with injections of HMW-AGEs would give more insights in the involvement of PM in neutralizing HMW-AGEs and the therapeutic strategy targeting HMW-AGEs.

7.5.3 Is there a role for HMW-AGEs in chemotherapy-related cardiotoxicity?

Heart failure and cancer are the two leading causes of mortality worldwide, accounting for 46.1 % of deaths [317, 318]. Improved oncologic treatments have contributed to increased survival in cancer patients. However, chemotherapy-related cardiotoxicity are a major cause of mortality in people living with or surviving cancer [319, 320]. Despite successful progresses in the understanding of molecular and cellular mechanisms behind chemotherapy-related cardiotoxicity, the treatments for these patients are still suboptimal [321, 322]. It is known that the generation of reactive oxygen species (ROS) and oxygen free radicals play an important role in chemotherapy-related cardiotoxicity [321, 323]. As already stated in the introduction, AGEs can be formed in situations of increased oxidative stress. Although there is no evidence in literature about the role of AGEs in chemotherapy-related cardiotoxicity, increased AGEs levels in these patients are expected but remain to be further confirmed. In this context, pre-treatment of cancer patients with for example PM could possible attenuate chemotherapy-related cardiotoxicity. However, this remains speculative and future experiments are necessary to proof this hypothesis.

8

REFERENCES

Reference list

1.   U N. United Nations population division: Population aged 65 or over 2012. 2012.

2.   WH. O. Cardiovascular disease 2013. 2013.

3.   Braunwald E. Research advances in heart failure: a compendium. Circulation research. 2013;113(6):633-45.

4.   LS L. Pathophysiology of heart failure. Fifth, North American Edition: Williams & Wilkins. 2010.

5.   Marzilli M, Merz CN, Boden WE, Bonow RO, Capozza PG, Chilian WM, et al. Obstructive coronary atherosclerosis and ischemic heart disease: an elusive link! J Am Coll Cardiol. 2012;60(11):951-6.

6.   Fukami K, Yamagishi SI, Okuda S. Role of AGEs-RAGE system in cardiovascular disease. Curr Pharm Des. 2013.

7.   Hartog JW, Voors AA, Bakker SJ, Smit AJ, van Veldhuisen DJ. Advanced glycation end-products (AGEs) and heart failure: pathophysiology and clinical implications. European journal of heart failure. 2007;9(12):1146-55.

8.   Jandeleit-Dahm K, Cooper ME. The role of AGEs in cardiovascular disease. Curr Pharm Des. 2008;14(10):979-86.

9.   Acharya AS, Manning JM. Reaction of glycolaldehyde with proteins: latent crosslinking potential of alpha-hydroxyaldehydes. Proceedings of the National Academy of Sciences of the United States of America. 1983;80(12):3590-4.

10.   Singh R, Barden A, Mori T, Beilin L. Advanced glycation end-products: a review. Diabetologia. 2001;44(2):129-46.

11.   Thornalley PJ. Clinical significance of glycation. Clin Lab. 1999;45:263-73.

12.   LC. M. Action des acides aminés sur les sucres: formation des mélanoïdines par voie méthodique. C R Acad Sci. 1912;154:66-8.

13.   Luevano-Contreras C, Chapman-Novakofski K. Dietary advanced glycation end products and aging. Nutrients. 2010;2(12):1247-65.

14.   Rerat A, Calmes R, Vaissade P, Finot PA. Nutritional and metabolic consequences of the early Maillard reaction of heat treated milk in the pig. Significance for man. European journal of nutrition. 2002;41(1):1-11.

15.   Seiquer I, Diaz-Alguacil J, Delgado-Andrade C, Lopez-Frias M, Munoz Hoyos A, Galdo G, et al. Diets rich in Maillard reaction products affect protein digestibility in adolescent males aged 11-14 y. The American journal of clinical nutrition. 2006;83(5):1082-8.

16.   Vlassara H, Striker GE. Advanced glycation endproducts in diabetes and diabetic complications. Endocrinology and metabolism clinics of North America. 2013;42(4):697-719.

17.   Goldberg T, Cai W, Peppa M, Dardaine V, Baliga BS, Uribarri J, et al. Advanced glycoxidation end products in commonly consumed foods. Journal of the American Dietetic Association. 2004;104(8):1287-91.

18.   Uribarri J, Woodruff S, Goodman S, Cai W, Chen X, Pyzik R, et al. Advanced glycation end products in foods and a practical guide to their reduction in the diet. Journal of the American Dietetic Association. 2010;110(6):911-16 e12.

19.   Brownlee M. Advanced protein glycosylation in diabetes and aging. Annual review of medicine. 1995;46:223-34.

20.   Abate G, Marziano M, Rungratanawanich W, Memo M, Uberti D. Nutrition and AGE-ing: Focusing on Alzheimer's Disease. Oxid Med Cell Longev. 2017;2017:7039816.

21.   Hasegawa S, Jao TM, Inagi R. Dietary Metabolites and Chronic Kidney Disease. Nutrients. 2017;9(4).

22.   McNair ED, Wells CR, Qureshi AM, Basran RS, Pearce C, Orvold J, et al. Low levels of soluble receptor for advanced glycation end products in non-ST elevation myocardial infarction patients. The International journal of angiology : official publication of the International College of Angiology, Inc. 2009;18(4):187-92.

23.   Willemsen S, Hartog JW, Heiner-Fokkema MR, van Veldhuisen DJ, Voors AA. Advanced glycation end-products, a pathophysiological pathway in the cardiorenal syndrome. Heart Fail Rev. 2012;17(2):221-8.

24.   Nagai R, Matsumoto K, Ling X, Suzuki H, Araki T, Horiuchi S. Glycolaldehyde, a reactive intermediate for advanced glycation end products, plays an important role in the generation of an active ligand for the macrophage scavenger receptor. Diabetes. 2000;49(10):1714-23.

25.   Ott C, Jacobs K, Haucke E, Navarrete Santos A, Grune T, Simm A. Role of advanced glycation end products in cellular signaling. Redox Biol. 2014;2:411-29.

26.   Takeuchi M, Takino J, Furuno S, Shirai H, Kawakami M, Muramatsu M, et al. Assessment of the concentrations of various advanced glycation end-products in beverages and foods that are commonly consumed in Japan. PloS one. 2015;10(3):e0118652.

27.   Goldin A, Beckman JA, Schmidt AM, Creager MA. Advanced glycation end products: sparking the development of diabetic vascular injury. Circulation. 2006;114(6):597-605.

28.   Monnier VM, Sun W, Sell DR, Fan X, Nemet I, Genuth S. Glucosepane: a poorly understood advanced glycation end product of growing importance for diabetes and its complications. Clinical chemistry and laboratory medicine. 2014;52(1):21-32.

29.   Peyroux J, Sternberg M. Advanced glycation endproducts (AGEs): Pharmacological inhibition in diabetes. Pathol Biol (Paris). 2006;54(7):405-19.

30.   Hegab Z, Gibbons S, Neyses L, Mamas MA. Role of advanced glycation end products in cardiovascular disease. World J Cardiol. 2012;4(4):90-102.

31.   Zieman SJ. Advanced glycation end products cross-linking pathophysiologic role and therapeutic target in cardiovascular disease. Le Jacq. 2004.

32.   Koyama Y, Takeishi Y, Arimoto T, Niizeki T, Shishido T, Takahashi H, et al. High serum level of pentosidine, an advanced glycation end product (AGE), is a risk factor of patients with heart failure. Journal of cardiac failure. 2007;13(3):199-206.

33.   Willemsen S, Hartog JW, van Veldhuisen DJ, van der Meer P, Roze JF, Jaarsma T, et al. The role of advanced glycation end-products and their receptor on outcome in heart failure patients with preserved and reduced ejection fraction. American heart journal. 2012;164(5):742-9 e3.

34.   Lorenzi M. The polyol pathway as a mechanism for diabetic retinopathy: attractive, elusive, and resilient. Experimental diabetes research. 2007;2007:61038.

35.   Schalkwijk CG, Stehouwer CD, van Hinsbergh VW. Fructose-mediated non-enzymatic glycation: sweet coupling or bad modification. Diabetes/metabolism research and reviews. 2004;20(5):369-82.

36.   Takeuchi M, Yanase Y, Matsuura N, Yamagishi Si S, Kameda Y, Bucala R, et al. Immunological detection of a novel advanced glycation end-product. Molecular medicine. 2001;7(11):783-91.

37.   Marino L, Maya-Aguirre CA, Pauwels K, Vilanova B, Ortega-Castro J, Frau J, et al. Glycation of Lysozyme by Glycolaldehyde Provides New Mechanistic Insights in Diabetes-Related Protein Aggregation. ACS Chem Biol. 2017;12(4):1152-62.

38.   Thornalley PJ. Dicarbonyl intermediates in the maillard reaction. Annals of the New York Academy of Sciences. 2005;1043:111-7.

39.   Glomb MA, Monnier VM. Mechanism of protein modification by glyoxal and glycolaldehyde, reactive intermediates of the Maillard reaction. The Journal of biological chemistry. 1995;270(17):10017-26.

40.   Moheimani F, Morgan PE, van Reyk DM, Davies MJ. Deleterious effects of reactive aldehydes and glycated proteins on macrophage proteasomal function: possible links between diabetes and atherosclerosis. Biochimica et biophysica acta. 2010;1802(6):561-71.

41.   Ahmed N. Advanced glycation endproducts--role in pathology of diabetic complications. Diabetes research and clinical practice. 2005;67(1):3-21.

42.   Ahmed N, Babaei-Jadidi R, Howell SK, Beisswenger PJ, Thornalley PJ. Degradation products of proteins damaged by glycation, oxidation and nitration in clinical type 1 diabetes. Diabetologia. 2005;48(8):1590-603.

43.   Kisugi R, Kouzuma T, Yamamoto T, Akizuki S, Miyamoto H, Someya Y, et al. Structural and glycation site changes of albumin in diabetic patient with very high glycated albumin. Clinica chimica acta; international journal of clinical chemistry. 2007;382(1-2):59-64.

44.   Anderson MM, Hazen SL, Hsu FF, Heinecke JW. Human neutrophils employ the myeloperoxidase-hydrogen peroxide-chloride system to convert hydroxy-amino acids into glycolaldehyde, 2-hydroxypropanal, and acrolein. A mechanism for the generation of highly reactive alpha-hydroxy and alpha,beta-unsaturated aldehydes by phagocytes at sites of inflammation. The Journal of clinical investigation. 1997;99(3):424-32.

45.   Nagaraj RH, Sady C. The presence of a glucose-derived Maillard reaction product in the human lens. FEBS letters. 1996;382(3):234-8.

46.   Robison TW, Zhou H, Kim KJ. Generation of glycolaldehyde from guinea pig airway epithelial monolayers exposed to nitrogen dioxide and its effects on sodium pump activity. Environmental health perspectives. 1996;104(8):852-6.

47.   Shinohara M, Thornalley PJ, Giardino I, Beisswenger P, Thorpe SR, Onorato J, et al. Overexpression of glyoxalase-I in bovine endothelial cells inhibits intracellular advanced glycation endproduct formation and prevents hyperglycemia-induced increases in macromolecular endocytosis. The Journal of clinical investigation. 1998;101(5):1142-7.

48.   Brown BE, Dean RT, Davies MJ. Glycation of low-density lipoproteins by methylglyoxal and glycolaldehyde gives rise to the in vitro formation of lipid-laden cells. Diabetologia. 2005;48(2):361-9.

49.   Morgan PE, Dean RT, Davies MJ. Inactivation of cellular enzymes by carbonyls and protein-bound glycation/glycoxidation products. Archives of biochemistry and biophysics. 2002;403(2):259-69.

50.   Ukeda H, Hasegawa Y, Ishi T, Sawamura M. Inactivation of Cu,Zn-superoxide dismutase by intermediates of Maillard reaction and glycolytic pathway and some sugars. Bioscience, biotechnology, and biochemistry. 1997;61(12):2039-42.

51.   Nauseef WM, Olsson I, Arnljots K. Biosynthesis and processing of myeloperoxidase--a marker for myeloid cell differentiation. European journal of haematology. 1988;40(2):97-110.

52.   Arena S, Renzone G, D'Ambrosio C, Salzano AM, Scaloni A. Dairy products and the Maillard reaction: A promising future for extensive food characterization by integrated proteomics studies. Food Chem. 2017;219:477-89.

53.   Arena S, Salzano AM, Renzone G, D'Ambrosio C, Scaloni A. Non-enzymatic glycation and glycoxidation protein products in foods and diseases: an interconnected, complex scenario fully open to innovative proteomic studies. Mass Spectrom Rev. 2014;33(1):49-77.

54.   Al-Enezi KS, Alkhalaf M, Benov LT. Glycolaldehyde induces growth inhibition and oxidative stress in human breast cancer cells. Free radical biology & medicine. 2006;40(7):1144-51.

55.   Andrades ME, Lorenzi R, Berger M, Guimaraes JA, Moreira JC, Dal-Pizzol F. Glycolaldehyde induces fibrinogen post-translational modification, delay in clotting and resistance to enzymatic digestion. Chemico-biological interactions. 2009;180(3):478-84.

56.   Mera K, Takeo K, Izumi M, Maruyama T, Nagai R, Otagiri M. Effect of reactive-aldehydes on the modification and dysfunction of human serum albumin. Journal of pharmaceutical sciences. 2010;99(3):1614-25.

57.   Koike S, Yano S, Tanaka S, Sheikh AM, Nagai A, Sugimoto T. Advanced Glycation End-Products Induce Apoptosis of Vascular Smooth Muscle Cells: A Mechanism for Vascular Calcification. Int J Mol Sci. 2016;17(9).

58.   Morita M, Yano S, Yamaguchi T, Sugimoto T. Advanced glycation end products-induced reactive oxygen species generation is partly through NF-kappa B activation in human aortic endothelial cells. J Diabetes Complications. 2013;27(1):11-5.

59.   Atkins TW, Thornally PJ. Erythrocyte glyoxalase activity in genetically obese (ob/ob) and streptozotocin diabetic mice. Diabetes research. 1989;11(3):125-9.

60.   Odani H, Shinzato T, Matsumoto Y, Usami J, Maeda K. Increase in three alpha,beta-dicarbonyl compound levels in human uremic plasma: specific in vivo determination of intermediates in advanced Maillard reaction. Biochemical and biophysical research communications. 1999;256(1):89-93.

61.   Campbell DJ, Somaratne JB, Jenkins AJ, Prior DL, Yii M, Kenny JF, et al. Diastolic dysfunction of aging is independent of myocardial structure but associated with plasma advanced glycation end-product levels. PloS one. 2012;7(11):e49813.

62.   Aronson D. Cross-linking of glycated collagen in the pathogenesis of arterial and myocardial stiffening of aging and diabetes. Journal of hypertension. 2003;21(1):3-12.

63.   Deluyker D, Ferferieva V, Noben JP, Swennen Q, Bronckaers A, Lambrichts I, et al. Cross-linking versus RAGE: How do high molecular weight advanced glycation products induce cardiac dysfunction? Int J Cardiol. 2016;210:100-8.

64.   Zieman SJ. Advanced glycation end products cross-linking pathophysiologic role and therapeutic target in cardiovascular disease. Drugs. 2004;64(5):459-70.

65.   Corman B, Duriez M, Poitevin P, Heudes D, Bruneval P, Tedgui A, et al. Aminoguanidine prevents age-related arterial stiffening and cardiac hypertrophy. Proceedings of the National Academy of Sciences of the United States of America. 1998;95(3):1301-6.

66.   Little WC, Zile MR, Kitzman DW, Hundley WG, O'Brien TX, Degroof RC. The effect of alagebrium chloride (ALT-711), a novel glucose cross-link breaker, in the treatment of elderly patients with diastolic heart failure. Journal of cardiac failure. 2005;11(3):191-5.

67.   Candela P, Gosselet F, Saint-Pol J, Sevin E, Boucau MC, Boulanger E, et al. Apical-to-basolateral transport of amyloid-beta peptides through blood-brain barrier cells is mediated by the receptor for advanced glycation end-products and is restricted by P-glycoprotein. J Alzheimers Dis. 2010;22(3):849-59.

68.   Bers DM. Cardiac excitation-contraction coupling. Nature. 2002;415(6868):198-205.

69.   Fabiato A. Simulated calcium current can both cause calcium loading in and trigger calcium release from the sarcoplasmic reticulum of a skinned canine cardiac Purkinje cell. The Journal of general physiology. 1985;85(2):291-320.

70.   Bers DM, Despa S. Cardiac myocytes Ca2+ and Na+ regulation in normal and failing hearts. J Pharmacol Sci. 2006;100(5):315-22.

71.   MacLennan DH, Kranias EG. Phospholamban: a crucial regulator of cardiac contractility. Nat Rev Mol Cell Biol. 2003;4(7):566-77.

72.   Schwinger RH, Munch G, Bolck B, Karczewski P, Krause EG, Erdmann E. Reduced Ca(2+)-sensitivity of SERCA 2a in failing human myocardium due to reduced serin-16 phospholamban phosphorylation. Journal of molecular and cellular cardiology. 1999;31(3):479-91.

73.   Barry WH, Bridge JH. Intracellular calcium homeostasis in cardiac myocytes. Circulation. 1993;87(6):1806-15.

74.   Bidasee KR, Nallani K, Yu Y, Cocklin RR, Zhang Y, Wang M, et al. Chronic diabetes increases advances glycation end products on cardiac ryanodine receptors calcium-release channels (primers). Diabetes. 2003;52.

75.   Bidasee KR, Zhang Y, Shao CH, Wang M, Patel KP, Dincer UD, et al. Diabetes increases formation of advanced glycation end products on Sarco(endo)plasmic reticulum Ca2+-ATPase. Diabetes. 2004;53(2):463-73.

76.   Bidasee KR, Xu L, Meissner G, Besch HR, Jr. Diketopyridylryanodine has three concentration-dependent effects on the cardiac calcium-release channel/ryanodine receptor. The Journal of biological chemistry. 2003;278(16):14237-48.

77.   Lagadic-Gossmann D, Buckler KJ, Le Prigent K, Feuvray D. Altered Ca2+ handling in ventricular myocytes isolated from diabetic rats. The American journal of physiology. 1996;270(5 Pt 2):H1529-37.

78.   Kranstuber AL, Del Rio C, Biesiadecki BJ, Hamlin RL, Ottobre J, Gyorke S, et al. Advanced glycation end product cross-link breaker attenuates diabetes-induced cardiac dysfunction by improving sarcoplasmic reticulum calcium handling. Front Physiol. 2012;3:292.

79.   Vazzana N, Santilli F, Cuccurullo C, Davi G. Soluble forms of RAGE in internal medicine. Internal and emergency medicine. 2009;4(5):389-401.

80.   Brett J, Schmidt AM, Yan SD, Zou YS, Weidman E, Pinsky D, et al. Survey of the distribution of a newly characterized receptor for advanced glycation end products in tissues. The American journal of pathology. 1993;143(6):1699-712.

81.   Tekabe Y, Luma J, Li Q, Schmidt AM, Ramasamy R, Johnson LL. Imaging of receptors for advanced glycation end products in experimental myocardial ischemia and reperfusion injury. JACC Cardiovasc Imaging. 2012;5(1):59-67.

82.   Bucciarelli LG, Kaneko M, Ananthakrishnan R, Harja E, Lee LK, Hwang YC, et al. Receptor for advanced-glycation end products: key modulator of myocardial ischemic injury. Circulation. 2006;113(9):1226-34.

83.   Hong J, Ku SH, Lee MS, Jeong JH, Mok H, Choi D, et al. Cardiac RNAi therapy using RAGE siRNA/deoxycholic acid-modified polyethylenimine complexes for myocardial infarction. Biomaterials. 2014;35(26):7562-73.

84.   Jabaudon M, Perbet S, Pereira B, Soummer A, Roszyk L, Guerin R, et al. Plasma levels of sRAGE, loss of aeration and weaning failure in ICU patients: a prospective observational multicenter study. PloS one. 2013;8(5):e64083.

85.   Neeper M, Schmidt AM, Brett J, Yan SD, Wang F, Pan YC, et al. Cloning and expression of a cell surface receptor for advanced glycosylation end

products of proteins. The Journal of biological chemistry. 1992;267(21):14998-5004.

86.   Vlassara H, Cai W, Goodman S, Pyzik R, Yong A, Chen X, et al. Protection against loss of innate defenses in adulthood by low advanced glycation end products (AGE) intake: role of the antiinflammatory AGE receptor-1. The Journal of clinical endocrinology and metabolism. 2009;94(11):4483-91.

87.   Vlassara H. The AGE-receptor in the pathogenesis of diabetic complications. Diabetes/metabolism research and reviews. 2001;17(6):436-43.

88.   Cai W, He JC, Zhu L, Lu C, Vlassara H. Advanced glycation end product (AGE) receptor 1 suppresses cell oxidant stress and activation signaling via EGF receptor. Proceedings of the National Academy of Sciences of the United States of America. 2006;103(37):13801-6.

89.   Prasad K, Mishra M. AGE-RAGE Stress, Stressors, and Antistressors in Health and Disease. The International journal of angiology : official publication of the International College of Angiology, Inc. 2018;27(1):1-12.

90.   Ramasamy R, Schmidt AM. Receptor for advanced glycation end products (RAGE) and implications for the pathophysiology of heart failure. Curr Heart Fail Rep. 2012;9(2):107-16.

91.   Yan SF, Ramasamy R, Schmidt AM. The receptor for advanced glycation endproducts (RAGE) and cardiovascular disease. Expert Rev Mol Med. 2009;11:e9.

92.   Nielsen JM, Kristiansen SB, Norregaard R, Andersen CL, Denner L, Nielsen TT, et al. Blockage of receptor for advanced glycation end products prevents development of cardiac dysfunction in db/db type 2 diabetic mice. European journal of heart failure. 2009;11(7):638-47.

93.   Bucciarelli LG, Ananthakrishnan R, Hwang YC, Kaneko M, Song F, Sell DR, et al. RAGE and modulation of ischemic injury in the diabetic myocardium. Diabetes. 2008;57(7):1941-51.

94.   Aleshin A, Ananthakrishnan R, Li Q, Rosario R, Lu Y, Qu W, et al. RAGE modulates myocardial injury consequent to LAD infarction via impact on JNK and STAT signaling in a murine model. American journal of physiology Heart and circulatory physiology. 2008;294(4):H1823-32.

95.   Petrova R, Yamamoto Y, Muraki K, Yonekura H, Sakurai S, Watanabe T, et al. Advanced glycation endproduct-induced calcium handling impairment in

mouse cardiac myocytes. Journal of molecular and cellular cardiology. 2002;34(10):1425-31.

96.   Ma H, Li SY, Xu P, Babcock SA, Dolence EK, Brownlee M, et al. Advanced glycation endproduct (AGE) accumulation and AGE receptor (RAGE) up-regulation contribute to the onset of diabetic cardiomyopathy. J Cell Mol Med. 2009;13(8B):1751-64.

97.   Yan D, Luo X, Li Y, Liu W, Deng J, Zheng N, et al. Effects of advanced glycation end products on calcium handling in cardiomyocytes. Cardiology. 2014;129(2):75-83.

98.   Rojas A, Mercadal E, Figueroa H, Morales MA. Advanced Glycation and ROS: a link between diabetes and heart failure. Current vascular pharmacology. 2008;6(1):44-51.

99.   Lopez B, Gonzalez A, Hermida N, Valencia F, de Teresa E, Diez J. Role of lysyl oxidase in myocardial fibrosis: from basic science to clinical aspects. American journal of physiology Heart and circulatory physiology. 2010;299(1):H1-9.

100.   Yan SF, Ramasamy R, Schmidt AM. The RAGE axis: a fundamental mechanism signaling danger to the vulnerable vasculature. Circulation research. 2010;106(5):842-53.

101.   Li SY, Sigmon VK, Babcock SA, Ren J. Advanced glycation endproduct induces ROS accumulation, apoptosis, MAP kinase activation and nuclear O-GlcNAcylation in human cardiac myocytes. Life sciences. 2007;80(11):1051-6.

102.   Zhang L, Huang D, Shen D, Zhang C, Ma Y, Babcock SA, et al. Inhibition of protein kinase C betaII isoform ameliorates methylglyoxal advanced glycation endproduct-induced cardiomyocyte contractile dysfunction. Life sciences. 2014;94(1):83-91.

103.   Bucala R, Tracey KJ, Cerami A. Advanced glycosylation products quench nitric oxide and mediate defective endothelium-dependent vasodilatation in experimental diabetes. The Journal of clinical investigation. 1991;87(2):432-8.

104.   Esposito C, Gerlach H, Brett J, Stern D, Vlassara H. Endothelial receptor-mediated binding of glucose-modified albumin is associated with increased monolayer permeability and modulation of cell surface coagulant properties. The Journal of experimental medicine. 1989;170(4):1387-407.

105.   Wautier JL, Zoukourian C, Chappey O, Wautier MP, Guillausseau PJ, Cao R, et al. Receptor-mediated endothelial cell dysfunction in diabetic vasculopathy. Soluble receptor for advanced glycation end products blocks hyperpermeability in diabetic rats. The Journal of clinical investigation. 1996;97(1):238-43.

106.   Hegab Z, Mohamed TMA, Stafford N, Mamas M, Cartwright EJ, Oceandy D. Advanced glycation end products reduce the calcium transient in cardiomyocytes by increasing production of reactive oxygen species and nitric oxide. FEBS Open Bio. 2017;7(11):1672-85.

107.   Schmidt AM. Soluble RAGEs - Prospects for treating & tracking metabolic and inflammatory disease. Vascular pharmacology. 2015;72:1-8.

108.   Falcone C, Emanuele E, D'Angelo A, Buzzi MP, Belvito C, Cuccia M, et al. Plasma levels of soluble receptor for advanced glycation end products and coronary artery disease in nondiabetic men. Arterioscler Thromb Vasc Biol. 2005;25(5):1032-7.

109.   Prasad K, Mishra M. Do Advanced Glycation End Products and Its Receptor Play a Role in Pathophysiology of Hypertension? The International journal of angiology : official publication of the International College of Angiology, Inc. 2017;26(1):1-11.

110.   Smith DJ, Yerkovich ST, Towers MA, Carroll ML, Thomas R, Upham JW. Reduced soluble receptor for advanced glycation end-products in COPD. Eur Respir J. 2011;37(3):516-22.

111.   Bopp C, Hofer S, Weitz J, Bierhaus A, Nawroth PP, Martin E, et al. sRAGE is elevated in septic patients and associated with patients outcome. The Journal of surgical research. 2008;147(1):79-83.

112.   Jensen LJ, Lindberg S, Hoffmann S, Iversen AZ, Pedersen SH, Mogelvang R, et al. Dynamic changes in sRAGE levels and relationship with cardiac function in STEMI patients. Clin Biochem. 2015;48(4-5):297-301.

113.   Raposeiras-Roubin S, Rodino-Janeiro BK, Grigorian-Shamagian L, Moure-Gonzalez M, Seoane-Blanco A, Varela-Roman A, et al. Soluble receptor of advanced glycation end products levels are related to ischaemic aetiology and extent of coronary disease in chronic heart failure patients, independent of advanced glycation end products levels: New Roles for Soluble RAGE. European journal of heart failure. 2010;12(10):1092-100.

114.   Prasad K, Sarkar A, Zafar MA, Shoker A, Moselhi HE, Tranquilli M, et al. Advanced Glycation End Products and its Soluble Receptors in the Pathogenesis of Thoracic Aortic Aneurysm. Aorta (Stamford). 2016;4(1):1-10.

115.   Cai W, He JC, Zhu L, Chen X, Striker GE, Vlassara H. AGE-receptor-1 counteracts cellular oxidant stress induced by AGEs via negative regulation of p66shc-dependent FKHRL1 phosphorylation. American journal of physiology Cell physiology. 2008;294(1):C145-52.

116.   He CJ, Koschinsky T, Buenting C, Vlassara H. Presence of diabetic complications in type 1 diabetic patients correlates with low expression of mononuclear cell AGE-receptor-1 and elevated serum AGE. Molecular medicine. 2001;7(3):159-68.

117.   Uribarri J, Cai W, Peppa M, Goodman S, Ferrucci L, Striker G, et al. Circulating glycotoxins and dietary advanced glycation endproducts: two links to inflammatory response, oxidative stress, and aging. The journals of gerontology Series A, Biological sciences and medical sciences. 2007;62(4):427-33.

118.   Lin J, Tang Y, Kang Q, Feng Y, Chen A. Curcumin inhibits gene expression of receptor for advanced glycation end-products (RAGE) in hepatic stellate cells in vitro by elevating PPARgamma activity and attenuating oxidative stress. British journal of pharmacology. 2012;166(8):2212-27.

119.   Smedsrod B, Melkko J, Araki N, Sano H, Horiuchi S. Advanced glycation end products are eliminated by scavenger-receptor-mediated endocytosis in hepatic sinusoidal Kupffer and endothelial cells. The Biochemical journal. 1997;322 (Pt 2):567-73.

120.   Tang Y, Chen A. Curcumin eliminates the effect of advanced glycation end-products (AGEs) on the divergent regulation of gene expression of receptors of AGEs by interrupting leptin signaling. Laboratory investigation; a journal of technical methods and pathology. 2014;94(5):503-16.

121.   Furth AJ. Glycated proteins in diabetes. British journal of biomedical science. 1997;54(3):192-200.

122.   Thornalley PJ, Langborg A, Minhas HS. Formation of glyoxal, methylglyoxal and 3-deoxyglucosone in the glycation of proteins by glucose. The Biochemical journal. 1999;344 Pt 1:109-16.

123.   Henle T. AGEs in foods: Do they play a role in uremia? Kidney international. 2003;63:S145-S7.

124.	Heidland A, Sebekova K, Frangiosa A, De Santo LS, Cirillo M, Rossi F, et al. Paradox of circulating advanced glycation end product concentrations in patients with congestive heart failure and after heart transplantation. Heart. 2004;90(11):1269-74.

125.	Kilhovd BK, Berg TJ, Birkeland KI, Thorsby P, Hanssen KF. Serum levels of advanced glycation end products are increased in patients with type 2 diabetes and coronary heart disease. Diabetes care. 1999;22(9):1543-8.

126.	Gerdemann A, Lemke HD, Nothdurft A, Heidland A, Munch G, Bahner U, et al. Low-molecular but not high molecular advanced glycation end products (AGEs) are removed by high-flux dialysis. Clinical nephrology. 2000;54(4):276-83.

127.	Grzebyk E, Knapik-Kordecka M, Piwowar A. Advanced glycation end-products and cathepsin cysteine protease in type 2 diabetic patients. Polskie Archiwum Medycyny Wewnetrznej. 2013;123(7-8):364-70.

128.	Thomas MC, Forbes JM, MacIsaac R, Jerums G, Cooper ME. Low-molecular weight advanced glycation end products: markers of tissue AGE accumulation and more? Annals of the New York Academy of Sciences. 2005;1043:644-54.

129.	Poulsen MW, Andersen JM, Hedegaard RV, Madsen AN, Krath BN, Monosik R, et al. Short-term effects of dietary advanced glycation end products in rats. The British journal of nutrition. 2016;115(4):629-36.

130.	Davies KJ. Degradation of oxidized proteins by the 20S proteasome. Biochimie. 2001;83(3-4):301-10.

131.	Grunwald S, Krause R, Bruch M, Henle T, Brandsch M. Transepithelial flux of early and advanced glycation compounds across Caco-2 cell monolayers and their interaction with intestinal amino acid and peptide transport systems. The British journal of nutrition. 2006;95(6):1221-8.

132.	Hellwig M, Geissler S, Matthes R, Peto A, Silow C, Brandsch M, et al. Transport of free and peptide-bound glycated amino acids: synthesis, transepithelial flux at Caco-2 cell monolayers, and interaction with apical membrane transport proteins. Chembiochem : a European journal of chemical biology. 2011;12(8):1270-9.

133.   He C, Sabol J, Mitsuhashi T, Vlassara H. Dietary glycotoxins: inhibition of reactive products by aminoguanidine facilitates renal clearance and reduces tissue sequestration. Diabetes. 1999;48(6):1308-15.

134.   Koschinsky T, He CJ, Mitsuhashi T, Bucala R, Liu C, Buenting C, et al. Orally absorbed reactive glycation products (glycotoxins): an environmental risk factor in diabetic nephropathy. Proceedings of the National Academy of Sciences of the United States of America. 1997;94(12):6474-9.

135.   Thomas MC, Tsalamandris C, MacIsaac R, Medley T, Kingwell B, Cooper ME, et al. Low-molecular-weight AGEs are associated with GFR and anemia in patients with type 2 diabetes. Kidney international. 2004;66(3):1167-72.

136.   Poulsen MW, Hedegaard RV, Andersen JM, de Courten B, Bugel S, Nielsen J, et al. Advanced glycation endproducts in food and their effects on health. Food and chemical toxicology : an international journal published for the British Industrial Biological Research Association. 2013;60:10-37.

137.   Finot PA, Magnenat E. Metabolic transit of early and advanced Maillard products. Progress in food & nutrition science. 1981;5(1-6):193-207.

138.   Foerster A. KY, Henle T. Studies on absorption and elimination of dietary maillard reaction products. Ann N Y Acad Sci. 2005;1043:474-81.

139.   Deuther-Conrad W, Franke S, Sommer M, Henle T, Stein G. Differences in the modulating potential of advanced glycation end product (AGE) peptides versus AGE proteins. Kidney international Supplement. 2001;78:S63-6.

140.   Jara N, Leal MJ, Bunout D, Hirsch S, Barrera G, Leiva L, et al. Dietary intake increases serum levels of carboxymethil-lysine (CML) in diabetic patients. Nutr Hosp. 2012;27(4):1272-8.

141.   Wang Z, Jiang Y, Liu N, Ren L, Zhu Y, An Y, et al. Advanced glycation end-product Nepsilon-carboxymethyl-Lysine accelerates progression of atherosclerotic calcification in diabetes. Atherosclerosis. 2012;221(2):387-96.

142.   Donaldson C, Taatjes DJ, Zile M, Palmer B, VanBuren P, Spinale F, et al. Combined immunoelectron microscopic and computer-assisted image analyses to detect advanced glycation end-products in human myocardium. Histochem Cell Biol. 2010;134(1):23-30.

143.   Takeuchi M, Makita Z, Yanagisawa K, Kameda Y, Koike T. Detection of noncarboxymethyllysine and carboxymethyllysine advanced glycation end

products (AGE) in serum of diabetic patients. Molecular medicine. 1999;5(6):393-405.

144.   Berg TJ, Snorgaard O, Faber J, Torjesen PA, Hildebrandt P, Mehlsen J, et al. Serum levels of advanced glycation end products are associated with left ventricular diastolic function in patients with type 1 diabetes. Diabetes care. 1999;22(7):1186-90.

145.   Miura J, Yamagishi S, Uchigata Y, Takeuchi M, Yamamoto H, Makita Z, et al. Serum levels of non-carboxymethyllysine advanced glycation endproducts are correlated to severity of microvascular complications in patients with Type 1 diabetes. J Diabetes Complications. 2003;17(1):16-21.

146.   Sharp PS, Rainbow S, Mukherjee S. Serum levels of low molecular weight advanced glycation end products in diabetic subjects. Diabetic medicine : a journal of the British Diabetic Association. 2003;20(7):575-9.

147.   Penfold SA, Coughlan MT, Patel SK, Srivastava PM, Sourris KC, Steer D, et al. Circulating high molecular-weight RAGE ligands activate pathways implicated in the development of diabetic nephropathy. Kidney international. 2010;78(3):287-95.

148.   Ahmed N, Thornalley PJ. Advanced glycation endproducts: what is their relevance to diabetic complications? Diabetes Obes Metab. 2007;9(3):233-45.

149.   Makita Z, Bucala R, Rayfield EJ, Friedman EA, Kaufman AM, Korbet SM, et al. Reactive glycosylation endproducts in diabetic uraemia and treatment of renal failure. Lancet. 1994;343(8912):1519-22.

150.   Vlassara H, Striker GE. AGE restriction in diabetes mellitus: a paradigm shift. Nature reviews Endocrinology. 2011;7(9):526-39.

151.   Brownlee M, Vlassara H, Kooney A, Ulrich P, Cerami A. Aminoguanidine prevents diabetes-induced arterial wall protein cross-linking. Science. 1986;232(4758):1629-32.

152.   Borg DJ, Forbes JM. Targeting advanced glycation with pharmaceutical agents: where are we now? Glycoconj J. 2016;33(4):653-70.

153.   Soulis T, Cooper ME, Vranes D, Bucala R, Jerums G. Effects of aminoguanidine in preventing experimental diabetic nephropathy are related to the duration of treatment. Kidney international. 1996;50(2):627-34.

154.   Hammes HP, Martin S, Federlin K, Geisen K, Brownlee M. Aminoguanidine treatment inhibits the development of experimental diabetic

retinopathy. Proceedings of the National Academy of Sciences of the United States of America. 1991;88(24):11555-8.

155.   Kihara M, Schmelzer JD, Poduslo JF, Curran GL, Nickander KK, Low PA. Aminoguanidine effects on nerve blood flow, vascular permeability, electrophysiology, and oxygen free radicals. Proceedings of the National Academy of Sciences of the United States of America. 1991;88(14):6107-11.

156.   Miyauchi Y, Shikama H, Takasu T, Okamiya H, Umeda M, Hirasaki E, et al. Slowing of peripheral motor nerve conduction was ameliorated by aminoguanidine in streptozocin-induced diabetic rats. Eur J Endocrinol. 1996;134(4):467-73.

157.   Yagihashi S, Kamijo M, Baba M, Yagihashi N, Nagai K. Effect of aminoguanidine on functional and structural abnormalities in peripheral nerve of STZ-induced diabetic rats. Diabetes. 1992;41(1):47-52.

158.   Bolton WK, Cattran DC, Williams ME, Adler SG, Appel GB, Cartwright K, et al. Randomized trial of an inhibitor of formation of advanced glycation end products in diabetic nephropathy. Am J Nephrol. 2004;24(1):32-40.

159.   Freedman BI, Wuerth JP, Cartwright K, Bain RP, Dippe S, Hershon K, et al. Design and baseline characteristics for the aminoguanidine Clinical Trial in Overt Type 2 Diabetic Nephropathy (ACTION II). Control Clin Trials. 1999;20(5):493-510.

160.   Booth AA, Khalifah RG, Todd P, Hudson BG. In vitro kinetic studies of formation of antigenic advanced glycation end products (AGEs). Novel inhibition of post-Amadori glycation pathways. The Journal of biological chemistry. 1997;272(9):5430-7.

161.   Voziyan PA, Khalifah RG, Thibaudeau C, Yildiz A, Jacob J, Serianni AS, et al. Modification of proteins in vitro by physiological levels of glucose: pyridoxamine inhibits conversion of Amadori intermediate to advanced glycation end-products through binding of redox metal ions. The Journal of biological chemistry. 2003;278(47):46616-24.

162.   Alderson NL, Chachich ME, Youssef NN, Beattie RJ, Nachtigal M, Thorpe SR, et al. The AGE inhibitor pyridoxamine inhibits lipemia and development of renal and vascular disease in Zucker obese rats. Kidney international. 2003;63(6):2123-33.

163.   Degenhardt TP, Alderson NL, Arrington DD, Beattie RJ, Basgen JM, Steffes MW, et al. Pyridoxamine inhibits early renal disease and dyslipidemia in the streptozotocin-diabetic rat. Kidney international. 2002;61(3):939-50.

164.   Zheng F, Zeng YJ, Plati AR, Elliot SJ, Berho M, Potier M, et al. Combined AGE inhibition and ACEi decreases the progression of established diabetic nephropathy in B6 db/db mice. Kidney international. 2006;70(3):507-14.

165.   Nagaraj RH, Sarkar P, Mally A, Biemel KM, Lederer MO, Padayatti PS. Effect of pyridoxamine on chemical modification of proteins by carbonyls in diabetic rats: characterization of a major product from the reaction of pyridoxamine and methylglyoxal. Archives of biochemistry and biophysics. 2002;402(1):110-9.

166.   Wu CH, Huang SM, Lin JA, Yen GC. Inhibition of advanced glycation endproduct formation by foodstuffs. Food Funct. 2011;2(5):224-34.

167.   Giardino I, Edelstein D, Horiuchi S, Araki N, Brownlee M. Vitamin-E Prevents Diabetes-Induced Formation of Arterial-Wall Intracellular Advanced Glycation Endproducts (Ages). Diabetes. 1995;44:A73-A.

168.   Ceriello A, Giugliano D, Quatraro A, Donzella C, Dipalo G, Lefebvre PJ. Vitamin-E Reduction of Protein Glycosylation in Diabetes - New Prospect for Prevention of Diabetic Complications. Diabetes care. 1991;14(1):68-72.

169.   Aoki Y, Yanagisawa Y, Yazaki K, Oguchi H, Kiyosawa K, Furuta S. Protective effect of vitamin E supplementation on increased thermal stability of collagen in diabetic rats. Diabetologia. 1992;35(10):913-6.

170.   Forbes JM, Thomas MC, Thorpe SR, Alderson NL, Cooper ME. The effects of valsartan on the accumulation of circulating and renal advanced glycation end products in experimental diabetes. Kidney international Supplement. 2004(92):S105-7.

171.   Watson AM, Soro-Paavonen A, Sheehy K, Li J, Calkin AC, Koitka A, et al. Delayed intervention with AGE inhibitors attenuates the progression of diabetes-accelerated atherosclerosis in diabetic apolipoprotein E knockout mice. Diabetologia. 2011;54(3):681-9.

172.   Candido R, Forbes JM, Thomas MC, Thallas V, Dean RG, Burns WC, et al. A breaker of advanced glycation end products attenuates diabetes-induced myocardial structural changes. Circulation research. 2003;92(7):785-92.

173.   Kim BJ, Choi SY, Lee SH, Kim CK, Ryu WS, Han MK, et al. Advanced coronary artery calcification is associated with ischemic stroke. Cerebrovasc Dis. 2010;30(1):93-100.

174.   Mentink CJ, Hendriks M, Levels AA, Wolffenbuttel BH. Glucose-mediated cross-linking of collagen in rat tendon and skin. Clinica chimica acta; international journal of clinical chemistry. 2002;321(1-2):69-76.

175.   Shapiro BP, Owan TE, Mohammed SF, Meyer DM, Mills LD, Schalkwijk CG, et al. Advanced glycation end products accumulate in vascular smooth muscle and modify vascular but not ventricular properties in elderly hypertensive canines. Circulation. 2008;118(10):1002-10.

176.   Forbes JM, Thallas V, Thomas MC, Founds HW, Burns WC, Jerums G, et al. The breakdown of preexisting advanced glycation end products is associated with reduced renal fibrosis in experimental diabetes. FASEB journal : official publication of the Federation of American Societies for Experimental Biology. 2003;17(12):1762-4.

177.   Lassila M, Seah KK, Allen TJ, Thallas V, Thomas MC, Candido R, et al. Accelerated nephropathy in diabetic apolipoprotein e-knockout mouse: role of advanced glycation end products. Journal of the American Society of Nephrology : JASN. 2004;15(8):2125-38.

178.   Susic D, Varagic J, Ahn J, Frohlich ED. Cardiovascular and renal effects of a collagen cross-link breaker (ALT 711) in adult and aged spontaneously hypertensive rats. American journal of hypertension. 2004;17(4):328-33.

179.   Thallas-Bonke V, Lindschau C, Rizkalla B, Bach LA, Boner G, Meier M, et al. Attenuation of extracellular matrix accumulation in diabetic nephropathy by the advanced glycation end product cross-link breaker ALT-711 via a protein kinase C-alpha-dependent pathway. Diabetes. 2004;53(11):2921-30.

180.   Yang S, Litchfield JE, Baynes JW. AGE-breakers cleave model compounds, but do not break Maillard crosslinks in skin and tail collagen from diabetic rats. Archives of biochemistry and biophysics. 2003;412(1):42-6.

181.   Price DL, Rhett PM, Thorpe SR, Baynes JW. Chelating activity of advanced glycation end-product inhibitors. The Journal of biological chemistry. 2001;276(52):48967-72.

182.   Nenna A, Nappi F, Avtaar Singh SS, Sutherland FW, Di Domenico F, Chello M, et al. Pharmacologic Approaches Against Advanced Glycation End

Products (AGEs) in Diabetic Cardiovascular Disease. Res Cardiovasc Med. 2015;4(2):e26949.

183.   Kass DA, Shapiro EP, Kawaguchi M, Capriotti AR, Scuteri A, deGroof RC, et al. Improved arterial compliance by a novel advanced glycation end-product crosslink breaker. Circulation. 2001;104(13):1464-70.

184.   Willemsen S, Hartog JW, Hummel YM, Posma JL, van Wijk LM, van Veldhuisen DJ, et al. Effects of alagebrium, an advanced glycation end-product breaker, in patients with chronic heart failure: study design and baseline characteristics of the BENEFICIAL trial. European journal of heart failure. 2010;12(3):294-300.

185.   Fujimoto N, Hastings JL, Carrick-Ranson G, Shafer KM, Shibata S, Bhella PS, et al. Cardiovascular effects of 1 year of alagebrium and endurance exercise training in healthy older individuals. Circ Heart Fail. 2013;6(6):1155-64.

186.   Oudegeest-Sander MH, Olde Rikkert MG, Smits P, Thijssen DH, van Dijk AP, Levine BD, et al. The effect of an advanced glycation end-product crosslink breaker and exercise training on vascular function in older individuals: a randomized factorial design trial. Experimental gerontology. 2013;48(12):1509-17.

187.   Flyvbjerg A, Denner L, Schrijvers BF, Tilton RG, Mogensen TH, Paludan SR, et al. Long-term renal effects of a neutralizing RAGE antibody in obese type 2 diabetic mice. Diabetes. 2004;53(1):166-72.

188.   Jensen LJ, Denner L, Schrijvers BF, Tilton RG, Rasch R, Flyvbjerg A. Renal effects of a neutralising RAGE-antibody in long-term streptozotocin-diabetic mice. J Endocrinol. 2006;188(3):493-501.

189.   Okamoto T, Yamagishi S, Inagaki Y, Amano S, Koga K, Abe R, et al. Angiogenesis induced by advanced glycation end products and its prevention by cerivastatin. FASEB journal : official publication of the Federation of American Societies for Experimental Biology. 2002;16(14):1928-30.

190.   Yu W, Wu J, Cai F, Xiang J, Zha W, Fan D, et al. Curcumin alleviates diabetic cardiomyopathy in experimental diabetic rats. PloS one. 2012;7(12):e52013.

191.   Alizadeh M, Kheirouri S. Curcumin against advanced glycation end products (AGEs) and AGEs-induced detrimental agents. Crit Rev Food Sci Nutr. 2017:1-9.

192.   Cerami C, Founds H, Nicholl I, Mitsuhashi T, Giordano D, Vanpatten S, et al. Tobacco smoke is a source of toxic reactive glycation products. Proceedings of the National Academy of Sciences of the United States of America. 1997;94(25):13915-20.

193.   Uribarri J, Peppa M, Cai W, Goldberg T, Lu M, He C, et al. Restriction of dietary glycotoxins reduces excessive advanced glycation end products in renal failure patients. Journal of the American Society of Nephrology : JASN. 2003;14(3):728-31.

194.   Ross R, Dagnone D, Jones PJ, Smith H, Paddags A, Hudson R, et al. Reduction in obesity and related comorbid conditions after diet-induced weight loss or exercise-induced weight loss in men. A randomized, controlled trial. Annals of internal medicine. 2000;133(2):92-103.

195.   Brooks JH, Ferro A. The physician's role in prescribing physical activity for the prevention and treatment of essential hypertension. JRSM Cardiovasc Dis. 2012;1(4).

196.   Gillett M, Royle P, Snaith A, Scotland G, Poobalan A, Imamura M, et al. Non-pharmacological interventions to reduce the risk of diabetes in people with impaired glucose regulation: a systematic review and economic evaluation. Health Technol Assess. 2012;16(33):1-236, iii-iv.

197.   Goon JA, Aini AH, Musalmah M, Anum MY, Nazaimoon WM, Ngah WZ. Effect of Tai Chi exercise on DNA damage, antioxidant enzymes, and oxidative stress in middle-age adults. J Phys Act Health. 2009;6(1):43-54.

198.   Macias-Cervantes MH, Rodriguez-Soto JM, Uribarri J, Diaz-Cisneros FJ, Cai W, Garay-Sevilla ME. Effect of an advanced glycation end product-restricted diet and exercise on metabolic parameters in adult overweight men. Nutrition. 2015;31(3):446-51.

199.   Jessup M, Brozena S. Heart failure. N Engl J Med. 2003;348(20):2007-18.

200.   Cai XY, Lu L, Wang YN, Jin C, Zhang RY, Zhang Q, et al. Association of increased S100B, S100A6 and S100P in serum levels with acute coronary syndrome and also with the severity of myocardial infarction in cardiac tissue of rat models with ischemia-reperfusion injury. Atherosclerosis. 2011;217(2):536-42.

201.	Bodiga VL, Eda SR, Bodiga S. Advanced glycation end products: role in pathology of diabetic cardiomyopathy. Heart Fail Rev. 2014;19(1):49-63.

202.	Raj DS, Choudhury D, Welbourne TC, Levi M. Advanced glycation end products: a Nephrologist's perspective. American journal of kidney diseases : the official journal of the National Kidney Foundation. 2000;35(3):365-80.

203.	Bauer M, Cheng S, Jain M, Ngoy S, Theodoropoulos C, Trujillo A, et al. Echocardiographic speckle-tracking based strain imaging for rapid cardiovascular phenotyping in mice. Circulation research. 2011;108(8):908-16.

204.	Ferferieva V, Van den Bergh A, Claus P, Jasaityte R, Veulemans P, Pellens M, et al. The relative value of strain and strain rate for defining intrinsic myocardial function. American journal of physiology Heart and circulatory physiology. 2012;302(1):H188-95.

205.	Popovic ZB, Sun JP, Yamada H, Drinko J, Mauer K, Greenberg NL, et al. Differences in left ventricular long-axis function from mice to humans follow allometric scaling to ventricular size. J Physiol. 2005;568(Pt 1):255-65.

206.	Valencia JV, Mone M, Koehne C, Rediske J, Hughes TE. Binding of receptor for advanced glycation end products (RAGE) ligands is not sufficient to induce inflammatory signals: lack of activity of endotoxin-free albumin-derived advanced glycation end products. Diabetologia. 2004;47(5):844-52.

207.	Makita Z, Vlassara H, Cerami A, Bucala R. Immunochemical Detection of Advanced Glycosylation End-Products Invivo. Journal of Biological Chemistry. 1992;267(8):5133-8.

208.	Wrobel K, Wrobel K, Garay-Sevilla ME, Nava LE, Malacara JM. Novel analytical approach to monitoring advanced glycosylation end products in human serum with on-line spectrophotometric and spectrofluorometric detection in a flow system. Clinical chemistry. 1997;43(9):1563-9.

209.	Tong L, Huang C, Ramalli A, Tortoli P, Luo J, D'Hooge J, et al. Poster session 1: Wednesday 3 December 2014, 09:00-16:00Location: Poster area. Eur Heart J Cardiovasc Imaging. 2014;15(suppl 2):ii25-ii51.

210.	Ichinose F, Bloch KD, Wu JC, Hataishi R, Aretz HT, Picard MH, et al. Pressure overload-induced LV hypertrophy and dysfunction in mice are exacerbated by congenital NOS3 deficiency. American journal of physiology Heart and circulatory physiology. 2004;286(3):H1070-5.

211.   Derveaux S, Vandesompele J, Hellemans J. How to do successful gene expression analysis using real-time PCR. Methods (San Diego, Calif). 2010;50(4):227-30.

212.   Bustin SA, Benes V, Garson JA, Hellemans J, Huggett J, Kubista M, et al. The MIQE guidelines: minimum information for publication of quantitative real-time PCR experiments. Clinical chemistry. 2009;55(4):611-22.

213.   Yamagishi S, Matsui T, Takenaka K, Nakamura K, Takeuchi M, Inoue H. Pigment epithelium-derived factor (PEDF) prevents platelet activation and aggregation in diabetic rats by blocking deleterious effects of advanced glycation end products (AGEs). Diabetes/metabolism research and reviews. 2009;25(3):266-71.

214.   Greven WL, Smit JM, Rommes JH, Spronk PE. Accumulation of advanced glycation end (AGEs) products in intensive care patients: an observational, prospective study. BMC Clin Pathol. 2010;10:4.

215.   Raposeiras-Roubin S, Rodino-Janeiro BK, Paradela-Dobarro B, Grigorian-Shamagian L, Garcia-Acuna JM, Aguiar-Souto P, et al. Predictive value of advanced glycation end products for the development of post-infarction heart failure: a preliminary report. Cardiovascular Diabetology. 2012;11.

216.   Ferferieva V, Van den Bergh A, Claus P, Jasaityte R, La Gerche A, Rademakers F, et al. Assessment of strain and strain rate by two-dimensional speckle tracking in mice: comparison with tissue Doppler echocardiography and conductance catheter measurements. Eur Heart J Cardiovasc Imaging. 2013;14(8):765-73.

217.   Zhang Q, Ames JM, Smith RD, Baynes JW, Metz TO. A perspective on the Maillard reaction and the analysis of protein glycation by mass spectrometry: probing the pathogenesis of chronic disease. J Proteome Res. 2009;8(2):754-69.

218.   Hermida N, Lopez B, Gonzalez A, Dotor J, Lasarte JJ, Sarobe P, et al. A synthetic peptide from transforming growth factor-beta1 type III receptor prevents myocardial fibrosis in spontaneously hypertensive rats. Cardiovascular research. 2009;81(3):601-9.

219.   Sivakumar P, Gupta S, Sarkar S, Sen S. Upregulation of lysyl oxidase and MMPs during cardiac remodeling in human dilated cardiomyopathy. Molecular and cellular biochemistry. 2008;307(1-2):159-67.

220. Lopez B, Querejeta R, Gonzalez A, Beaumont J, Larman M, Diez J. Impact of treatment on myocardial lysyl oxidase expression and collagen cross-linking in patients with heart failure. Hypertension. 2009;53(2):236-42.

221. Koyama H, Yamamoto H, Nishizawa Y. RAGE and soluble RAGE: potential therapeutic targets for cardiovascular diseases. Molecular medicine. 2007;13(11-12):625-35.

222. Deluyker D, Evens L, Bito V. Advanced glycation end products (AGEs) and cardiovascular dysfunction: focus on high molecular weight AGEs. Amino Acids. 2017.

223. Bito V, Macquaide N, Sipido KR. Characterizing the trigger for sarcoplasmic reticulum Ca2+ release in cardiac myocytes. Cold Spring Harbor protocols. 2015;2015(4):398-402.

224. Vornanen M. Na+/Ca2+ exchange current in ventricular myocytes of fish heart: contribution to sarcolemmal Ca2+ influx. J Exp Biol. 1999;202 (Pt 13):1763-75.

225. Ginsburg KS, Bers DM. Modulation of excitation-contraction coupling by isoproterenol in cardiomyocytes with controlled SR Ca2+ load and Ca2+ current trigger. J Physiol. 2004;556(Pt 2):463-80.

226. Grossman W, Jones D, McLaurin LP. Wall stress and patterns of hypertrophy in the human left ventricle. The Journal of clinical investigation. 1975;56(1):56-64.

227. Gerdes AM. Cardiac myocyte remodeling in hypertrophy and progression to failure. Journal of cardiac failure. 2002;8(6 Suppl):S264-8.

228. Bernardo BC, Weeks KL, Pretorius L, McMullen JR. Molecular distinction between physiological and pathological cardiac hypertrophy: Experimental findings and therapeutic strategies. Pharmacol Therapeut. 2010;128(1):191-227.

229. Piacentino V, 3rd, Weber CR, Chen X, Weisser-Thomas J, Margulies KB, Bers DM, et al. Cellular basis of abnormal calcium transients of failing human ventricular myocytes. Circulation research. 2003;92(6):651-8.

230. Bracken N, Howarth FC, Singh J. Effects of streptozotocin-induced diabetes on contraction and calcium transport in rat ventricular cardiomyocytes. Annals of the New York Academy of Sciences. 2006;1084:208-22.

231.   Bracken NK, Woodall AJ, Howarth FC, Singh J. Voltage-dependence of contraction in streptozotocin-induced diabetic myocytes. Molecular and cellular biochemistry. 2004;261(1-2):235-43.

232.   Lu Z, Ballou LM, Jiang YP, Cohen IS, Lin RZ. Restoration of defective L-type Ca2+ current in cardiac myocytes of type 2 diabetic db/db mice by Akt and PKC-iota. J Cardiovasc Pharmacol. 2011;58(4):439-45.

233.   Pereira L, Matthes J, Schuster I, Valdivia HH, Herzig S, Richard S, et al. Mechanisms of [Ca2+]i transient decrease in cardiomyopathy of db/db type 2 diabetic mice. Diabetes. 2006;55(3):608-15.

234.   He J, Conklin MW, Foell JD, Wolff MR, Haworth RA, Coronado R, et al. Reduction in density of transverse tubules and L-type Ca(2+) channels in canine tachycardia-induced heart failure. Cardiovascular research. 2001;49(2):298-307.

235.   Heinzel FR, Bito V, Biesmans L, Wu M, Detre E, von Wegner F, et al. Remodeling of T-tubules and reduced synchrony of Ca2+ release in myocytes from chronically ischemic myocardium. Circulation research. 2008;102(3):338-46.

236.   Louch WE, Bito V, Heinzel FR, Macianskiene R, Vanhaecke J, Flameng W, et al. Reduced synchrony of Ca2+ release with loss of T-tubules-a comparison to Ca2+ release in human failing cardiomyocytes. Cardiovascular research. 2004;62(1):63-73.

237.   Louch WE, Mork HK, Sexton J, Stromme TA, Laake P, Sjaastad I, et al. T-tubule disorganization and reduced synchrony of Ca2+ release in murine cardiomyocytes following myocardial infarction. J Physiol. 2006;574(Pt 2):519-33.

238.   Lyon AR, MacLeod KT, Zhang Y, Garcia E, Kanda GK, Lab MJ, et al. Loss of T-tubules and other changes to surface topography in ventricular myocytes from failing human and rat heart. Proceedings of the National Academy of Sciences of the United States of America. 2009;106(16):6854-9.

239.   Brette F, Orchard C. T-tubule function in mammalian cardiac myocytes. Circulation research. 2003;92(11):1182-92.

240.   Ibrahim M, Gorelik J, Yacoub MH, Terracciano CM. The structure and function of cardiac t-tubules in health and disease. Proc Biol Sci. 2011;278(1719):2714-23.

241.   Yuill KH, Al Kury LT, Howarth FC. Characterization of L-type calcium channel activity in atrioventricular nodal myocytes from rats with streptozotocin-induced Diabetes mellitus. Physiological reports. 2015;3(11).

242.   Bito V, Heinzel FR, Weidemann F, Dommke C, van der Velden J, Verbeken E, et al. Cellular mechanisms of contractile dysfunction in hibernating myocardium. Circulation research. 2004;94(6):794-801.

243.   Bito V, van der Velden J, Claus P, Dommke C, Van Lommel A, Mortelmans L, et al. Reduced force generating capacity in myocytes from chronically ischemic, hibernating myocardium. Circulation research. 2007;100(2):229-37.

244.   Allen DL, Leinwand LA. Postnatal myosin heavy chain isoform expression in normal mice and mice null for IIb or IId myosin heavy chains. Dev Biol. 2001;229(2):383-95.

245.   Everett AW, Sinha AM, Umeda PK, Jakovcic S, Rabinowitz M, Zak R. Regulation of myosin synthesis by thyroid hormone: relative change in the alpha- and beta-myosin heavy chain mRNA levels in rabbit heart. Biochemistry. 1984;23(8):1596-9.

246.   Krenz M, Robbins J. Impact of beta-myosin heavy chain expression on cardiac function during stress. J Am Coll Cardiol. 2004;44(12):2390-7.

247.   Jones WK, Grupp IL, Doetschman T, Grupp G, Osinska H, Hewett TE, et al. Ablation of the murine alpha myosin heavy chain gene leads to dosage effects and functional deficits in the heart. The Journal of clinical investigation. 1996;98(8):1906-17.

248.   Periasamy M, Janssen PM. Molecular basis of diastolic dysfunction. Heart Fail Clin. 2008;4(1):13-21.

249.   Zarain-Herzberg A, Garcia-Rivas G, Estrada-Aviles R. Regulation of SERCA pumps expression in diabetes. Cell Calcium. 2014;56(5):302-10.

250.   Zhao XY, Hu SJ, Li J, Mou Y, Chen BP, Xia Q. Decreased cardiac sarcoplasmic reticulum Ca2+ -ATPase activity contributes to cardiac dysfunction in streptozotocin-induced diabetic rats. J Physiol Biochem. 2006;62(1):1-8.

251.   Kim HW, Ch YS, Lee HR, Park SY, Kim YH. Diabetic alterations in cardiac sarcoplasmic reticulum Ca2+-ATPase and phospholamban protein expression. Life sciences. 2001;70(4):367-79.

252. Teshima Y, Takahashi N, Saikawa T, Hara M, Yasunaga S, Hidaka S, et al. Diminished expression of sarcoplasmic reticulum Ca(2+)-ATPase and ryanodine sensitive Ca(2+)Channel mRNA in streptozotocin-induced diabetic rat heart. Journal of molecular and cellular cardiology. 2000;32(4):655-64.

253. Allen DG, Kentish JC. The cellular basis of the length-tension relation in cardiac muscle. Journal of molecular and cellular cardiology. 1985;17(9):821-40.

254. Belus A, Piroddi N, Ferrantini C, Tesi C, Cazorla O, Toniolo L, et al. Effects of chronic atrial fibrillation on active and passive force generation in human atrial myofibrils. Circulation research. 2010;107(1):144-52.

255. Makarenko I, Opitz CA, Leake MC, Neagoe C, Kulke M, Gwathmey JK, et al. Passive stiffness changes caused by upregulation of compliant titin isoforms in human dilated cardiomyopathy hearts. Circulation research. 2004;95(7):708-16.

256. Bollen IAE, Ehler E, Fleischanderl K, Bouwman F, Kempers L, Ricke-Hoch M, et al. Myofilament Remodeling and Function Is More Impaired in Peripartum Cardiomyopathy Compared with Dilated Cardiomyopathy and Ischemic Heart Disease. The American journal of pathology. 2017.

257. Deluyker D FV, Noben JP, Swennen Q, Bronckaers A, Lambrichts I, Rigo JM, Bito V. Cross-linking versus RAGE: How do high molecular weight advanced glycation products induce cardiac dysfunction? International Journal of Cardiology. 2016;210:100-8.

258. Naser N, Januszewski AS, Brown BE, Jenkins AJ, Hill MA, Murphy TV. Advanced glycation end products acutely impair ca(2+) signaling in bovine aortic endothelial cells. Front Physiol. 2013;4:38.

259. Sipido KR, Macquaide N, Bito V. A systematic approach for assessing Ca(2)(+) handling in cardiac myocytes. Cold Spring Harbor protocols. 2015;2015(5):431-3.

260. Xue J, Ray R, Singer D, Bohme D, Burz DS, Rai V, et al. The receptor for advanced glycation end products (RAGE) specifically recognizes methylglyoxal-derived AGEs. Biochemistry. 2014;53(20):3327-35.

261. Rosamond W, Flegal K, Furie K, Go A, Greenlund K, Haase N, et al. Heart disease and stroke statistics--2008 update: a report from the American Heart

Association Statistics Committee and Stroke Statistics Subcommittee. Circulation. 2008;117(4):e25-146.

262.   Berner AK, Brouwers O, Pringle R, Klaassen I, Colhoun L, McVicar C, et al. Protection against methylglyoxal-derived AGEs by regulation of glyoxalase 1 prevents retinal neuroglial and vasodegenerative pathology. Diabetologia. 2012;55(3):845-54.

263.   Mulder DJ, van Haelst PL, Graaff R, Gans RO, Zijlstra F, Smit AJ. Skin autofluorescence is elevated in acute myocardial infarction and is associated with the one-year incidence of major adverse cardiac events. Neth Heart J. 2009;17(4):162-8.

264.   Blackburn NJR, Vulesevic B, McNeill B, Cimenci CE, Ahmadi A, Gonzalez-Gomez M, et al. Methylglyoxal-derived advanced glycation end products contribute to negative cardiac remodeling and dysfunction post-myocardial infarction. Basic Res Cardiol. 2017;112(5):57.

265.   Guo Y, Lu M, Qian J, Cheng YL. Alagebrium chloride protects the heart against oxidative stress in aging rats. The journals of gerontology Series A, Biological sciences and medical sciences. 2009;64(6):629-35.

266.   Steppan J, Tran H, Benjo AM, Pellakuru L, Barodka V, Ryoo S, et al. Alagebrium in combination with exercise ameliorates age-associated ventricular and vascular stiffness. Experimental gerontology. 2012;47(8):565-72.

267.   Wang CH, Wu ET, Wu MS, Tsai MS, Ko YH, Chang RW, et al. Pyridoxamine protects against mechanical defects in cardiac ageing in rats: studies on load dependence of myocardial relaxation. Experimental physiology. 2014;99(11):1488-98.

268.   Wu ET, Liang JT, Wu MS, Chang KC. Pyridoxamine prevents age-related aortic stiffening and vascular resistance in association with reduced collagen glycation. Experimental gerontology. 2011;46(6):482-8.

269.   Desai CK, Huang J, Lokhandwala A, Fernandez A, Riaz IB, Alpert JS. The role of vitamin supplementation in the prevention of cardiovascular disease events. Clin Cardiol. 2014;37(9):576-81.

270.   Hartog JW, Willemsen S, van Veldhuisen DJ, Posma JL, van Wijk LM, Hummel YM, et al. Effects of alagebrium, an advanced glycation endproduct breaker, on exercise tolerance and cardiac function in patients with chronic heart failure. European journal of heart failure. 2011;13(8):899-908.

271.   Almeida F, Santos-Silva D, Rodrigues T, Matafome P, Crisostomo J, Sena C, et al. Pyridoxamine reverts methylglyoxal-induced impairment of survival pathways during heart ischemia. Cardiovasc Ther. 2013;31(6):e79-85.

272.   Shang L, Ananthakrishnan R, Li Q, Quadri N, Abdillahi M, Zhu Z, et al. RAGE modulates hypoxia/reoxygenation injury in adult murine cardiomyocytes via JNK and GSK-3beta signaling pathways. PloS one. 2010;5(4):e10092.

273.   Muellenbach EM, Diehl CJ, Teachey MK, Lindborg KA, Hasselwander O, Matuschek M, et al. Metabolic interactions of AGE inhibitor pyridoxamine and antioxidant alpha-lipoic acid following 22 weeks of treatment in obese Zucker rats. Life sciences. 2009;84(15-16):563-8.

274.   Dhalla NS, Takeda S, Elimban V. Mechanisms of the beneficial effects of vitamin B6 and pyridoxal 5-phosphate on cardiac performance in ischemic heart disease. Clinical chemistry and laboratory medicine. 2013;51(3):535-43.

275.   Kandzari DE, Dery JP, Armstrong PW, Douglas DA, Zettler ME, Hidinger GK, et al. MC-1 (pyridoxal 5'-phosphate): novel therapeutic applications to reduce ischaemic injury. Expert Opin Investig Drugs. 2005;14(11):1435-42.

276.   Richardson WJ, Clarke SA, Quinn TA, Holmes JW. Physiological Implications of Myocardial Scar Structure. Compr Physiol. 2015;5(4):1877-909.

277.   Nakatani S. Left ventricular rotation and twist: why should we learn? J Cardiovasc Ultrasound. 2011;19(1):1-6.

278.   Peng Y, Popovic ZB, Sopko N, Drinko J, Zhang Z, Thomas JD, et al. Speckle tracking echocardiography in the assessment of mouse models of cardiac dysfunction. American journal of physiology Heart and circulatory physiology. 2009;297(2):H811-20.

279.   Wang J, Khoury DS, Yue Y, Torre-Amione G, Nagueh SF. Left ventricular untwisting rate by speckle tracking echocardiography. Circulation. 2007;116(22):2580-6.

280.   Iwasaki M, Masuda K, Asanuma T, Nakatani S. Effects of mechanical limitation of apical rotation on left ventricular relaxation and end-diastolic pressure. American journal of physiology Heart and circulatory physiology. 2011;301(4):H1456-60.

281.   Celec P, Hodosy J, Jani P, Janega P, Kudela M, Kalousova M, et al. Advanced glycation end products in myocardial reperfusion injury. Heart Vessels. 2012;27(2):208-15.

282.   Kralev S, Zimmerer E, Brueckmann M, Lang S, Kalsch T, Rippert A, et al. Elevation of the glycoxidation product N(epsilon)-(carboxymethyl)lysine in patients presenting with acute myocardial infarction. Clinical chemistry and laboratory medicine. 2009;47(4):446-51.

283.   Gonzalez-Santamaria J, Villalba M, Busnadiego O, Lopez-Olaneta MM, Sandoval P, Snabel J, et al. Matrix cross-linking lysyl oxidases are induced in response to myocardial infarction and promote cardiac dysfunction. Cardiovascular research. 2016;109(1):67-78.

284.   El Hajj EC, El Hajj MC, Ninh VK, Bradley JM, Claudino MA, Gardner JD. Detrimental role of lysyl oxidase in cardiac remodeling. Journal of molecular and cellular cardiology. 2017;109:17-26.

285.   Hartog JW, van de Wal RM, Schalkwijk CG, Miyata T, Jaarsma W, Plokker HW, et al. Advanced glycation end-products, anti-hypertensive treatment and diastolic function in patients with hypertension and diastolic dysfunction. European journal of heart failure. 2010;12(4):397-403.

286.   Jellis C, Martin J, Narula J, Marwick TH. Assessment of nonischemic myocardial fibrosis. J Am Coll Cardiol. 2010;56(2):89-97.

287.   Willemsen S, Hartog JWL, Hummel YM, Posma JL, van Wijk LM, van Veldhuisen DJ, et al. Effects of alagebrium, an advanced glycation end-product breaker, in patients with chronic heart failure: study design and baseline characteristics of the BENEFICIAL trial. European journal of heart failure. 2010;12(3):294-300.

288.   Metz TO, Alderson NL, Thorpe SR, Baynes JW. Pyridoxamine, an inhibitor of advanced glycation and lipoxidation reactions: a novel therapy for treatment of diabetic complications. Archives of biochemistry and biophysics. 2003;419(1):41-9.

289.   Wu M, D'Hooge J, Ganame J, Ferferieva V, Sipido KR, Maes F, et al. Non-invasive characterization of the area-at-risk using magnetic resonance imaging in chronic ischaemia. Cardiovascular research. 2011;89(1):166-74.

290.   Voloshenyuk TG, Landesman ES, Khoutorova E, Hart AD, Gardner JD. Induction of cardiac fibroblast lysyl oxidase by TGF-beta1 requires PI3K/Akt, Smad3, and MAPK signaling. Cytokine. 2011;55(1):90-7.

291.   Dean RG, Balding LC, Candido R, Burns WC, Cao Z, Twigg SM, et al. Connective tissue growth factor and cardiac fibrosis after myocardial infarction. J Histochem Cytochem. 2005;53(10):1245-56.

292.   Petrov VV, van Pelt JF, Vermeesch JR, Van Duppen VJ, Vekemans K, Fagard RH, et al. TGF-beta1-induced cardiac myofibroblasts are nonproliferating functional cells carrying DNA damages. Experimental cell research. 2008;314(7):1480-94.

293.   Lopez B, Gonzalez A, Lindner D, Westermann D, Ravassa S, Beaumont J, et al. Osteopontin-mediated myocardial fibrosis in heart failure: a role for lysyl oxidase? Cardiovascular research. 2013;99(1):111-20.

294.   Shimazaki M, Nakamura K, Kii I, Kashima T, Amizuka N, Li M, et al. Periostin is essential for cardiac healing after acute myocardial infarction. Journal of Experimental Medicine. 2008;205(2):295-303.

295.   Sarrazy V, Koehler A, Chow ML, Zimina E, Li CX, Kato H, et al. Integrins alphavbeta5 and alphavbeta3 promote latent TGF-beta1 activation by human cardiac fibroblast contraction. Cardiovascular research. 2014;102(3):407-17.

296.   Jobling MF, Mott JD, Finnegan MT, Jurukovski V, Erickson AC, Walian PJ, et al. Isoform-specific activation of latent transforming growth factor beta (LTGF-beta) by reactive oxygen species. Radiation research. 2006;166(6):839-48.

297.   Midaoui AE, Elimadi A, Wu L, Haddad PS, de Champlain J. Lipoic acid prevents hypertension, hyperglycemia, and the increase in heart mitochondrial superoxide production. American journal of hypertension. 2003;16(3):173-9.

298.   Adam O, Theobald K, Lavall D, Grube M, Kroemer HK, Ameling S, et al. Increased lysyl oxidase expression and collagen cross-linking during atrial fibrillation. Journal of molecular and cellular cardiology. 2011;50(4):678-85.

299.   Nishizawa Y, Koyama H, Inaba M. AGEs and cardiovascular diseases in patients with end-stage renal diseases. J Ren Nutr. 2012;22(1):128-33.

300.   Chen SC, Guh JY, Hwang CC, Chiou SJ, Lin TD, Ko YM, et al. Advanced glycation end-products activate extracellular signal-regulated kinase via the oxidative stress-EGF receptor pathway in renal fibroblasts. J Cell Biochem. 2010;109(1):38-48.

301.   Greven WL, Waanders F, Nagai R, van den Heuvel MC, Navis G, van Goor H. Mesangial accumulation of GA-pyridine, a novel glycolaldehyde-derived AGE, in human renal disease. Kidney international. 2005;68(2):595-602.

302.   Nagai R, Hayashi CM, Xia L, Takeya M, Horiuchi S. Identification in human atherosclerotic lesions of GA-pyridine, a novel structure derived from glycolaldehyde-modified proteins. The Journal of biological chemistry. 2002;277(50):48905-12.

303.   Takeuchi M, Makita Z, Bucala R, Suzuki T, Koikie T, Kameda Y. Immunological evidence that non-carboxymethyllysine advanced glycation end-products are produced from short chain sugars and dicarbonyl compounds in vivo. Molecular medicine. 2000;6(2):114-25.

304.   Scheijen J, Clevers E, Engelen L, Dagnelie PC, Brouns F, Stehouwer CDA, et al. Analysis of advanced glycation endproducts in selected food items by ultra-performance liquid chromatography tandem mass spectrometry: Presentation of a dietary AGE database. Food Chem. 2016;190:1145-50.

305.   Scheijen JL, Schalkwijk CG. Quantification of glyoxal, methylglyoxal and 3-deoxyglucosone in blood and plasma by ultra performance liquid chromatography tandem mass spectrometry: evaluation of blood specimen. Clinical chemistry and laboratory medicine. 2014;52(1):85-91.

306.   Teerlink T, Barto R, Ten Brink HJ, Schalkwijk CG. Measurement of Nepsilon-(carboxymethyl)lysine and Nepsilon-(carboxyethyl)lysine in human plasma protein by stable-isotope-dilution tandem mass spectrometry. Clinical chemistry. 2004;50(7):1222-8.

307.   Hanssen NM, Wouters K, Huijberts MS, Gijbels MJ, Sluimer JC, Scheijen JL, et al. Higher levels of advanced glycation endproducts in human carotid atherosclerotic plaques are associated with a rupture-prone phenotype. Eur Heart J. 2014;35(17):1137-46.

308.   Milani-Nejad N, Janssen PM. Small and large animal models in cardiac contraction research: advantages and disadvantages. Pharmacol Ther. 2014;141(3):235-49.

309.   Cingolani OH, Kass DA. Pressure-volume relation analysis of mouse ventricular function. American journal of physiology Heart and circulatory physiology. 2011;301(6):H2198-206.

310. Hartley CJ, Reddy AK, Madala S, Entman ML, Michael LH, Taffet GE. Doppler velocity measurements from large and small arteries of mice. American journal of physiology Heart and circulatory physiology. 2011;301(2):H269-78.

311. Fedorov VV, Glukhov AV, Ambrosi CM, Kostecki G, Chang R, Janks D, et al. Effects of KATP channel openers diazoxide and pinacidil in coronary-perfused atria and ventricles from failing and non-failing human hearts. Journal of molecular and cellular cardiology. 2011;51(2):215-25.

312. Glukhov AV, Fedorov VV, Lou Q, Ravikumar VK, Kalish PW, Schuessler RB, et al. Transmural dispersion of repolarization in failing and nonfailing human ventricle. Circulation research. 2010;106(5):981-91.

313. Nerbonne JM. Studying cardiac arrhythmias in the mouse--a reasonable model for probing mechanisms? Trends Cardiovasc Med. 2004;14(3):83-93.

314. Bassani JW, Bassani RA, Bers DM. Relaxation in rabbit and rat cardiac cells: species-dependent differences in cellular mechanisms. J Physiol. 1994;476(2):279-93.

315. Li L, Chu G, Kranias EG, Bers DM. Cardiac myocyte calcium transport in phospholamban knockout mouse: relaxation and endogenous CaMKII effects. The American journal of physiology. 1998;274(4 Pt 2):H1335-47.

316. Pott C, Eckardt L, Goldhaber JI. Triple threat: the Na+/Ca2+ exchanger in the pathophysiology of cardiac arrhythmia, ischemia and heart failure. Curr Drug Targets. 2011;12(5):737-47.

317. American Cancer Society. Cancer Facts & Figures 2017. Amercian Cancer Society.

318. Weir HK, Anderson RN, Coleman King SM, Soman A, Thompson TD, Hong Y, et al. Heart Disease and Cancer Deaths - Trends and Projections in the United States, 1969-2020. Prev Chronic Dis. 2016;13:E157.

319. Ferlay J, Autier P, Boniol M, Heanue M, Colombet M, Boyle P. Estimates of the cancer incidence and mortality in Europe in 2006. Annals of oncology : official journal of the European Society for Medical Oncology / ESMO. 2007;18(3):581-92.

320. Mariotto AB, Yabroff KR, Shao Y, Feuer EJ, Brown ML. Projections of the cost of cancer care in the United States: 2010-2020. Journal of the National Cancer Institute. 2011;103(2):117-28.

321.   Han X, Zhou Y, Liu W. Precision cardio-oncology: understanding the cardiotoxicity of cancer therapy. NPJ Precis Oncol. 2017;1(1):31.

322.   Kenigsberg B, Wellstein A, Barac A. Left Ventricular Dysfunction in Cancer Treatment: Is it Relevant? JACC Heart Fail. 2018;6(2):87-95.

323.   Zheng PP, Li J, Kros JM. Breakthroughs in modern cancer therapy and elusive cardiotoxicity: Critical research-practice gaps, challenges, and insights. Med Res Rev. 2018;38(1):325-76.

9

NEDERLANDSE SAMENVATTING

Nederlandse samenvatting

Hartfalen is wereldwijd de voornaamste doodsoorzaak. Het hart is niet meer in staat om voldoende bloed rond te pompen om aan de energiebehoeftes van het lichaam te voldoen. De ontwikkeling van hartfalen is een complex proces gekenmerkt door zowel structurele als functionele veranderingen. De laatste jaren komen er steeds meer aanwijzingen dat advanced glycation end products (AGEs) een rol spelen in de ontwikkeling van hartfalen. AGEs zijn eiwitten gemodificeerd met suikergroepen. In normale fysiologische omstandigheden stapelen AGEs zich op in het lichaam naarmate men ouder wordt. Dit proces wordt echter versneld in pathologische omstandigheden zoals hartfalen.

AGEs kunnen *in vivo* en *in vitro* gevormd worden via verschillende pathways. Aangezien verscheidene routes kunnen leiden tot de vorming van AGEs, zijn er diverse AGEs moleculen *in vivo* aanwezig. Op basis van hun moleculaire grootte kunnen ze worden onderverdeeld in twee groepen: AGEs met een hoog moleculair gewicht (HMW-AGEs) en AGEs met een laag moleculair gewicht (LMW-AGEs). Tot nu toe focuste het wetenschappelijk onderzoek zich voornamelijk op LMW-AGEs. Recent onderzoek heeft aangetoond dat HMW-AGEs even belangrijk zijn als LMW-AGEs zijn in een pathologische setting.

Deze doctoraatsdissertatie focust zich op de rol van HMW-AGEs binnen cardiale dysfunctie. Dit werk kaart meer specifiek de volgende vragen aan: Kunnen HMW-AGEs leiden tot cardiale dysfunctie in gezonde dieren? Kan chronische blootstelling aan HMW-AGEs leiden tot structurele en morfologische verandering op cellulair niveau? Spelen HMW-AGEs een rol in acute omstandigheden? Kan behandeling met pyridoxamine, een vitamine dat de vorming van AGEs voorkomt, leiden tot een verbeterde cardiale functie na een myocardinfarct?

De resultaten gepresenteerd in deze dissertatie tonen aan dat HMW-AGEs *in vivo* kunnen leiden tot verdikking van de anterior en posterior wand van de ventrikels. Deze hypertrofie gaat samen met een verhoogde myocardiale fibrose **(hoofdstuk 3)**. Op cellulair niveau wordt er eveneens hypertrofie waargenomen. Chronisch HMW-AGEs toediening leidt tot een verstoorde calciumhuishouding, aangetoond door verminderde calciuminstroom en een veranderde beschikbaarheid van de calciumkanalen. Meer in detail werd ook

gezien dat de eigenschappen van de myofilamenten veranderen **(hoofdstuk 4)**. Acute toediening van HMW-AGEs aan cardiomyocyten *in vitro* veroorzaakt een verminderde contractiliteit en verminderde calcium instroom via de L-type calcium kanalen **(hoofdstuk 5)**. Ten slotte geeft dit werk aan dat de behandeling van een myocardinfarct met pyridoxamine leidt tot een verminderde mortaliteit in vergelijking met dieren die geen behandeling kregen. Verder leidt behandeling met pyridoxamine tot verlaagde AGEs levels en verminderde hoeveelheid myocardiale fibrose **(hoofdstuk 6)**.

Uit deze dissertatie kunnen de volgende conclusies getrokken worden. (1) HMW-AGEs leiden tot cardiale dysfunctie. (2) HMW-AGEs veroorzaken zowel structurele als functionele veranderingen op cellulair niveau. (3) HMW-AGEs spelen een rol in acute omstandigheden. (4) Pyridoxamine verlaagt de mortaliteit en vermindert de cardiale dysfunctie na een myocardinfarct.

10

OTHER

Curriculum Vitae

Dorien Deluyker was born on 21st of July 1989 in Maaseik, Belgium. In 2007, she graduated from Koninklijk Atheneum Maaseik, latin-mathematics. In 2012, she obtained a Master's degree at Hasselt University/transnational University Limburg in Biomedical Sciences, option environmental health sciences. Dorien conducted her Master dissertation entitled 'Stem cell dynamics after exposure to cadmium and hexavalent chromium in Schmidtea mediterranea: regenerating vs intact worms' at centrum voor Milieukunde (CMK) in the lab of prof. dr. Karen Smeets.

In October 2012, she started her PhD at Biomedical research institute in the group of prof. dr. Virginie Bito. Dorien followed several courses and workshops, including project and time managment, professional education and teaching, FLAMES summerschool, LC-MS summerschool and organized together with 6 other PhD students the PhD symposium 'Recent Advanced in neuronal and cardiac tissue engineering: From lab to Clinic'.

The results obtained during the course of her PhD were partially published in international peer reviewed journals and were presented at several (inter)national conferences.

Bibliography

Publications

- Verboven M, **Deluyker D**, Ferferieva V, Lambrichts I, Hansen D, Eijnde B, Bito V. Western diet given to healthy rats mimics the human phenotype of diabetic cardiomyopathy. The Journal of Nutritional Biochemistry (2018); *In press.* (IF: 4.41)

- **Deluyker D***, Ferferieva V*, Driesen RB, Verboven M, Lambrichts I, Bito V. Pyridoxamine improves survival and limits cardiac dysfunction after MI. Scientific reports (2017); 7(1):16010. (IF: 4.12)
  *authors equally contributed to the study

- **Deluyker D**, Evens L, Bito V. Advanced glycation end products (AGEs) and cardiovascular dysfunction: focus on high molecular weight AGEs. Amino Acids (2017); 49:1535-1541. (IF: 3.17)

- **Deluyker D**, Ferferieva V. Noben JP, Swennen Q, Bronckaers A, Lambrichts I, Rigo JM, Bito V. Cross-linking versus RAGE: how do high molecular weight advanced glycation products induce cardiac dysfunction? International Journal Cardiology (2016); 210:100-108. (IF: 6.19)

- Stevens AL, Ferferieva V, Bito V, Wens I, Verboven K, **Deluyker D**, Voet A, Vanhoof J, Dendale P, Eijnde BO. Exercise improves cardiac function and attenuates insulin resistance in Dahl salt-sensitive rats. International Journal of Cardiology (2015); 186:154-160. (IF: 4.86)

*Authors equally contributed to the study

Published Posters

- Verboven M, **Deluyker D**, Hansen D, Eijnde B, Bito V. The origin of diabetes: high-sugar diet to induce diabetic cardiomyopathy in rats. *European Heart Journal* (2017)

- Ferferieva V, **Deluyker D**, Verboven M, Bito V. Pyridoxamine treatment improves diastolic function in a rat model of chronic myocardial infarction. *European Heart Journal* (2016);37 (1), 1331

- **Deluyker D**, Bito V. HMW-AGEs application acutely reduces ICaL in adult cardiomyocytes. *Cardiovascular Research* (2016): 111 Suppl 1; S108-S108

- **Deluyker D**, Bito V. HMW-AGEs induces Ca^{2+} imbalance in rat cardiomyocytes. *Journa of International Society of Antioxidants in Nutrition & Health* (2016); 3 (2)
- Ferferieva V, **Deluyker D**, Bito V. Advanced glycation end products play a role in adverse LV remodeling following MI. European Heart Joural Cardiovascular Imaging. (2015)
- Ferferieva F, **Deluyker D**, Lambrichts I, Rigo JM, Bito V. Assessment of left ventricular twist and untwist rate in a rat model of myocardial infarction. European Heart Journal Cardiovascular Imaging. (2014);15 Suppl 2; ii168-ii195
- Ferferieva V, **Deluyker D**, Arslan T, Lambrichts I, Rigo JM, Bito V. Strain and strain rate identify accurately myocardial dysfunction in rats injected with advanced glycation end products. European Heart Journal Cardiovascular Imaging. (2014);15 Suppl 2; ii55-ii56

Selected Poster presentations

- Verboven M, Evens L, **Deluyker D**, Colson D, Eijnde BO, Hansen D, Bito V. High-Intensity Interval Training is as efficient as Moderate Intensity Training in reversing diabetic cardiomyopathy. American Heart Association, 2018.
- **Deluyker D***, Evens L*, Kuster D, Verboven M, van der Velden J, Bito V. Impact of glycated proteins on cardiomyocyte function. International Society for Heart Research, 2018.
  *authors equally contributed to the study
- Lize Evens, **Deluyker D**, Verboven M, Bito V. Do glycated proteins change cardiomyocyte function? MOSA conference, 2017.
- Verboven M, **Deluyker D**, Eijnde BO, Hansen D, Bito V. High-intensity interval training is as efficient as moderate intensity training for cardiac function. Exercise metabolism, 2017.
- **Deluyker D**, Ferferieva V, Rigo JM, Bito V. sRAGE levels correlate with strain in a rat model of cardiac dysfunction. BIOMEDICA, 2015.
- **Deluyker D**, Ferferieva V, Rigo JM, Bito V. sRAGE limits cardiac dysfunction induced by advanced glycation end products in rats. Belgian society of physiology and pharmacology, 2014.

Bursaries

- FWO travel grant (2016) to attend the 3rd world congress on Glycation & Maillard reaction
- FWO grant for short stay (2017) to stay and work in Amsterdam in the lab of Prof. dr. Jolanda van der Velden at VUmc Amsterdam.

Dankwoord

Er bestaat geen protocol voor het doorlopen van een doctoraat maar er zijn wel een aantal voorwaarden, die nodig zijn om een doctoraat succesvol af te ronden. Zo is het essentieel om lieve, zotte en behulpzame mensen rond je te hebben zodat je zelfs de zwaarste bergetappes tijdens je doctoraat kan overleven. Daarom schrijven mensen op het einde van hun doctoraat meestal een dankwoord om deze mensen te bedanken. Maar de kans bestaat ook dat je onbewust iemand vergeet en om dit te voorkomen heb ik een schema gemaakt.